NASA CR-54700
LMSC-A852007

SMALL AMPLITUDE LATERAL SLOSHING IN A CYLINDRICAL TANK WITH A HEMISPHERICAL BOTTOM UNDER LOW GRAVITATIONAL CONDITIONS

by

P. Concus, G. E. Crane, H. M. Satterlee

Prepared for
NATIONAL AERONAUTICS AND SPACE ADMINISTRATION
CONTRACT NAS 3-7119

Lockheed

MISSILES & SPACE COMPANY

A GROUP DIVISION OF LOCKHEED AIRCRAFT CORPORATION

SUNNYVALE CALIFORNIA

LMSC/A852007
NASA CR-54700

SUMMARY REPORT

SMALL AMPLITUDE LATERAL SLOSHING IN A CYLINDRICAL TANK WITH A HEMISPHERICAL BOTTOM UNDER LOW GRAVITATIONAL CONDITIONS

by

P. Concus
G. E. Crane
H. M. Satterlee

Prepared for

NATIONAL AERONAUTICS AND SPACE ADMINISTRATION
January 20, 1967
CONTRACT NAS 3-7119

Technical Management
NASA Lewis Research Center
Cleveland, Ohio

LOCKHEED MISSILES AND SPACE COMPANY
1111 Lockheed Way
Sunnyvale, California

ABSTRACT

A finite difference technique utilizing an irregular triangular mesh and the Wielandt inverse iteration method has been used to compute normal mode lateral sloshing in a cylindrical tank with a hemispherical bottom under reduced but still positive gravitational conditions for a contact angle of five (5) degrees. Results of these computations have been used to calculate, using a Fourier series expansion, the liquid response to sinusoidal, square wave and periodic-pulse lateral perturbing accelerations. Reduction of liquid volume, gravity level, and contact angle reduce the fundamental (most important) lateral sloshing frequency.

TABLE OF CONTENTS

LIST OF ILLUSTRATIONS

LIST OF TABLES

NOMENCLATURE

Variables topped by bars are dimensional quantities, those without are generally nondimensional. Underlined variables are generally vectors. Subscripted variables are either derivatives or values of the unsubscripted variable at the mesh point indicated by the subscript.

English Alphabet

a - Area of zone on free-surface divided by 2π.

A - Diagonal matrix whose entries are a_j;

- Matrix in generalized eigenvalue-vector problem;

- Area of triangle with vertices at mesh points P_1, P_2, P_3.

A_k - Coefficient of Φ_k in Fourier expansion of perturbed velocity potential.

$A_k^{(m)}$ - Coefficient of $\Phi_k \cos(m\omega_o t)$ in Fourier expansion of perturbed velocity potential.

A_1 - Coefficient of φ in approximating Φ/r^2 at vertex P_1.

B - Matrix in generalized eigenvalue-vector problem.

B_α - Axial Bond number = $\rho\, g_\alpha\, r_o^2/\sigma$.

B_τ - Transverse time-varying Bond number = $\rho g_\tau r_o^2/\sigma$.

$\hat{B}_\tau$ - Transverse Bond number based upon maximum lateral perturbing acceleration = $\rho\, \hat{g}_\tau\, r_o^2/\sigma$.

c - r-coordinate of centroid of triangle $P_1P_2P_3$.

c_{12} c_{13} - Coefficients in difference equations connecting φ_1 at P_1 to φ_2 and φ_3 at P_2 and P_3.

C - Matrix in symmetric eigenvalue-vector problem.

C_m - Coefficient of $\sin(m\omega_o t)$ in Fourier expansion of periodic perturbation.

d_i - Coefficients of φ_i in difference equation for 7-point star.

D - Interior of two-dimensional domain bounded by f, w, and the center line;

- Matrix approximating the Laplace equation in D with zero normal derivative on f and w and zero potential on the center line.

D_k - Fourier coefficient in the expansion of r in terms of Φ_k.

DL - Left triangular factor of the matrix $D(\lambda)$.

DR - Right triangular factor of the matrix $D(\lambda)$.

$D(\lambda)$ - Matrix of linear system approximating the normal mode eigenvalue-vector problem.

$D_{1,j}$
$D_{1,N}$
D_2
$D_{3,j}$ - Terms in the diagonal entries of the matrix T.

$D_{\mu\nu}$ - Submatrices of D.

$DL_{\mu\nu}$ - Submatrices of DL.

$DR_{\mu\nu}$ - Submatrices of DR.

E - Set of eigenvectors.

f - Shape of the equilibrium free-surface.

F - Arbitrary function of time in the nonsteady Bernoulli equation;
- Input ratio used in constructing the finite-difference mesh.

F_x - Maximum lateral force for kth mode.

g - $= (1+f_r^2)^{1/2}$.

g_N - Value of g at s_N.

g_α - Dimensional steady axial acceleration.

g_τ - Dimensional time-varying lateral acceleration.

$\hat{g}_\tau$ - Maximum value of g_τ.

G - Diagonal matrix with g_i as entries.

h - Sloshing perturbation of equilibrium free-surface (eigenmode);
- Maximum mesh spacing in triangular mesh.

h_k - Sloshing perturbation in kth normal mode.

h_o - Liquid depth measured along tank axis.

h_w - Maximum vertical excursion at wall.

h^* - Eigenmode of related problem.

h_{k_w} - Maximum vertical excursion at wall of kth normal eigenmode.

H - Mean curvature of free-surface.

i - Index, usually for points and values associated with mesh triangles or stars.

I_o, I_1 - Modified Bessel functions of first kind of orders zero and one.

j - Index, usually for points and values belonging to the equilibrium free-surface.

J_1 - Bessel function of first kind of order one.

k - Index, usually for functions and vectors related to kth normal mode.

K - Abbreviation for boundary condition satisfied by the equilibrium free-surface when $r_w < 1$;

- Rectangular coordinate in logical, equilateral triangular mesh;

- a large constant.

ℓ - Index for eigenmodes.

L - Left triangular factor of the matrix S;

- Rectangular coordinate in logical, equilateral triangular mesh.

$\underline{L}$ - Second order differential operator representing combined free-surface boundary conditions.

m - Index in Fourier sine expansion of perturbing function.

m_i - Vector from mid-point of side s_i to centroid of a mesh triangle.

M - Total number of mesh points.

M_y - Maximum moment of the lateral force caused by liquid sloshing in the kth normal mode.

$\mathcal{M}$ - Equivalent sloshing mass for mechanical analog for kth normal mode.

n - Denotes differentiation in exterior normal direction.

N - Number of mesh points on free-surface.

$\mathcal{N}$ - Euclidean vector norm.

p - Pressure.

p_g - Gas pressure.

p_i - Vector from mid-point of side s_i to intersection of perpendicular bisectors of a mesh triangle.

p_o - Static liquid pressure at center of equilibrium free-surface.

P_i - Mesh point viewed as a vertex of a mesh triangle.

q_{12} - r-coordinate of mid-point of side s_1 of a mesh triangle.

r - Radial coordinate.

r_o - Dimensional tank radius defined in Figure 1;
- also $r_o = r(s_o)$.

r_t - Radial coordinate of point on meridian of w.

r_w - Radius of latitude line in which f meets w.

R - Right triangular factor of the matrix S.

$\underline{R}$ - Radius vector from the origin of the tank fixed coordinate system.

s - Shape of the time varying free-surface;
- Arc length along the equilibrium free-surface.

s_i - Vector from P_i to $P_i + 1$, i=1, 2, 2 (mod 3) in a mesh triangle.

s_j - s-coordinate of mesh point of f.

s_N - s-coordinate of intersection of f with w.

s_o - s-coordinate of mesh point on f at tank axis;
- s-coordinate at which $U = K$ holds in iterative determination of f.

s_w - $s_w = s_N$.

S - Tridiagonal matrix $S = \frac{1}{2} A^{-1} T A^{-1}$.

t - Time.

t_1
t_2 - s-coordinates of mid-points of two adjacent mesh intervals.

T - Tridiagonal matrix approximating the free-surface boundary operator $\underline{L}$;
- As superscript denotes transposition;
- Period of perturbing function.

$\bar{u}$ - Radial velocity $\partial\varphi/\partial\bar{r}$.

$\underline{u}$ - Intermediate vector produced by downsweep.

$\bar{v}$ - Angular velocity $\partial\varphi/\bar{r}\partial\theta$.

V - $= 2\bar{V}/\pi(1+B_\alpha)\sigma r_o^2$;
- Coefficient in integration formula;
- Volume.

$\bar{V}$ - Maximum potential energy in kth normal mode sloshing.

w - Tank wall.

$\bar{w}$ - Vertical velocity $\partial\varphi/\partial\bar{z}$.

W - Coefficient in integration formula;

- Arbitrary function.

$W_{\mu\nu}$ - Submatrices used in the Wielandt inverse-iteration.

$\bar{x}$ - Maximum lateral displacement of the mass of the mechanical analog.

$\underline{x}$ - Arbitrary vector.

$\underline{x}^{(1)}$ - Vector of approximations to Φ for mesh points not on the free-surface or mesh line below it.

y - Pitch axis about which lateral sloshing forces operate.

$\underline{y}$ - Vector of approximations to Φ for mesh points not on free-surface.

$\underline{y}^{(1)}$ - Initially $\underline{y}^{(1)} \equiv \underline{y}$;

- Vector of approximations to Φ on the first mesh line below the free-surface.

z - Axial coordinate.

z_t - Axial coordinate of points on meridian of w .

$\underline{z}$ - Vector approximations to Φ on the free-surface.

$\underline{z}_k$ - kth and jth eigenvectors in an orthonormal (B-orthonormal) eigensystem.

$\underline{z}_j$

$\underline{z}^{(0)}$ - Initial guess for $\underline{z}$.

$\underline{z}^{(1)}$ - Improved approximation for $\underline{z}$.

Z - Lateral force action point for the mechanical analog.

Greek Alphabet

α - As subscript denotes the axial direction.

α_k - Coefficient of $\underline{z}_k$ in Fourier expansion of $\underline{z}^{(0)}$.

β - Angle between normal to tank wall and vertical.

β_k - Coefficient of $\underline{z}_k$ in Fourier expansion of $\underline{z}^{(1)}$.

δ - Ratio of periodic pulse width to half period of the perturbing acceleration.

δ_{jk} - Kronecker delta = 1 if j = k, otherwise = 0.

Δs - Mesh spacing on s.

Δt - Perturbing pulse width.

θ - Angular coordinate.

Θ - Contact angle.

$\varkappa$ - Spring constant for mechanical analog.

λ - Approximation to the eigenvalue ω^2;

- Twice the curvature of f at r = 0;

- Eigenvalue in generalized eigenvalue problem.

λ_j - Eigenvalues in an orthonormal (B-orthonormal) eigensystem.
λ_k

λ_o - Guessed value of λ in calculating f .

$\lambda^{(0)}$ - Guessed λ in Wielandt inverse-iteration.

$\lambda^{(1)}$ - Improved λ in Wielandt inverse-iteration.

μ - Number of diametrical nodes in perturbed surface;

- Integer index.

ν - Integer index.

ξ - Arc length along meridian of tank.

ξ_o - Total length of meridian tank.

ρ - Dimensional liquid density.

σ - Dimensional surface tension.

τ - As subscript denotes transverse (lateral) direction.

φ - Dimensional velocity potential.

φ_i - Approximation to Φ at the ith mesh point in a mesh triangle or star.

$\underline{\varphi}$ - Vector of approximation to Φ.

$\underline{\varphi}_n$ - Vector approximating Φ_n on f.

$\varphi_{n,j}$ - jth component of $\underline{\varphi}_n$.

$\underline{\varphi}_1$ - Vector component of $\underline{\varphi}$ for points on f.

$\underline{\varphi}_2$ - Vector component of φ for points not on f.

$\underline{\varphi}_{1,k}$ - $\underline{\varphi}_1$ corresponding to kth normal mode.

$\underline{\varphi}_{2,k}$ - $\underline{\varphi}_2$ corresponding to kth normal mode.

$\underline{\varphi}_1^{(0)}$ - Initial guess for eigenvector on f.

Φ - Dimensionless velocity potential.

Φ_k - Φ for kth normal mode.

Φ_n - $\partial\Phi/\partial n$.

Φ_k^* - Modified Φ_k to give $\bar{h}_{k_w}$ as vertical excursion at r_w.

Ψ_k - Normalization factor for Φ_k^*;

- Eigenvector in orthonormal (B-orthonormal) eigensystem.

$\Psi_k(r)$ - $= \omega_k h_k(r)$.

ω - Frequency;

- ω^2 is eigenvalue for normal mode sloshing corresponding to Φ.

ω_k - ω_k^2 is eigenvalue for normal mode sloshing corrpsponding to Φ_k.

ω_o - Circular frequency of periodic perturbing functions.

$\underline{\Omega}$ - Angular rotation rate of tank-fixed coordinate system.

SUMMARY

Lateral sloshing of liquids in a cylindrical tank with a hemispherical bottom under reduced but positive gravitational conditions for various tank fill volumes has been analyzed for both normal mode oscillations and forced oscillations produced by sinusoidal, square wave, and periodic pulse lateral perturbing accelerations. Calculated results are limited to a constant contact angle condition of 5 degrees. The range of gravitational conditions considered is limited to cases in which the dimensionless Bond number $B_\alpha = \rho g_\alpha r_o^2/\sigma$ (ρ , g_α, r_o and σ being the liquid density, steady axial gravitational body force per unit mass, tank radius and surface tension) ranges from zero to 50. The liquid volume is varied so that the centerline depth, between the liquid meniscus and the tank bottom, ranges from 0.1 to $3 r_o$.

Normal modes are calculated by finite-difference methods. Difference equations are constructed on an irregular triangular mesh; and eigenvalues and eigenfunctions are obtained by the Wielandt inverse-iteration technique. The response to the specified periodic lateral perturbing accelerations is calculated by a finite Fourier analysis utilizing results of the normal mode calculations.

General conclusions include: (a) The fundamental sloshing frequency is low-

ered by reducing liquid volume, axial gravitational body force, and the contact angle. (b) The computation of the response to lateral perturbing accelerations is easily effected by the method used; but engineering sloshing computations are more readily made with the aid of an equivalent spring-mass mechanical analog. Mechanical analog parameters have therefore been computed, and those for the first normal sloshing mode are presented. These are adequate for engineering computations when the first term is dominant in the Fourier series for forced liquid motion. (c) The irregular-triangular, finite-difference, Wielandt inverse-iteration scheme appears adquate for this type of problem when currently available digital computers are fully utilized.

INTRODUCTION

The oscillation of bodies of liquids has been of interest to scientists and mathematicians for over one-hundred years (See references given by Lamb[1]*). In the recent past, this subject has been of special importance to the designers of rocket propelled space vehicles because liquids comprise a large percentage of the total mass. The oscillation of liquids in rocket propellant tanks imposes reaction forces on the tank walls which are important in the design of guidance, control, and propulsion systems. This problem has been thoroughly studied and there now exists a large literature about sloshing under conditions when surface tension is not important. The bulk of currently available analysis of sloshing is limited to small amplitude analysis and has until recently[2,3] avoided complications arising from surface tension effects such as the curvature of the equilibrium surface. Up to date examples of conventional sloshing literature include the work of Moiseev[4] and Abramson[5].

The technical objective of this study is to extend calculation of linear sloshing to cases where the effective gravitational acceleration acting on the liquid is so small that surface tension effects become important.

* Reference numbers are superscripted in parentheses.

Specific objectives of this study include (a) determination of natural frequencies of liquids in cylindrical tanks with hemispherical bottoms as affected by the level of steady axial acceleration, surface tension and density properties of the liquid, and the volume of liquid in the tank; and (b) determination of the response of liquids to lateral perturbing accelerations.

The linear analysis used here does not treat large amplitude effects; results must be cautiously interpreted for finite amplitude. It has been shown[2,5] that the resonant sloshing frequency of a liquid of moderate viscosity is acceptably close to the first normal mode sloshing frequency obtained from inviscid analysis, even in small scale experiments. Hence, viscosity is neglected. It is also assumed that surface tension, density, and wetting properties are constant and do not vary dynamically.

Analysis for this study uses a frame of reference fixed to the container. This is shown in Figure 1. A space vehicle acted upon by a lateral perturbing force will be translated laterally and rotated relative to an external fixed coordinate system. The liquid contained in the tank will not be directly acted upon by the lateral force but, rather, indirectly acted upon by the moving walls of the tank. From an analytic viewpoint, it is more convenient to consider the tank fixed. When a transformation is effected from the fixed coordinate system to the coordinate system moving with the tank, the liquid can be considered as being

influenced directly by lateral perturbing accelerations relative to a tank fixed with respect to the moving coordinate system.

The mathematical problem attacked in this study takes the form of a linear boundary value problem. Basic assumptions are that the liquid is incompressible, inviscid, and its motion irrotational. Solution of this problem involves obtaining solutions to Laplace's equation in the interior of the liquid subject to a zero normal-velocity boundary condition at solid walls and a condition on the free-surface derived from the non-steady state Bernoulli equation. The problem is posed completely by the following set of equations in dimensionless form:

$$\Phi_{rr} + \frac{1}{r}\Phi_r + \frac{1}{r^2}\Phi_{\theta\theta} + \Phi_{zz} = 0 \quad \text{in} \quad D \,, \tag{1}$$

$$\Phi_n = 0 \quad \text{on} \; w \,, \tag{2}$$

$$\frac{1}{r}\frac{\partial}{\partial r}\frac{rh_r}{(1+f_r^2)^{3/2}} + \frac{1}{r^2}\frac{h_{\theta\theta}}{(1+f_r^2)^{1/2}} - B_\alpha h + B_\tau r\cos\theta - (1+B_\alpha)\Phi_t = 0 \quad \text{on} \quad f \,, \tag{3}$$

$$h_t = \Phi_z - f_r\Phi_r = (1+f_r^2)^{1/2}\Phi_n \quad \text{on} \quad f \,, \text{ and} \tag{4}$$

$$\left.\begin{aligned} &h_r = 0 \text{ at } r = r_w \text{ if } r_w = 1 \,, \text{ or} \\ &h_r = (1+f_r^2)^{1/2}\left[(1-r_w^2)^{1/2}\cos\Theta + r_w\sin\Theta\right]\frac{h}{r_w} \text{ at } r = r_w \\ &\text{if } r_w < 1 \,. \end{aligned}\right\} \tag{5}$$

The first two terms of Equation (3) contain the effect of surface tension and the fourth contains the effect of lateral perturbing accelerations. In this analysis it is assumed that the contact angle is constant, hence the end conditions on h_r given by Equation (5).

Solution of the problem just posed falls into two parts. First, eigenvalues and eigenfunctions of the normal mode sloshing problem are obtained for the case when the perturbing accelerations are zero. Second, the functions thus obtained are used to expand the periodic time history of the perturbing accelerations in a Fourier series.

Several schemes were briefly considered for obtaining numerical solutions to the problem. Among these one involves construction of the velocity potential as a series of the product-type solutions obtained by separating variables in Laplace's equation. Boundary conditions are satisfied by a least-squares collocation method[6]--that is, the boundary conditions are applied at a number of points on the boundary larger than the number of terms in the series used; and the set of equations thus obtained is solved in the least-squares sense. Alternatively, finite-difference techniques offer more promise of accuracy, particularly when the contact angle is small. Other investigators[7] have experienced numerical difficulties in obtaining satisfactory convergence for the series expansion in the same type of problem. Further, the use of an irregular-triangular, finite-difference mesh offers significant advantages. First, the mesh is

space-filling; no difficulties are encountered in applying boundary conditions at places where the boundary intersects mesh lines. Second, the mesh can be constructed so as to facilitate obtaining accurate representation of the boundary conditions.

PROBLEM FORMULATION

The purpose of this section is to detail the derivation of the boundary conditions peculiar to this problem. The assumptions used in this analysis are that the liquid is incompressible, inviscid, and that it behaves irrotationally. This allows application of the nonsteady state Bernoulli equation to the free-surface

$$\frac{p}{\rho} + \frac{1}{2}\left|\underline{\nabla}\,\varphi - \underline{\Omega}\times\underline{\bar{R}}\right|^2 + g_\alpha(\bar{f}+\bar{h}) - g_\tau \bar{r}\cos\theta + \varphi_{\bar{t}} + \frac{1}{2}\,(\underline{\Omega}\cdot\underline{\bar{R}})^2 - \frac{1}{2}\,|\underline{\Omega}|^2|\underline{\bar{R}}|^2 = F(\bar{t})\,, \tag{6}$$

where φ is the velocity potential defined by

$$\left.\begin{aligned} \bar{u} &= \varphi_{\bar{r}}\,, \\ \bar{v} &= \frac{1}{\bar{r}}\,\varphi_\theta\,, \quad \text{and} \\ \bar{w} &= \varphi_{\bar{z}}\,. \end{aligned}\right\} \tag{7}$$

The choice of the function of time on the right hand side of this equation is arbitrary and, for convenience, is set equal to p_o/ρ, the static liquid pressure at the center of the equilibrium meniscus divided by the liquid density. The liquid pressure at the interface is related to the gas pressure through the surface-tension and the mean curvature of the free-

surface by means of the equation

$$p_g - p = 2\sigma H = \sigma \left\{ \frac{1}{\bar{r}} \frac{\partial}{\partial \bar{r}} \frac{\bar{r}\bar{s}_{\bar{r}}}{\left(1 + \bar{s}_{\bar{r}}^2 + \frac{1}{\bar{r}^2}\bar{s}_\theta^2\right)^{1/2}} + \frac{1}{\bar{r}^2} \frac{\partial}{\partial \theta} \frac{\bar{s}_\theta}{\left(1 + \bar{s}_{\bar{r}}^2 + \frac{1}{\bar{r}^2}\bar{s}_\theta^2\right)^{1/2}} \right\} . \tag{8}$$

Substitution of this relation and p_o/ρ for $F(\bar{t})$ into equation (6) results in

$$\frac{\sigma}{\rho} 2H - \frac{1}{2}\left|\underline{\nabla} \varphi - \underline{\Omega}\times\underline{\bar{R}}\right|^2 - g_\alpha(\bar{f}+\bar{h}) + g_\tau \bar{r} \cos\theta - \varphi_{\bar{t}}$$

$$- \frac{1}{2}(\underline{\Omega} \cdot \underline{\bar{R}})^2 - \frac{1}{2}|\underline{\Omega}|^2|\underline{\bar{R}}|^2 = \frac{p_g - p_o}{\rho} . \tag{9}$$

The kinematic condition is derived as follows. Consider $\bar{s} = \bar{s}(\bar{r}, \theta, \bar{t})$. The total derivative of $\bar{s}$ with respect to time is written

$$\frac{d\bar{s}}{d\bar{t}} = \bar{s}_{\bar{t}} + \bar{s}_{\bar{r}} \frac{d\bar{r}}{d\bar{t}} + \frac{1}{\bar{r}^2} \bar{s}_\theta \frac{d\theta}{d\bar{t}} .$$

Use of the definition of the velocity potential results in the following familiar form for the kinematic condition

$$\bar{s}_{\bar{t}} = \varphi_{\bar{z}} - \varphi_{\bar{r}} \bar{s}_{\bar{r}} - \frac{1}{\bar{r}^2} \varphi_\theta \bar{s}_\theta . \tag{10}$$

The non linearities of the problem appear in the free-surface boundary conditions, Equations (9) and (10). These can be linearized by assuming

that the free-surface is the sum of an axisymmetric equilibrium surface $\bar{f}$ and a small time-varying perturbation $\bar{h}$,

$$\bar{s}(r, \theta, \bar{t}) = \bar{f}(\bar{r}) + \bar{h}(\bar{r}, \theta, \bar{t}) . \tag{11}$$

Substituting this into Equation (9) and neglecting the $O(\bar{h}^2)$ terms (all angular velocity terms are of this order) yield

$$\frac{\sigma}{\rho}\left\{ \frac{1}{\bar{r}} \frac{\partial}{\partial \bar{r}} \frac{\bar{r}\bar{f}_{\bar{r}}}{\left(1 + \bar{f}_{\bar{r}}^2\right)^{1/2}} + \frac{1}{\bar{r}} \frac{\partial}{\partial \bar{r}} \frac{\bar{r}\bar{h}_{\bar{r}}}{\left(1 + \bar{f}_{\bar{r}}^2\right)^{3/2}} + \frac{1}{\bar{r}^2} \frac{\bar{h}_{\theta\theta}}{\left(1 + \bar{f}_{\bar{r}}^2\right)^{1/2}} \right\}$$

$$-g_\alpha \bar{f} - g_\alpha \bar{h} + g_\tau \bar{r} \cos\theta - \varphi_{\bar{t}} - \frac{p_g - p_o}{\sigma} = 0 .$$

The first, fourth, and last terms sum to zero; they form the equation of the equilibrium surface

$$\frac{\sigma}{\rho} \frac{1}{\bar{r}} \frac{d}{d\bar{r}} \frac{\bar{r}\bar{f}_{\bar{r}}}{\left(1 + \bar{f}_{\bar{r}}^2\right)^{1/2}} - g_\alpha \bar{f} - \frac{p_g - p_o}{\sigma} = 0 . \tag{12}$$

With these deleted, the linearized free-surface condition becomes

$$\frac{\sigma}{\rho}\left\{ \frac{1}{\bar{r}} \frac{\partial}{\partial \bar{r}} \frac{\bar{r}\bar{h}_{\bar{r}}}{\left(1 + \bar{f}_{\bar{r}}^2\right)^{3/2}} + \frac{1}{\bar{r}^2} \frac{\bar{h}_{\theta\theta}}{\left(1 + \bar{f}_{\bar{r}}^2\right)^{1/2}} \right\} - g_\alpha \bar{h}$$

$$+ g_\tau \bar{r} \cos\theta - \varphi_{\bar{t}} = 0 . \tag{13}$$

Substituting Equation (11) into Equation (10) and linearizing give the kinematic condition in the form

$$\bar{h}_{\bar{t}} = \varphi_{\bar{z}} - \varphi_{\bar{r}} \frac{d\bar{f}}{d\bar{r}} \quad . \tag{14}$$

Formulation of the problem is completed by nondimensionalization with the use of the following definitions

$$\left.\begin{aligned} r &= \frac{\bar{r}}{r_o}, \quad z = \frac{\bar{z}}{r_o}, \quad s = \frac{\bar{s}}{r_o}, \quad f = \frac{\bar{f}}{r_o}, \quad h = \frac{\bar{h}}{r_o}, \\ t &= \bar{t}\left((1 + B_\alpha)\frac{\sigma}{\rho r_o^3}\right)^{1/2}, \quad \Phi = \frac{\varphi}{\left((1 + B_\alpha)\frac{\sigma r_o}{\rho}\right)^{1/2}}, \\ B_\alpha &= \frac{\rho g_\alpha r_o^2}{\sigma}, \quad B_\tau = \frac{\rho g_\tau r_o^2}{\sigma} . \end{aligned}\right\} \tag{15}$$

Introducing Equations (15) yields the problem statment given in the Introduction:

$$\Phi_{rr} + \frac{1}{r}\Phi_r + \frac{1}{r^2}\Phi_{\theta\theta} + \Phi_{zz} = 0 \quad \text{in} \quad D \ , \tag{1}$$

$$\Phi_n = 0 \quad \text{on} \quad w \ , \tag{2}$$

$$\frac{1}{r}\frac{\partial}{\partial r}\frac{rh_r}{\sqrt{1 + f_r^2}^3} + \frac{1}{r^2}\frac{h_{\theta\theta}}{\sqrt{1 + f_r^2}} - B_\alpha h + B_\tau r\cos\theta - (1 + B_\alpha)\Phi_t = 0 \quad \text{on} \quad f \ , \tag{3}$$

$$h_t = \Phi_z - f_r \Phi_r \quad \text{on} \quad f \text{ , and} \tag{4}$$

$$\left.\begin{aligned} &h_r = 0 \quad \text{at } r = r_w \quad \text{if } r_w = 1 \text{ , or} \\ &h_r = (1 + f_r^2)^{1/2} \left[(1 - r_w^2)^{1/2} \cos\Theta + r_w \sin\Theta \right] \frac{h}{r_w} \text{ at } r = r_w \\ &\text{if } r_w < 1 \text{ .} \end{aligned}\right\} \tag{5}$$

with the equilibrium surface defined by the following equation and boundary conditions

$$\frac{1}{r}\frac{d}{dr}\frac{rf_r}{\sqrt{1 + f_r^2}} - B_\alpha f - \lambda = 0 \text{ ,} \tag{16}$$

$$\left.\begin{aligned} &\frac{df}{dr} = 0 \quad \text{at} \quad r = 0 \text{ ,} \qquad \text{and} \\ &\frac{df}{dr} = (1 + f_r^2)^{1/2} \left[r_w \cos\Theta - (1 - r_w^2)^{1/2} \sin\Theta \right] \text{at } r = r_w \text{ .} \end{aligned}\right\} \tag{17}$$

Here λ is a parameter related to the pressure difference across the vertex of the equilibrium surface located at the origin.

In the foregoing, it is assumed that $B_\alpha \geq 0$. Oscillation can take place for $B_\alpha < 0$, but only for small values of $|B_\alpha|$ beyond which the surface becomes unstable. This region is not considered in this study.

The problem posed by Equations (1) - (5) and (16) and (17) is a linear boundary value problem. Equation (3) is

inhomogeneous. The implication is that the solution can be obtained in two parts. The problem is first made homogeneous by setting B_T to zero and solving the normal mode problem. The result of this is a set of eigenfunctions which is then used in a Fourier series expansion to obtain the response to transverse perturbing accelerations.

Normal Mode Problem

Let the periodic time dependence and the angular dependence of φ and h for the kth normal mode be

$$\Phi = \Phi_k (r, z) \cos\theta \cos\omega_k t$$

$$h = h_k (r) \cos\theta \sin\omega_k t \ .$$

When these expressions are substituted into Equation (3) with $B_T = 0$ and Equation (4), there follows

$$\left.\begin{aligned} &(1 + B_\alpha)\omega_k\Phi_k - B_\alpha h_k + \frac{1}{r}\frac{\partial}{\partial r}\frac{rh_{k_r}}{\left(1 + f_r^2\right)^{3/2}} - \frac{1}{r^2}\frac{h_k}{\left(1 + f_r^2\right)^{1/2}} = 0 \\ &\omega_k h_k = \Phi_{k_z} - f_r \Phi_{k_r} = \left(1 + f_r^2\right)^{1/2} \Phi_{k_n} \end{aligned}\right\} z = f(r) \quad (18)$$

The boundary conditions on h_k and Φ_k are the one on h in Equation (5) and

$$h_k(0) = 0, \quad \Phi_{k_n} = 0 \quad \text{on} \quad \underline{w} \ , \text{ and } \quad \Phi_k(0,z) = 0 \ . \tag{19}$$

Solution of this problem yields a set of eigenfunctions $\{\Phi_k\}$, eigenvalues $\{\omega_k^2\}$, and eigenmodes $\{h_k\}$. The method used in this study to obtain these quantities is detailed in the next part of this report.

Response to Perturbing Accelerations

Fourier Series Expansions: For a sinusoidal perturbation of amplitude $\hat{B}_\tau$,

$$B_\tau = \hat{B}_\tau \sin \omega_o t \ ,$$

the velocity potential of the perturbed motion can be represented as a Fourier series

$$\Phi = \cos \theta \cos \omega_o t \sum_k A_k \Phi_k(r, z) \tag{20}$$

where the solution to the normal mode problem, $\Phi_k(r, z)$, satisfies Equations (18) and (19), but not (3) and (4). Inserting the series into Equations (3) and (4), the free surface and kinematic boundary conditions for the perturbed motion, and combining the results lead to

$$(1 + B_\alpha) \sum_k (\omega_k^2 - \omega_o^2) A_k \Phi_k = \hat{B}_\tau \omega_o r \quad \text{on} \quad z = f(r) \ .$$

Now, r can be expressed as an expansion in Φ_k evaluated on $z = f(r)$,

$$r = \sum_k D_k \Phi_k[r, f(r)] \ . \tag{21}$$

The Φ_k's and corresponding h_k's form a biorthogonal set with the orthogonality condition[8]

$$\int_o^{r_w} r\, \Phi_k\, h_\ell\, dr \begin{cases} = 0 & \text{for } k \neq \ell\,, \\ \neq 0 & \text{for } k = \ell\,. \end{cases} \tag{22}$$

Use of this in Equation (21) yields an expression for the Fourier coefficient

$$D_k = \frac{\int_o^{r_w} h_k\, r^2 dr}{\int_o^{r_w} \Phi_k\, h_k\, r dr}\,. \tag{23}$$

Thus, the solution for A_k for sinusoidal excitation is

$$A_k = \frac{1}{(1 + B_\alpha)} \frac{\hat{B}_\tau\, D_k\, \omega_o}{\omega_k^2 - \omega_o^2} \tag{24}$$

so that the velocity potential for the sinusoidally perturbed motion becomes

$$\Phi = \frac{\hat{B}_\tau \cos\theta \cos\omega_o t}{1 + B_\alpha} \sum_k \frac{D_k\, \omega_o}{\omega_k^2 - \omega_o^2}\, \Phi_k\,(r, z)\,. \tag{25}$$

The procedure for obtaining the solution for any periodic perturbation that possesses a Fourier series expansion of the form

$$B_\tau = \hat{B}_\tau \sum_m C_m \sin(m\omega_o t)$$

is similar. The solution is

$$\Phi = \cos\theta \sum_k \Phi_k\,(r, z) \sum_m A_k^{(m)} \cos(m\omega_o t) \tag{26}$$

where

$$A_k^{(m)} = \frac{D_k\, \hat{B}_\tau}{(1 + B_\alpha)} \frac{m\, C_m\, \omega_o}{\omega_k^2 - m^2\omega_o^2}\,.$$

Particular perturbations of interest are the square wave and the periodic pulsing accelerations. The coefficients D_k are computed from Equation (23) and the C_m's are obtained by the expanding the perturbing acceleration function in a Fourier series. The C_m's for square wave and periodic pulse perturbations of amplitude $\hat{B}_\tau$ (see Figure 11) are as follows.

Square wave:

$$C_m = \begin{cases} 0 , & m \text{ even} , \\ \dfrac{4}{m\pi} , & m \text{ odd} ; \end{cases}$$

Periodic Pulse:

$$C_m = \begin{cases} 0 , & m \text{ even} , \\ \dfrac{4}{m\pi} (-1)^{\frac{m-1}{2}} \sin \dfrac{m\delta\pi}{2} , & m \text{ odd} , \end{cases}$$

where δ is the ratio of Δt to $\frac{1}{2}T = \pi/\omega_o$, the ratio of the perturbing pulse width to half the period of the perturbing function.

Use of these gives the following solutions for the velocity potential.

Square wave:

$$\Phi = \frac{\hat{B}_\tau \cos\theta}{1 + B_\alpha} \sum_{k=1}^{\infty} \frac{D_k \Phi_k}{\pi} \sum_{\substack{m=1 \\ m \text{ odd}}}^{\infty} \frac{4\omega_o \cos(m\omega_o t)}{\omega_k^2 - m^2\omega_o^2} \qquad (27)$$

Periodic Pulse:

$$\Phi = \frac{\hat{B}_\tau \cos\theta}{1 + B_\alpha} \sum_{k=1}^{\infty} \frac{D_k \Phi_k}{\pi} \sum_{\substack{m=1 \\ m \text{ odd}}}^{\infty} \frac{4\omega_o (-1)^{\frac{m-1}{2}} \sin \frac{m\delta\pi}{2} \cos(m\omega_o t)}{\omega_k^2 - m^2\omega_o^2} \qquad (28)$$

Most interest, however, is centered on the vertical rise of the liquid at the wall when perturbed by lateral accelerations. The basis for the calculation is, of course, the kinematic condition, Equation (4). Use of this together with the velocity potentials for sinusoidal, square wave, and periodic pulse lateral perturbing accelerations yields the following.

Sinusoidal:

$$h\Big]_{\substack{\theta=0\\ r=r_w}} = \frac{\hat{B}_\tau(1+f_r^2)^{1/2}}{1+B_\alpha} \sin\omega_o t \sum_{k=1}^{\infty} \frac{D_k}{\omega_k^2 - \omega_o^2} \Phi_{k_n}\Big]_{\substack{z=f(r)\\ r=r_w}} \quad (29)$$

Square wave:

$$h\Big]_{\substack{\theta=0\\ r=r_w}} = \frac{\hat{B}_\tau(1+f_r^2)^{1/2}}{1+B_\alpha} \frac{4}{\pi} \sum_{k=1}^{\infty} D_k\Big[\sum_{\substack{m=1\\ m\ \text{odd}}}^{\infty} \frac{\sin(m\omega_o t)}{m(\omega_k^2 - m^2\omega_o^2)}\Big] \Phi_{k_n}\Big]_{\substack{z=f(r)\\ r=r_w}} \quad (30)$$

Periodic Pulse:

$$h\Big]_{\substack{\theta=0\\ r=r_w}} = \frac{\hat{B}_\tau(1+f_r^2)^{1/2}}{1+B_\alpha} \frac{4}{\pi} \sum_{k=1}^{\infty} D_k\Big[\sum_{\substack{m=1\\ m\ \text{odd}}}^{\infty} \frac{(-1)^{\frac{m-1}{2}} \sin\frac{m\delta\pi}{2} \sin(m\omega_o t)}{m(\omega_k^2 - m^2\omega_o^2)}\Big] \Phi_{k_n}\Big]_{\substack{z=f(r)\\ r=r_w}} \quad (31)$$

A Simpler Approximation: Calculations using the techniques just described can, in general, be used to compute, with the aid of the tabulated results of this study, the response of liquids in cylindrical tanks with hemispherical bottoms to any periodic lateral perturbing acceleration

with period $T = 2\pi/\omega_o$. It is often desirable, however, to treat dynamic problems in a simpler way. The normal mode calculations to be described in the next part of this report can be used to compute parameters of an equivalent mechanical analog with which approximate dynamic computations can be made with somewhat less effort. The theoretical basis for this is outlined below.

The pressure in a liquid which is sloshing in a container can be computed from a knowledge of the velocity potential using the nonsteady state Bernoulli equation (Equation (6)) and the relation for the pressure difference across the free surface (Equation (8)). It may be shown that the pressure within the liquid consistent with the limitations of the linearization of the lateral sloshing problem is given by

$$\frac{p}{\rho} = \frac{p_g}{\rho} + g_\alpha \bar{f} - \frac{\sigma}{\rho}\,\frac{1}{\bar{r}}\,\frac{\partial}{\partial \bar{r}}\,\frac{\bar{r}\bar{f}_{\bar{r}}}{\left(1+\bar{f}_{\bar{r}}^{\,2}\right)^{1/2}} - g_\alpha \bar{z} - \frac{\partial \varphi}{\partial \bar{t}} \qquad (32)$$

The first four terms on the right in this equation represent the contributions due to surface tension and gravitational body forces, second and fourth are merely the hydrostatic head, and the third appears only if surface tension effects are considered. The last term in this equation is the contribution due to sloshing of the liquid. The first four terms will contribute nothing to lateral forces on the tank since they represent the static equilibrium balance, only.

Equation (32) can be used to determine the lateral force acting on the tank due to k-th normal mode sloshing from the velocity potential $\Phi_k(r,z) \cos\theta \cos\omega_k t$. Using the notation of Figure 1, the lateral force due to the k-th mode is given by

$$\int_0^{2\pi} \int_{\bar{\xi}=0}^{\bar{\xi}=\bar{\xi}_0} p \sin\beta \cos\theta \, \bar{r}_t \, d\bar{\xi} \, d\theta$$

and its maximal value is

$$\bar{F}_x = \pi \bar{\omega}_k \int_0^{\bar{\xi}_0} \rho \Phi_k(\bar{r}_t, \bar{z}_t) \, \bar{r}_t \sin\beta \, d\bar{\xi} \, . \tag{33}$$

The expression, obtained in a similar fashion, for the maximum moment of the lateral forces generated by the k-th normal mode is

$$\bar{M}_y = \pi \bar{\omega}_k \int_0^{\bar{\xi}_0} \rho \Phi_k(\bar{r}_t, \bar{z}_t) \, \bar{r}_t \, \bar{z}_t \sin\beta \, d\bar{\xi} \, . \tag{34}$$

The ratio of $\bar{M}_y$ to $\bar{F}_x$ is, of course, the point of action, $\bar{Z}$, of a single force on the axis which can be substituted for the integral of the lateral component of pressure forces acting on the tank.

The quantities just calculated can be related to parameters of an equivalent spring-mass oscillator as follows. The maximum force imposed by an oscillator and the maximum potential energy stored are given by

$$\bar{F}_x = \bar{\kappa} \bar{x}$$

and

$$\bar{V} = \frac{\bar{\kappa}}{2} \bar{x}^2 \tag{35}$$

where $\bar{x}$ is the maximum displacement. Elimination of the parameter $\bar{x}$ results in a formula for the spring constant as a function of the maximum lateral force and potential energy stored in the system

$$\bar{\kappa} = \frac{\bar{F}_x^2}{2\bar{V}} . \tag{36}$$

This constant can be calculated by use of the integral

$$\bar{V} = \frac{\pi\rho}{2}\int_o^{\bar{r}_w} \Phi_k(\bar{r},\bar{z}) \frac{\partial}{\partial n} \Phi_k(\bar{r},\bar{z})(1+\bar{f}_{\bar{r}}^2)^{1/2}\, \bar{r}d\bar{r} \tag{37}$$

taken over a meridian of the equilibrium free surface.

The magnitude of the mass to be substituted for the liquid sloshing in the k-th mode is obtained by dividing the spring constant by the square of the appropriate frequency.

$$\bar{\mathcal{M}} = \frac{\bar{F}_x^2}{2\bar{\omega}_k^2 \bar{V}} \tag{38}$$

For convenience in making calculations, these expressions can be non-dimensionalized with the use of Equation (15). The mechanical analog parameters equivalent to k-th normal mode sloshing are as follows.

Maximum lateral force:

$$F_x = \frac{\bar{F}_x}{\sigma r_o} = \pi(1+B_\alpha)\omega_k \int_o^{\xi_o} \Phi_k(r_t, z_t)\, r_t \sin\beta\, d\xi \tag{39}$$

Maximum moment:

$$M_y = \frac{\bar{M}_y}{\sigma r_o^2} = \pi(1+B_\alpha)\omega_k \int_o^{\xi_o} \Phi_k(r_t, z_t)\, r_t\, z_t \sin\beta\, d\xi \quad . \quad (40)$$

Lateral force action point:

$$Z = \frac{\bar{Z}}{r_o} = \frac{M_y}{F_x} \quad (41)$$

Equivalent spring constant:

$$\kappa = \frac{\bar{\kappa}}{\sigma} = \frac{\pi(1+B_\alpha)\omega_k^2 \left[\int_o^{\xi_o} \Phi_k(r_t, z_t) r_t \sin\beta\, d\xi\right]^2}{V} \quad (42)$$

Equivalent sloshing mass:

$$\mathcal{M} = \frac{\bar{\mathcal{M}}}{\rho r_o^3} = \frac{\pi\left[\int_o^{\xi_o} \Phi_k(r_t, z_t) r_t \sin\beta\, d\xi\right]^2}{V} \quad (43)$$

where V is given by

$$V = \int_o^{r_w} \Phi_k(r,z) \frac{\partial \Phi_k(r,z)}{\partial n} (1+f_r^2)^{1/2}\, rdr$$

the integral being taken over a meridian of the equilibrium free-surface.

The quantities Z, $\varkappa$ and $\mathcal{M}$ are homogeneous in Φ_k and therefore independent of the amplitude of the eigenfunction; however, F_x and M_y depend linearly upon the amplitude. From these facts, the displacement history of an equivalent mechanical analog of kth mode sloshing can be computed as the solution of a dynamics problem that is much simpler than determining the motion of the liquid. The procedure is to compute an equivalent spring constant and sloshing mass from Equations (42) and (43). These can be used in the simple, spring-mass dynamical model shown in Figure 1 and the excursion $\bar{x}$ produced by a lateral perturbing acceleration computed. The maximum value of $\bar{x}$ can be inserted into the first of Equations (35) to establish the maximum lateral force. The maximum vertical excursion at the wall of the kth mode wave, $\bar{h}_{k_w}$, can be determined by modifying the amplitude of the eigenfunction Φ_k in Equation (39). In fact, replacing Φ_k by

$$\Phi_k^* = \frac{\omega_k \bar{h}_{k_w}}{r_o \Psi_k} \Phi_k$$

with

$$\Psi_k = \left[(1+f_r^2)^{1/2} \frac{\partial \Phi_k}{\partial n} \right]_{\substack{z=f(r) \\ r=r_w}}$$

gives a normalization in which the vertical excursion at the wall is $\bar{h}_{k_w}$. Consequently, $\bar{h}_{k_w}$ can be determined from

$$\frac{\bar{F}_x}{\sigma \bar{h}_{k_w}} = \frac{\pi(1+B_\alpha)\omega_k^2}{\Psi_k} \int_0^{\xi_o} \Phi_k(r_t, z_t) r_t \sin \beta \, d\xi \, . \qquad (44)$$

The corresponding moment and action point are determined from

$$\frac{\bar{M}_y}{\sigma r_o \bar{h}_{k_w}} = \frac{\pi(1+B_\alpha)\omega_k^2}{\Psi_k} \int_0^{\xi_o} \Phi_k(r_t, z_t) r_t z_t \sin \beta \, d\xi \qquad (45)$$

and Equation (41).

NUMERICAL ANALYSIS

Choice of Method

Computational Formulation of the Problem. Introducing

$$\left.\begin{aligned} \Phi &= \phi(r,z)\cos\mu\theta\cos\omega t\ , \\ h &= h(r)\cos\mu\theta\sin\omega t\ , \\ &\text{and} \\ B_\tau &= 0 \end{aligned}\right\} \tag{46}$$

in (1) - (5), setting $B_\alpha \geq 0$, and combining the two free-surface equations into a single one by eliminating h yield the well-posed eigenvalue-function problems:

$$-\left(\phi_{rr} + \frac{1}{r}\phi_r + \phi_{zz}\right) + \frac{\mu^2}{r^2}\phi = 0 \quad \text{in} \quad D\ , \tag{47}$$

$$\phi_n = 0 \quad \text{on} \quad w\ , \text{ and} \tag{48}$$

$$\frac{1}{1+B_\alpha}\left(-\frac{1}{r}\frac{\partial}{\partial r}\left[\frac{r}{g^3}\frac{\partial}{\partial r}(g\phi_n)\right] + \left(B_\alpha g + \frac{\mu^2}{r^2}\right)\phi_n\right)$$

$$-\omega^2\phi = 0 \quad \text{on} \quad f \tag{49}$$

with the boundary conditions

$$\phi_n = 0 \quad \text{for} \quad \mu \quad \text{odd} \quad \text{or} \quad \frac{\partial}{\partial r}(g\phi_n) = 0 \quad \text{for} \quad \mu \quad \text{even} \tag{50}$$

at $r = 0$ and either

$$\frac{\partial}{\partial r}(g\phi_n) = 0 \quad \text{at} \quad r = 1 \tag{51}$$

when the equilibrium free-surface intersects the wall in the cylinder or

$$\frac{\partial}{\partial s}(g\Phi_n) = \left[(1 - r_w^2)^{1/2} \cos\Theta + r_w \sin\Theta\right] g\Phi_n / r_w \qquad (52)$$

at $r = r_w$ when the intersection lies in the hemisphere. Here s denotes arc length on f. The special case in which the equilibrium free-surface, the cylinder, and the hemisphere have a common point is not covered in this formulation.

Because the boundary condition (50) holds, the second order differential operator, say $\underline{L}$, acting on Φ_n in (49), including the boundary conditions (50) and (51) or (52), is invertible when μ and B_α are not both zero, that is,

$$\Phi_n = \underline{L}^{-1}(\omega^2 \Phi) \quad \text{on} \quad f. \qquad (53)$$

From the circular and angular symmetry of (46), (47), and (48),

$$\Phi(0, z) = 0 \qquad \text{for} \quad \mu \quad \text{odd} \qquad (54)$$

and

$$\Phi_r(0, z) = 0 \qquad \text{for} \quad \mu \quad \text{even} \qquad (55)$$

are the boundary conditions on the axis, $r = 0$.

Note that the introduction of (46), removes the θ-dependence from (47) and (48); nevertheless, the solution $\Phi(r, z)$ may be viewed as circularly symmetric in three dimensions because it is a function of only r and z -- this approach aids in understanding the finite difference formulation to follow.

The discussion is now restricted to the case of particular engineering interest, namely $\mu = 1$, in which the eigenmodes have a single diametral node and vibrate in an anti-symmetric manner. Mathematically the problem is a mixed boundary value problem for the eigenvalue-function pairs $[\omega, \Phi]$ that satisfy the potential equation (47) within the liquid subject to prescribed values along the axis (54) and to normal derivative boundary conditions on the wall (48) and on the equilibrium free-surface (53).

The range of parameters for which the solutions to the problem are required include, at least, the intervals

$$0 \leq B_\alpha \leq 50 \text{ , for axial Bond numbers ,}$$

and

$$0.1 \leq h_o \leq 3 \text{ , for center depths.}$$

Even for a fixed contact angle ($\Theta = 5$ degrees is used in most of the calculations), the domains D vary widely in shape: some resemble puddles in the center of the hemisphere, some half-filled test tubes, some thin crescents covering most of the hemispherical surface, some have a hemispherical free-surface, some a nearly flat surface with a pronounced meniscus. In view of the variety of shapes involved and experience with similar problems with a limited range of shapes, it seems unlikely that any reasonable linear combination of known special functions or harmonic polynomials could be made to satisfy both the potential equation and the boundary conditions efficiently for such a variety of domains.

On the other hand, the system determining the eigenvalue-function pairs

$[\omega, \Phi]$ is of a form suitable for solution by finite difference methods provided that an adequate mesh can be generated for each domain.

The Mesh. Viewing the mesh, which is two-dimensional, as circularly symmetric in three dimensions gives directly an insight into the correct normalization of the difference equations: each linear element must be rotated about the axis to generate a conical zone and each area must be rotated to generate a volume. The constant π will be removed from each equation.

A suitable two-dimensional mesh would:

(1) approximate the curved boundaries of a radial section of D by polygonal lines,

(2) be reasonably regular near the free-surface,

(3) have more points per unit area near the contact angle than elsewhere, and

(4) permit the potential equation (47) to be easily approximated by symmetric difference equations with a small truncation error.

An irregular-triangular mesh produced by a modification of a well-proven mesh generator developed at Lawrence Radiation Laboratory [9, 10] satisfies the first three criteria and the ease of approximation part of the fourth. The mesh points are the images of the vertices of a connected set of equilateral triangles forming a region similar in shape to a radial section of D; mesh lines map into mesh lines, boundaries map into boundaries, and each interior mesh point has six neighbors. If h is the maximum

mesh spacing, the truncation error is $O(h)$ when all triangles in the mesh are acute [11]. However, the almost unavoidable appearance of a few obtuse triangles produces a larger truncation error and also leads to asymmetric difference approximations. Fortunately, the obtuseness can be confined to regions where the potential gradient is small, well away from the free-surface.

The Finite-Difference Approximation. The finite-difference approximation to the free-surface boundary condition (53) takes the form

$$T\underline{\varphi}_n - \lambda A \underline{\varphi} = 0 \tag{56}$$

where

$\underline{\varphi}$ and $\underline{\varphi}_n$ are vectors of values approximating the potential and its normal derivative at the mesh points on f;

λ is an approximation to ω^2;

A is a diagonal matrix whose entries are $1/2\pi$ times the areas of the conical zones used to approximate the equilibrium free-surface; and

T is a tridiagonal, symmetric, irreducible, and probably positive definite matrix approximating the differential operator $\underline{L}$ (all examples of T have been positive definite).

It is routine to approximate the potential equation (47) by replacing the integral of the Laplacian of Φ over a mesh region by the integral of the normal derivative over the boundary of the region [10,12]. Each acute

triangle is subdivided into three quadrilaterals by its perpendicular bisectors; and the mesh region associated with each mesh point is the union of such quadrilaterals, six for interior points, two or three for boundary points, and one for the mesh point at the vertex of the contact angle. The difference quotient of the potential, φ_i, at adjacent mesh points approximates the normal derivative along bounding segments of the perpendicular bisector separating them; along the wall, the normal derivative vanishes; and along the free-surface, inverting T in (56) yields an approximation to the normal derivative in terms of all the values of the potential on the free-surface. Each approximation to the normal derivative must be multiplied by the area of the conical zone generated by the line segment to which it applies. A difference equation relates approximate potentials, φ_i, i=1, 7, in a seven-point mesh star, say

$$d_1 \varphi_1 + \ldots + d_4 \varphi_4 + \ldots + d_7 \varphi_7 = 0, \qquad (57)$$

and connects the value at the center, here φ_4, with the values of φ_i at the six neighboring mesh points. The coefficients d_i, $i \neq 4$, are negative and d_4 is, in general, the negative of the sum of the other d_i plus an approximation to the integral of $+ \Phi/r^2$ in (47), namely: twice the area of the mesh region divided by the radius of the mesh point with which it is associated (the approximation reflects the fact that the potential on the free-surface tends to vary linearly with r near the axis). As a consequence of (56), the difference equation for a mesh point on the free-surface involves every mesh point on the free-surface.

The boundary condition (54) is accommodated by suppressing the d_i belonging to points on the axis and leaving the other coefficients unchanged.

Let $\underline{\varphi}_2$ be the vector of approximations to the potential at mesh points not on the free-surface and let $\underline{\varphi}_1$ be the vector of approximations on the free-surface. With this partition, the linear system approximating the differential system (47), (48), (53), and (54), at mesh points in the interior of D, on the wall, and on the free-surface, but not on the axis, takes the form

$$D(\lambda)\underline{\varphi} = \begin{bmatrix} D_{22} & D_{21} \\ D_{12} & D_{11} - \lambda S^{-1} \end{bmatrix} \begin{bmatrix} \underline{\varphi}_2 \\ \underline{\varphi}_1 \end{bmatrix} = 0 \qquad (58)$$

with

$$S^{-1} = 2\, AT^{-1} A$$

representing the contribution of the free-surface boundary condition (56). The matrix D_{22} has seven nonzero diagonals (one for each of the coefficients in (57)); the matrix D_{11} is tridiagonal; the matrices D_{12} and D_{21} have two nonzero diagonals which are symmetric with respect to the principal diagonal of $D(\lambda)$. The matrix S, inheriting the properties of T, is tridiagonal, symmetric, irreducible, and positive definite; consequently, S^{-1} is strictly positive and has no zero entries.

For meshes consisting entirely of acute triangles, the matrix $D(\lambda)$ is symmetric; D_{11} and D_{22} are positive on the principal diagonal, nonpositive elsewhere, strictly diagonally dominant, and nonsingular; and D_{12} and D_{21} are nonpositive.

The introduction of obtuse triangles into the mesh does not change the location of the nonzero entries in $D(\lambda)$; however, the approximations used for obtuse triangles, detailed later, lead to asymmetric matrix entries--in fact, some off-diagonal entries may become positive. Nevertheless, because the eigenvalues and vectors of $D(\lambda)$ turn out to be real and well-separated, a continuity argument, verified by numerical experience, shows that some asymmetry, or obtuseness, can be tolerated far from the free-surface, without vitiating the methods derived for the strictly acute, symmetric case. Thus we follow Ostrowski's recommendation[13] and use the symmetric method for both cases.

The Transformed Eigenvalue-vector Problem. Expanding (58) gives the generalized eigenvalue-vector problem

$$\left[A - \lambda B \right] \underline{\varphi}_1 = 0 \qquad (59)$$

with

$$A = D_{11} - D_{12} D_{22}^{-1} D_{21}$$

and

$$B = S^{-1}$$

where B is positive definite and A and B are symmetric $N \times N$ matrices, N being the number of mesh points on the free-surface. Three facts concerning the eigensystem of (59) are relevant here[14]:

(1) there are N real eigenvalue-vector pairs $[\lambda_k, \underline{\psi}_k]$ such that

$$A \underline{\psi}_k = \lambda_k B \underline{\psi}_k ;$$

(2) the eigenvectors can be chosen so as to be B-orthonormal, that is,

$$\underline{\psi}_j^T B \underline{\psi}_k = \delta_{jk} = \begin{cases} 1 , & j = k , \\ 0 , & j \neq k , \end{cases} \tag{60}$$

with the superscript T denoting transposition; and

(3) if the variable vector $\underline{x}$ is B-orthogonal to a set of eigenvectors, E, then

$$\lambda = \min_{\underline{x}} \left[\frac{\underline{x}^T A \underline{x}}{\underline{x}^T B \underline{x}} \right] \tag{61}$$

is the smallest eigenvalue belonging to an eigenvector in the B-orthogonal complement of the subspace spanned by E.

The eigensystem of (58) consists of the N eigenvalue-vector pairs

$$[\lambda_k , (\underline{\varphi}_{2,k} , \underline{\varphi}_{1,k})^T] \tag{62}$$

connected to the solutions of (59) by the relations

$$\underline{\varphi}_{1,k} = \underline{\psi}_k$$

and

$$\underline{\varphi}_{2,k} = -D_{22}^{-1} D_{21} \underline{\varphi}_{1,k} .$$

A peculiarity of this problem is that only the N-dimensional subspace spanned by the vectors (62) is of interest within the M-dimensional space on which the matrix in (58) acts (M being the total number of mesh points and N the number of mesh points on the free-surface).

Because the matrices D_{11}^{-1} and S^{-1} have hundreds, if not thousands of entries, all nonzero, solving either (58) or (59) is infeasible. A congruence transformation on the matrix (58) by the nonsingular matrix

$$\begin{bmatrix} I & 0 \\ 0 & R \end{bmatrix} \tag{63}$$

where $S = LR$ and $R = L^T$ (and I is the $(M - N) \times (M - N)$ unit matrix) leaves the eigenvalues unchanged; the eigenvectors of the congruent matrix differ from those of (58) in that the surface component $\underline{\varphi}_1$ is replaced by

$$\underline{z} = L^{-1} \underline{\varphi}_1 . \tag{64}$$

Set $\underline{y} = \underline{\varphi}_2 .$

The resulting linear system

$$\begin{bmatrix} D_{22} & D_{21} L \\ RD_{12} & RD_{11} L - \lambda I \end{bmatrix} \begin{bmatrix} \underline{y} \\ \underline{z} \end{bmatrix} = 0 \tag{65}$$

is quite sparse (RD_{12} and $D_{21} L$ have three nonzero diagonals and $RD_{11} L$ has only five) and λ affects only the diagonal entries. Consequently, solving (65) and recovering the surface component of the eigenvector via (64) seems a practical way to solve (58).

The Modified Wielandt Inverse-Iteration. Reducing (65) to a form analogous to (59), namely,

$$\left[C - \lambda I \right] \underline{z} = 0 \tag{66}$$

with

$$C = RD_{11} L - RD_{12} D_{22}^{-1} D_{21} L$$

and

$$\underline{y} = - D_{22}^{-1} D_{21} L \underline{z}$$

provides the motivation for the choice of algorithm to solve (65). (Observe that the three facts adduced about the eigensystem of (59) reduce, when A and B are replaced by C and I, to the ordinary facts about the eigensystem of the symmetric matrix C.) The Wielandt inverse-iteration with the eigenvalue improved by forming the Rayleigh quotient at each step[13,15] is a popular and efficient way to solve problems of the form (66). In this method one guesses a $\lambda^{(0)}$ which is, hopefully, close to some eigenvalue λ_j and chooses a vector $\underline{z}^{(0)}$ which is, hopefully, not deficient in the eigenvector $\underline{z}_j$; at each iterative step one solves the linear system.

$$\left[C - \lambda^{(0)} I \right] \underline{z}^{(1)} = \underline{z}^{(0)} , \tag{67}$$

forms the Rayleigh quotient

$$\lambda^{(1)} = \frac{\underline{z}^{(1)T} C \underline{z}^{(1)}}{\underline{z}^{(1)T} \underline{z}^{(1)}} , \tag{68}$$

and replaces

$$\lambda^{(0)} \text{ by } \lambda^{(1)}$$

and

$$\underline{z}^{(0)} \text{ by } \underline{z}^{(1)} / (\underline{z}^{(1)T} \underline{z}^{(1)})^{1/2} .$$

The iteration continues until appropriate convergence criteria are satisfied.

Let the pairs $[\lambda_k, \underline{z}_k]$, $k = 1, \ldots, n$, be the orthonormal eigensystem of C . If

$$\left.\begin{aligned} \underline{z}^{(0)} &= \sum \alpha_k \underline{z}_k \quad \text{with} \left(\sum \alpha_k^2\right)^{1/2} = 1 \\ \text{and} \\ \underline{z}^{(1)} &= \sum \beta_k \underline{z}_k \, , \end{aligned}\right\} \tag{69}$$

then it is easy to show that

$$\beta_k = \frac{\alpha_k}{\lambda_k - \lambda^{(0)}} \, , \quad \lambda^{(1)} = \sum \lambda_k \frac{\beta_k^2}{\sum \beta_k^2} \, ,$$

and

$$\mathcal{N} = \left(\underline{z}^{(1)T} \underline{z}^{(1)}\right)^{1/2} = \left(\sum \beta_k^2\right)^{1/2} \geq \max_k \beta_k \, .$$

Thus, if $\lambda^{(0)}$ is nearer to λ_j than any other λ_k and α_j is not very small, then the iteration will magnify the component of $\underline{z}_j$ in $\underline{z}^{(1)}$ and make λ_k even more dominant in the expression for $\lambda^{(1)}$. Clearly as long as the norm $\mathcal{N}$ is increasing, the computation is gaining in accuracy. How large $\mathcal{N}$ can grow depends upon the accuracy to which $\lambda^{(0)}$ can approximate λ_k ; and the accuracy is limited by the noise level of the computation which depends upon the computer word length and the order and numerical nature of C . Thus one convergence criterion stops the iteration when the norm $\mathcal{N}$ exceeds a large constant K chosen to cut off the iteration just before the noise level is reached[16]. Because $\mathcal{N}$ grows very rapidly and overshoots a well chosen K in a few iterations, this criterion is effective in preventing excessive computation. If K is too large, then excess computation may occur

after the eigenvalue estimate runs out of digits in which to improve. Consequently, a second convergence criterion is used, namely: stop the iteration when $|\lambda^{(1)} - \lambda^{(0)}|/\lambda^{(1)}$ is less than the suspected noise level--again a matter of judgement.

Observe that if one defines

$$\underline{y}^{(1)} = - D_{22}^{-1} D_{21} L \underline{z}^{(1)} ,$$

then

$$C \underline{z}^{(1)} = RD_{11} L \underline{z}^{(1)} + RD_{12} \left[- D_{22}^{-1} D_{21} L \underline{z}^{(1)} \right]$$

$$= RD_{11} L \underline{z}^{(1)} + RD_{12} \underline{y}^{(1)} ;$$

thus the linear system (67) is equivalent to

$$\begin{bmatrix} D_{22} & D_{21} L \\ RD_{12} & RD_{11} L - \lambda^{(0)} I \end{bmatrix} \begin{bmatrix} \underline{y}^{(1)} \\ \underline{z}^{(1)} \end{bmatrix} = \begin{bmatrix} 0 \\ \underline{z}^{(0)} \end{bmatrix} \tag{70}$$

and the Rayleigh quotient (68) takes the form

$$\lambda^{(1)} = \frac{\underline{z}^{(1)T} \left[RD_{11} L \underline{z}^{(1)} + RD_{12} \underline{y}^{(1)} \right]}{\underline{z}^{(1)T} \underline{z}^{(1)}} . \tag{71}$$

The modified form of the Wielandt inverse-iteration (70) and (71) is used to compute the eigenvalues. The surface component of the eigenvector of (58) is recovered from the final $\underline{z}^{(0)}$ via (64), that is,

$$\underline{\varphi}_1 = L \underline{z}^{(0)} ; \tag{72}$$

the normal derivative on the surface is the solution to the system (cf. (56) and (58))

$$S(A\,\underline{\varphi}_n) = \frac{1}{2}\lambda\,\underline{\varphi}_1 \; ; \tag{73}$$

and the eigenmode is determined from (19) as

$$\underline{h} = \omega^{-1} G\,\underline{\varphi}_n \tag{74}$$

where G is the diagonal matrix whose entries are the values of $g = \left[1 + f_r^2\right]^{1/2}$ at the mesh points on the free-surface.

Solution of the Linear System and Reduction of Dimension. The linear system (70) is solved by direct triangular decomposition, with inner products accumulated in double precision, carried out in two stages. Because the matrix $D(\lambda)$ in (58) is symmetric and diagonally dominant in the upper left corner and (70) inherits these properties, a Cholesky decomposition [15] can be carried through for the majority of the matrix in case the mesh is strictly acute (this has also proved true in practice for meshes that are not strictly acute). Moreover, because the right side of (70) has a large initial component of zeros, the factorization permits reducing the order of the matrix used in the Wielandt inverse-iteration from M to $2N$ or $2N-1$. The effect of the first stage of the factorization is to consolidate all the information about the shape of the tank which appears throughout $D(\lambda)$ into a matrix of much smaller order.

Let $\underline{z}^{(0)}$ and $\underline{z}^{(1)}$ be, as before, vectors of values belonging to mesh points on the free-surface; let $\underline{y}^{(1)}$ now be a vector of values belonging to the first mesh line below and "parallel" to the free-surface; and let $\underline{x}^{(1)}$ be the vector of values belonging to the rest of the mesh points. The partition of the linear system (70) induced by this partition of the vectors is

$$\begin{bmatrix} D_{33} & D_{32} & 0 \\ D_{23} & D_{22} & D_{21} L \\ 0 & RD_{12} & RD_{11} L - \lambda^{(0)} I \end{bmatrix} \begin{bmatrix} \underline{x}^{(1)} \\ \underline{y}^{(1)} \\ \underline{z}^{(1)} \end{bmatrix} = \begin{bmatrix} 0 \\ 0 \\ \underline{z}^{(0)} \end{bmatrix} . \qquad (75)$$

The four matrices in the upper left are a partition of the former D_{22}. The nonzero entries in the new RD_{12} and $D_{21} L$ are identical with the nonzero entries in the previous matrices with the same names; consequently the form of the Rayleigh quotient (71) is unaffected by the new partition.

The factorization of the matrix in (75) into the form

$$(DL)\ (DR) \tag{76}$$

where

$$DL = \begin{bmatrix} DL_{33} & 0 & 0 \\ DL_{23} & I & 0 \\ 0 & 0 & I \end{bmatrix}$$

and

$$DR = \begin{bmatrix} DR_{33} & DR_{32} & 0 \\ 0 & W_{22} & W_{21} \\ 0 & W_{12} & W_{11} \end{bmatrix}$$

with

$$W_{22} = D_{22} - (DL_{23})\ (DR_{32}) ,$$

$$W_{21} = D_{21}\ L , \quad W_{12} = RD_{12} ,$$

and

$$W_{11} = RD_{11}\ L - \lambda^{(0)}\ I$$

can be accomplished without interchanges. Because the $\underline{x}$-component of the right side of (75) is zero, the downsweep simply reproduces the right side; that is, the solution of the equation

$$DL\ \underline{u} = \left[0,\ 0,\ \underline{z}^{(0)} \right]^T$$

gives

$$\underline{u} = \left[0,\ 0,\ \underline{z}^{(0)} \right]^T .$$

Because only the components $\underline{y}^{(1)}$ and $\underline{z}^{(1)}$ are needed to compute the Rayleigh quotient and the new right side for the next iteration, the upsweep, that is, the process of solving the equation

$$DR \left[\underline{x}^{(1)} , \underline{y}^{(1)} , \underline{z}^{(1)} \right]^T = \underline{u} , \tag{77}$$

can be truncated to a smaller system of order $2N$ or $2N-1$, namely,

$$\begin{bmatrix} W_{22} & W_{21} \\ W_{12} & W_{11} \end{bmatrix} \begin{bmatrix} \underline{y}^{(1)} \\ \underline{z}^{(1)} \end{bmatrix} = \begin{bmatrix} 0 \\ \underline{z}^{(0)} \end{bmatrix} . \tag{78}$$

The matrix W_{22} contains all the information about the tank shape from mesh lines below the first two. The matrix (78) can be viewed as a finite-difference formulation of the free-surface boundary condition (49) expressed in terms of the single variable, the potential φ, rather than in terms of the two variables φ and φ_n used in the previous representation (56). The fact that the potential drops off sharply from the surface is reflected by the fact that the entries in W_{22} are several orders of magnitude smaller than the fixed entries in the other three sub-matrices. This jump in magnitude seems to be the principal source of numerical difficulty; it seems to be in part physical and in part a result of the form of the congruence (63) used to avoid multiplying a full matrix by λ.

In the second stage of the direct triangular decomposition, factoring and solving (78), partial pivoting (row interchanges) is necessary to

maintain accuracy [15]. Because $\lambda^{(0)}$ in W_{11} changes, this factorization must be redone in each iterative step.

After the Wielandt inverse-iteration with (78) has converged, the full upsweep (77) expands the potential restricted to the first two mesh lines into the potential throughout the liquid.

The Initial Guesses. The rapidity with which the iteration converges depends upon how good the initial guesses for $\lambda^{(0)}$ and $\underline{z}^{(0)} = L^{-1}\underline{\varphi}_1^{(0)}$ are. If some eigenvalue-vector pairs $[\lambda_k, \underline{\varphi}_{1,k}]$, say $k = 1,2,$ and 4, have been determined, then clearly (cf. (61) and (69)), $\underline{\varphi}_1^{(0)}$ should be chosen to be B-orthogonal to the eigenvectors already determined; that is, $\underline{\varphi}_1(0)$ is repeatedly replaced by the new approximation

$$\underline{\varphi}_1^{(0)} - \left[\underline{\varphi}_{1,k}^{T} \, B\underline{\varphi}_1^{(0)} \right] \underline{\varphi}_{1,k} \tag{79}$$

for all known eigenvectors $\underline{\varphi}_{1,k}$.

Consider the mixed boundary value problem

$$\left.\begin{aligned} &-(\Phi_{rr} + \frac{1}{r}\Phi_r + \Phi_{zz}) + \frac{1}{r^2}\Phi = 0 \quad \text{in the liquid,} \\ &\Phi_n = 0 \quad \text{on the wall,} \quad \Phi = 0 \quad \text{on the axis,} \\ &\text{and} \\ &\Phi_n = \frac{1}{g} h^* \quad \text{on the free-surface} \end{aligned}\right\} \tag{80}$$

where h^* is an eigenmode from a related problem (the flat interface

case has been used in practice). The solution to (80) is a potential that at least belongs to the right domain, albeit with an incorrect normal derivative on the free-surface, and should have a strong component of the eigenfunction with the same index as h^*. The finite-difference form of (80) is

$$\begin{bmatrix} D_{22} & D_{21} \\ D_{12} & D_{11} \end{bmatrix} \begin{bmatrix} \varphi_2 \\ \varphi_1 \end{bmatrix} = \begin{bmatrix} 0 \\ AG^{-1}\, \underline{h}^* \end{bmatrix} \tag{81}$$

where the notation of (58) is used and $\underline{h}^*$ is a finite-difference approximation to h^*. Because only φ_1 is needed to start the iteration and because the first component on the right of (81) vanishes, only the left and right factors of D_{11} are needed to compute the guess. Thus the complete Cholesky factorization of the matrix in (81) is carried out--the first part is used in (76). In practice the vector $AG^{-1}\, \underline{h}^*$ is restricted to the B-orthogonal complement of the space spanned by the known eigenvectors by repeatedly applying (79). In addition, the same procedure is used to guarantee that the solution lies in the same space. These precautions have improved the guess $\underline{z}^{(0)} = L^{-1}\, \varphi_1$.

When external estimates of the eigenvalues are available, they may be used as the guessed $\lambda^{(0)}$. Two types of internal guesses are available under input control. The first is the Rayleigh quotient derived from the solution of (81), namely, with A and B defined as in (59),

$$\lambda^{(0)} = \frac{\underline{\varphi}_1^T A \underline{\varphi}_1}{\underline{\varphi}_1^T B \underline{\varphi}_1} . \qquad (82)$$

The guess (82) when based on an h^* from the flat interface case is good for the first few eigenvalues; however, it tends to be high for the later ones--in fact, so high that eigenvalue-vector pairs are skipped. When this occurs, the program switches to the second type of guess to recover the skipped pair.

The guessed eigenvector $\underline{z}^{(0)}$ produced by repeatedly applying (79) has no component in the space spanned by the known eigenvectors. Thus (61) implies that the first Rayleigh quotient produced by the Wielandt inverse iteration starting from a guess less than the first missing eigenvalue will tend to be near the smallest eigenvalue not yet determined. As a temporary expedient when the distribution of eigenvalues to be encountered was unknown, the second guess was taken as the zero guess, $\lambda^{(0)} = 0$. The zero guess proved so efficient in dealing with skipped eigenvalues for problems with less than 50 mesh points on the free-surface that it was never replaced. (Fortunately, few large problems have been needed.) In fact, many problems have been run with the zero guess to minimize skipping.

Both guesses produce cases in which the norm $\mathcal{N}$ (69) fails to grow appreciably after a few iterations (the eventual convergence is likely to be to an unwanted pair, one already determined or one with a high

index). When such a case is detected, the program switches to the other guess or stops if it has already been used. The strategies described have sufficed to produce the first five pairs for all problems run to completion.

Description of Techniques

Domain Definition. For given B_α, Θ, and r_w, the determination of the equilibrium free-surface f, the solution to the two-point boundary value problem (16) and (17), involves finding the value of λ for which the differential equation and both boundary conditions can be satisfied. Because the origin of the coordinate system lies at the vertex of the free-surface (cf. (16)), the condition $f(0) = 0$ is implicit. Thus, both f and f_r are known at $r = 0$ and the problem may be viewed as a sequence of initial value problems in which λ is to be determined so that the boundary condition at r_w is also satisfied. (Because λ is geometrically twice the curvature of f at $r = 0$, a range of acceptable values is known.)

To facilitate approximating the operator $\underline{L}$ on the free-surface, it is convenient to introduce s, arc length on f, as the independent variable and to replace (16) and (17) by a first order system

$$\left.\begin{aligned} \frac{\partial f}{\partial s} &= u \\ \frac{\partial u}{\partial s} &= (\lambda + B_\alpha f - u/r)\,(1 - u^2)^{1/2} \\ \frac{\partial r}{\partial s} &= (1 - u^2)^{1/2} \end{aligned}\right\} \qquad (83)$$

subject to the boundary conditions

$$u = 0 \text{ at } r = 0 \text{ and } u = K \text{ at } r_w \leq 1 \tag{84}$$

with

$$K = r_w \cos \Theta - (1 - r_w^2)^{1/2} \sin \Theta \ .$$

Integrating the initial value problem obtained by setting $f(0) = 0$ and guessing a λ, say λ_o, until $u = K$ holds, say at s_o with $r_o = r(s_o)$, gives functions $f(s, \lambda)$, $u(s, \lambda)$, and $r(s, \lambda)$ that satisfy (83) and (84)--except that the second boundary condition holds at r_o instead of at r_w. Applying Newton's method to correct λ_o gives

$$\lambda = \lambda_o + \frac{r_w - r_o}{\left[\frac{\partial r}{\partial \lambda} - \left(\frac{\partial u}{\partial \lambda} \frac{\partial r}{\partial s} \Big/ \frac{\partial u}{\partial s} \right) \right]} \ . \tag{85}$$

Geometrically this is equivalent to moving along the tangent to the curve $u(s, \lambda) = K$ at (s_o, λ_o) to a point (s, λ) at which $r(s, \lambda) = r_w$ to first order. Differentiating (83) with respect to λ and interchanging the order of differentiation yield a system that can be integrated simultaneously with (83) to give the derivatives necessary to evaluate (85), namely,

$$\left.\begin{aligned} \frac{\partial}{\partial s}\left(\frac{\partial f}{\partial \lambda} \right) &= \frac{\partial u}{\partial \lambda} \\ \frac{\partial}{\partial s}\left(\frac{\partial u}{\partial \lambda} \right) &= F\left(\lambda, B_\alpha, f, u, r, \frac{\partial f}{\partial \lambda}, \frac{\partial u}{\partial \lambda}, \frac{\partial r}{\partial \lambda} \right) \\ \frac{\partial}{\partial s}\left(\frac{\partial r}{\partial \lambda} \right) &= - (1 - u^2)^{1/2} \, u \, \frac{\partial u}{\partial \lambda} \end{aligned}\right\} \tag{86}$$

with the initial values

$$\frac{\partial f}{\partial \lambda} = \frac{\partial u}{\partial \lambda} = \frac{\partial r}{\partial \lambda} = 0 \quad \text{at} \quad s = 0 .$$

The numerical integration is carried out by a fourth-order Adams predictor-corrector method with double precision accumulation of inner products, double precision dependent variables, and single precision derivatives; this choice simplifies programming the approximation to $\underline{L}$. The starting values are obtained from the approximate solution, valid for $u^2 \ll 1$,

$$\left.\begin{aligned} f &= \lambda \left[I_o(B_\alpha^{1/2}\, s) - 1 \right] / B_\alpha , \\ u &= \lambda\, I_1(B_\alpha^{1/2}\, s)/B_\alpha^{1/2} , \end{aligned}\right\} \qquad (87)$$

and

$$r = s$$

where I_o and I_1 are the modified Bessel functions of the first kind of orders zero and one. The parameter λ is first determined on a rough mesh and then refined on the fine mesh used in approximating the operator $\underline{L}$. The iteration converges rapidly and yields a very accurate description of the free-shape. The actual approximation of $\underline{L}$ is carried out in a final integration pass with the converged λ in which only the system (83) is integrated.

The equilibrium free-surface is located with respect to the tank by transforming the origin from the vertex of the free-surface to the vertex of the tank (the spatial coordinates can now be taken as positive). For $r_w = 1$, when the free-surface intersects the cylinder, the transformation is controlled in practice by specifying the volume. For $r_w < 1$, when the surface intersects the hemisphere, the transformation is determined

by r_w itself. Thus, to vary the volume and/or the center depth, r_w must be varied. Because human judgement is needed between runs in producing an adequate mesh, the definition of the domain can be controlled by approximating r_w from working charts developed by Reynolds, et.al.[17] and refining the approximation by hand to get the desired property in the course of the mesh development.

Matrix Approximation for the Free-Surface Operator. To obtain both a symmetrical matrix approximation and a form useful in approximating the potential operator (47), it is convenient to put the differential equation (49) into self-adjoint form and introduce arc length, s, along the equilibrium free-surface as the independent variable. The result is

$$\frac{1}{1+B_\alpha}\left\{-\frac{1}{r}\frac{\partial}{\partial s}\left(r\frac{\partial \Phi_n}{\partial s}\right)+\left(B_\alpha g+\frac{1}{r^2}-\frac{g}{r}\frac{\partial}{\partial s}\left[\frac{r}{g^2}\frac{\partial g}{\partial s}\right)\right]\Phi_n\right\} \quad (88)$$

$$-\omega^2\Phi = 0 .$$

The boundary conditions (50) and either (51) or (52), which complete the definition of the free-surface operator $\underline{L}$ (58), can be put in the forms

$$\Phi_n = 0 \quad \text{at} \quad r = 0 \qquad (50)$$

and at $r = r_w$

$$-r_w\left(\frac{\partial \Phi_n}{\partial s}+\frac{1}{g}\frac{\partial g}{\partial s}\Phi_n\right)$$

$$= \begin{cases} 0 , & \text{if } r_w = 1 \text{ and } z_w > 1 , \\ -\left[(1-r_w^2)^{1/2}\cos\Theta + r_w \sin\Theta\right]\Phi_n , & \text{if } r_w < 1 , \end{cases} \qquad (89)$$

where (r_w, z_w) is the intersection of the tank wall, w, with f.

Let f be divided into N equal subintervals of length Δs by $N + 1$ mesh-points indexed by the integers $1 = 0, 1, \ldots, N$. Let φ_j and $\varphi_{n,j}$ denote the approximations to the potential and its normal derivative at the mesh points. Denote the value of other variables at a mesh point by attaching the mesh-point index as a subscript and choose the indices naturally: s_o lies on the axis and $s_N = s_w$ is the length of f. Let the interval $[t_1, t_2]$ contain a single mesh point s_j. In general, t_1 and t_2 are the s-coordinates of the mid-points of two adjacent mesh intervals; however, for $j = N$, t_1 is the mid-point of the mesh interval ending at s_N, and $t_2 = s_N$.

Approximations of the form, for an arbitrary function W,

$$\int_{t_1}^{t_2} \Phi_n W \, ds \doteq \varphi_{n,j} \int_{t_1}^{t_2} W \, ds \tag{90}$$

follow from the choice of the mesh; however, because Φ_n tends to vary linearly with r near the origin, better results are obtained when the combination Φ_n/r occurs in the integral by using an approximation of the form

$$\int_{t_1}^{t_2} (\Phi_n/r) W \, ds \doteq (\varphi_{n,j}/r_j) \int_{t_1}^{t_2} W \, ds \, . \tag{91}$$

Integrating (88) over $[t_1, t_2]$ and using approximations similar to (90) and (91) yield the approximate equation

$$\frac{1}{1+B_\alpha}\Bigg\{ -\left(r\frac{\partial\Phi_n}{\partial s}\right)_{t_2} + \left(r\frac{\partial\Phi_n}{\partial s}\right)_{t_1} + \left(B_\alpha\int_{t_1}^{t_2} g\, r\, ds + \frac{1}{r_j}\int_{t_1}^{t_2} ds - g_j\left[\left(\frac{r}{g^2}\frac{\partial g}{\partial s}\right)_{t_2} - \left(\frac{r}{g^2}\frac{\partial g}{\partial s}\right)_{t_1}\right]\right)\varphi_{n,j}\Bigg\} - \omega^2\varphi_j\int_{t_1}^{t_2} r\, ds \doteq 0 . \tag{92}$$

For $j = N$, the two terms to be evaluated at $t_2 = s_N$ combine into

$$-r_w\left[\left(\frac{\partial\Phi_n}{\partial s}\right)_{t_2} + \frac{1}{g_N}\left(\frac{\partial g}{\partial s}\right)_{t_2}\varphi_{n,N}\right] . \tag{93}$$

Because (93) approximates the left side of (89), the boundary condition at $r = r_w$ is satisfied accurately by replacing (93) by the right side of (89).

Set

$$\left.\begin{aligned} a_j &= \int_{t_1}^{t_2} r\, ds , \\ D_{1,j} &= \frac{B_\alpha}{1+B_\alpha}\int_{t_1}^{t_2} r\, g\, ds , \\ D_2 &= \Delta s/(1+B_\alpha) , \text{ and} \\ D_{3,j} &= \frac{g_j}{1+B_\alpha}\left[(r\,u\,g\frac{\partial u}{\partial s})_{t_2} - (r\,u\,g\frac{\partial u}{\partial s})_{t_1}\right] . \end{aligned}\right\} \tag{94}$$

The final expression follows from

$$\frac{1}{g^2}\frac{\partial g}{\partial s} = ug\frac{\partial u}{\partial s} \quad ,$$

which comes from noting that $g = (1+f_r^2)^{1/2} = (1-u^2)^{-1/2}$. Because the expressions (94) are evaluated in the final integration of the system (83) with a mesh interval twenty to forty times smaller that Δs , they contribute a negligible amount to the total error.

Because t_1 and t_2 are mid-points, the error in approximating the derivative by the difference quotient, for example

$$\left(r\frac{\partial \Phi_n}{\partial s}\right)_{t_1} \doteq r(t_1)\left[\varphi_{n,j} - \varphi_{n,j-1}\right]/\Delta s \quad , \tag{95}$$

is $O(\Delta s^2)$. The errors introduced by the approximations (90) and (91) are of the same order. Consequently, the total truncation error introduced by using the approximations (90) through (95) is $O(\Delta s^2)$--an order of magnitude smaller than the $O(h)$ obtained for the potential equation within the liquid.

Assembling the approximations (90) through (95) yields a difference equation of the form

$$\left.\begin{aligned} &- \frac{r(t_2)}{(1+B_\alpha)\Delta s}\ \varphi_{n,j+1} \\ &+ \left[\frac{r(t_2)}{(1+B_\alpha)\Delta s} + \frac{r(t_1)}{(1+B_\alpha)\Delta s} + D_{1,j} + \frac{D_2}{r_j} - D_{3,j}\right]\varphi_{n,j} \\ &- \frac{r(t_1)}{(1+B_\alpha)\Delta s}\ \varphi_{n,j-1} \\ &- \omega^2 a_j \varphi_j \doteq 0 \end{aligned}\right\} \quad (96)$$

as the approximation to (88) for $j = 2, 3, \ldots, N-1$. For $j = 1$, (96) is modified to accommodate the boundary condition (50) (see (95)) by suppressing the term involving $\varphi_{n,o} \equiv 0$. For $j = N$, as a consequence of (89) and (93), the difference equation takes the form

$$\left.\begin{aligned} &\left[\frac{r(t_1)}{(1+B_\alpha)\Delta s} + D_{1,N} + \frac{D_2}{2r_w}\right. \\ &\left. + g_N \left(r\, u\, g \frac{\partial u}{\partial s}\right)_{t_1} + K\right]\varphi_{n,N} \\ &- \frac{r(t_1)}{(1+B_\alpha)\Delta s}\ \varphi_{n,N-1} - \omega^2 a_N \varphi_N \doteq 0 \end{aligned}\right\} \quad (97)$$

with $$K = \begin{cases} 0 & , \text{ if } r_w = 1 \text{ and } z_w > 1 , \\ -\left[(1-r_w^2)^{1/2} \cos\Theta + r_w \sin\Theta\right] & , \text{ if } r_w < 1 \end{cases} .$$

The contact angle Θ occurs in (97) explicitly in the expression for K when $r_w < 1$ and implicitly through the shape of the equilibrium free-surface in the remaining variables. The care taken in the integration of f justifies fairing a smooth curve through the points (r, f) with the slope f_r at r_w obtained from the computed value of $g_N = (1+f_r^2)^{1/2}$.

The value of g_N is good to at least four digits. Consequently, the principal error in (97) comes from the size of Δs and not from the representation of the contact angle.

Assembling the difference equations (96) and (97) into a linear system gives

$$T\underline{\varphi}_n - \omega^2 A \underline{\varphi} = 0 . \tag{56}$$

The matrix T, which approximates the free-surface operator $\underline{L}$, is tridiagonal, symmetric, irreducible, and nonpositive off the diagonal. From (97) it is clear that T is positive on the diagonal and diagonally dominant in the N-th row when $K = 0$. If both K and $D_{3,j}$ are not too large, these properties hold in every row; and consequently T is positive definite. In spite of the fact that all constructed T have been positive definite, the "weasel word" "probably"(positive definite) is used to describe T because no a priori estimate is available for the relative magnitude of the terms which sum to the diagonal of T.

The matrix T is replaced in the program by the related matrices S, L, and R, defined by

$$S = \frac{1}{2} A^{-1} T A^{-1} \quad \text{and} \quad S = LR . \tag{98}$$

Mesh Generation. Four numbers are associated with each point in the mesh, two logical and two physical coordinates. The logical coordinates are integers numbering the mesh lines in a rectangular coordinate system $[K, L]$ imposed on an equilateral triangular grid by taking one set of parallel lines as the lines L = constant and taking the "perpendicular" broken lines as the lines K = constant. Figure 2 is the logical diagram for the computing mesh, physical cross-section of D, shown in Figure 3; the labeling of the boundaries of the heavily lined trapezoid in the former shows how they map into the latter; the logical coordinates $[K, L]$ of some points in Figure 2 are given along with the physical coordinates (r, z) of the corresponding points in Figure 3.

The logical diagram is a KMAX by LMAX rectangle in the first quadrant to which corresponds an RMAX by ZMAX physical rectangle. The regions 101 through 105 and their physical images are successively subtracted from the basic rectangles to leave the interior and boundaries of the heavily lined regions as the working logical domain and computing mesh. The logical and physical coordinates of each point on the heavily lined boundaries are explicitly constructed in the program. The physical coordinates of the equilibrium free-surface are associated with the logical coordinates of the lower boundary of the region 101. Because the boundary condition $\varphi(0) = 0$ holds, there is actually one more mesh point on the free-surface than the nominal number. The physical

height of region 104 and the physical width of region 105 is a small number, say 10^{-10}, so that the lines $K = 1$ and $L = 1$ effectively map into zero.

Because the contact angle Θ is small, only one triangle should be stuffed into its vertex; that is, the diagram of Figure 2 should have the form shown. Thus, the logical coordinates of the points on the cylinder wall are known if the L coordinate of the point that maps into the juncture of the cylinder and the hemisphere is specified. The physical coordinates of the end-points of the wetted part of the cylinder are also known, $(1, f(1))$ and $(1, 1)$. The first mesh space adjacent to the cylinder is a control segment, $\Delta S\ 102$: if $0 < \Delta S\ 102 < f(1) - 1$, the k mesh spaces along the cylinder form a geometric series with k terms which has $\Delta S\ 102$ as first term and sums to $f(1) - 1$; if $\Delta S\ 102 = 0$, the length of the last mesh interval on the free-surface is used as the first term of the geometric series; and if $\Delta S\ 102$ exceeds the length of the wetted cylinder, then k equal mesh intervals are used. Generally $\Delta S\ 102$ has been chosen to be slightly larger than Δs, the free-surface mesh spacing, and the number of points on the wetted cylinder has been chosen so that the mesh spacing increases slowly but observably as in Figure 3.

One other form of control over the mesh spacing on the wetted cylinder is available: the level of the free-surface may be raised or lowered

slightly. For example in the case illustrated in Figures 2 and 3, when the center depth, h_o, was precisly 1, five mesh spaces gave obtuse triangles at the free-surface and four mesh spaces gave obtuse triangles along the wall. Clearly using $h_o = 0.98$ and four mesh spaces yields an acceptable result. A better mesh could have been obtained were variable mesh spacing available along the free-surface.

The control for the mesh spacing on the inner boundary of region 105 is analogous to that for region 102. Observe in Figure 3 that alternate triangles along the axis are obtuse. This occurs in all meshes and is characteristic of points where only two triangles meet on a boundary. However, the potential is small near the axis because the boundary condition (50) holds so that obtuseness at the axis is not serious. To eliminate this, a major re-examination of the internal workings of the mesh generator would be necessary.

The hemisphere in Figure 3 is the image of two segments of the heavy boundary in Figure 2. The length of the image of the slanting heavy line is prescribed by giving F, the ratio of its length to the total length of the wetted part of the hemisphere. The control of the mesh spacing for region 103 follows the pattern used for region 102 except that, when $\Delta S\ 103 = 0$, the last mesh spacing from region 102 is used as the first in region 103. The control for region 104 is analogous to that for region 103.

Obtuse triangles occur most frequently in the neighborhood of the point on the hemisphere where only two triangles meet. Frequently, even with repeated trials, it has been impossible to eliminate such obtuseness--especially for cases with small fill levels.

When the free-surface intersects the hemisphere, the diagram of Figure 2 is modified by eliminating the region 102, by reducing LMAX considerably and by increasing KMAX.

Because the free-surface operator is approximated on a mesh much finer than that exhibited in Figures 3 and 4, what seems to be the contact angle is a gross over-estimate of the effective value used in forming the difference equation (97). As pointed out in the preceding section, the mesh points on the equilibrium free-surface, f , give its shape very accurately and the value of $g_N \doteq \sec(\pi/2 - \Theta)$ is a good measure of the overall accuracy of the determination of f . For example, in Figure 3, the seeming contact angle measures about 15 degrees; clearly, the curve faired through the mesh points on f leads to a much smaller estimate of the effective contact angle; and in fact, $g_N = 11.4766$ has four digits in common with 11.4737, the value of $\sec(\pi/2 - \Theta)$ for $\Theta = 5$ degrees. In addition, the rise height at the wall in a cylinder of a radius 1 with Bond number 50 would be 0.183 were $\Theta = 15$ degrees--not 0.203, the value for $\Theta = 5$ degrees, as in Figure 3. The situation for Figure 4 is less misleading. The seeming contact angle measures about 6 degrees; and $g_N = 11.4728$ has five digits of accuracy.

Although this discussion has emphasized the difficulty of obtaining good meshes, Figures 3 and 4 demonstrate that the procedures which have been explored can yield remarkably good meshes for difficult domains.

The mapping of the mesh points in the interior region of the logical diagram into the physical cross-section of D is constructed by solving iteratively a pair of coupled, non-linear elliptic partial differential equations. The input checking and expansion routines as well as the mapping routine are virtually in the form described by Winslow[9,10]. His plotting and matrix generation routines have been heavily modified, although the indexing structure is retained.

Matrix Approximation for the Potential Operator. In developing the restriction of the Wielandt inverse-iteration, the formulation of the sub-matrices in (58), (75), and (81) was sketched earlier only for a mesh consisting entirely of acute triangles. Here the description is completed by describing the approximations for obtuse triangles and sketching the assembly of the computing matrices.

Because the perpendicular bisectors intersect outside an obtuse triangle and the medians intersect within the triangle at the centroid, the argument that leads to the acute triangle approximation may be imitated for obtuse triangles with the line segments connecting the mid points of the sides to the centroid as the replacement for the segments of the

perpendicular bisectors. For obtuse triangles, assuming the potential to be linear within a mesh triangle gives an approximation consistent along sides of the triangle with that used for acute triangles. When obtuse triangles occur in the mesh, the mesh region that surrounds an interior mesh point is a dodecagon bounded by segments of perpendicular bisectors and medians.

Let P_i , $i = 1, 2, 3$ be the vertices of the triangle with indices increasing with positive rotation. At P_i , let φ_i be the approximate potential and r_i the r-coordinate. Let s_i be the vector from P_i to P_{i+1} and m_i be the vector from the mid point, $s_i/2$, to the centroid, $i = 1, 2, 3 \pmod 3$.

As in the acute case, the derivation of the difference equations approximating (47) is based upon replacing the integral of the Laplacian of Φ over a mesh region by the integral of the exterior normal derivative over the boundary. Here the relevant part of the boundary is the frustum of the cone generated by rotating m_1 about the center line, $r = 0$. The contribution from m_1 to the integral over the boundary of a region containing P_1 in its interior is, with the factor π divided out,

$$(c_{12} + c_{13})\,\varphi_1 - c_{12}\,\varphi_2 - c_{13}\,\varphi_3 \qquad (99)$$

where

$$\left.\begin{aligned} c_{12} &= (2s_3 \cdot s_3 + s_1 \cdot s_3)\,(q_{12} + c)/12A \\ \text{and} \\ c_{13} &= (2s_1 \cdot s_3 + s_1 \cdot s_1)\,(q_{12} + c)/12A \\ \text{where} \\ q_{12} &= (r_1 + r_2)/2 \quad , \quad c = (r_1 + r_2 + r_3)/3 \ , \end{aligned}\right\} \tag{100}$$

A is the area of the triangle $P_1P_2P_3$, and $s_1 \cdot s_3$ is the inner product of the two vectors. When m_1 is viewed from P_2, the direction of the exterior normal changes; thus the contribution from m_1 to the integral over the boundary of a region with P_2 in its interior is

$$c_{12}\,\varphi_2 + c_{13}\,\varphi_3 - (c_{12} + c_{13})\,\varphi_1 \ . \tag{101}$$

Because the quadrilateral bounded by m_1 and m_3 with vertex at P_1 has area $A/3$, the contributions from P_1 to the approximation for the coefficient of the term $+\,\Phi/r^2$ in (47) is

$$A_1 = 2A/3r_1 \ . \tag{102}$$

(The form of (102) is chosen to reflect the linear variation of φ with r near $r = 0$.) The contributions of an obtuse mesh triangle to the coefficients of the difference equations can be obtained from a set of nine numbers, c_{12}, c_{13}, A_1, and the six others obtained by permuting indices cyclicly.

Let p_i be the vector from $s_i/2$ to the intersection of the perpendicular bisectors. The analogue to (99) for an acute triangle has the form

$$c_{12}\,\varphi_1 - c_{12}\,\varphi_2 \tag{103}$$

where c_{12} is the lateral area divided by π of the frustum of the cone generated by rotating p_1 about the axis times the length of s_1. The analogue of (102) is an A_1 equal to twice the area of the quadrilateral bounded by p_1 and p_3 with vertex at P_1 divided by r_1. Although only c_{12} and A_1 need be associated with a vertex of an acute triangle, setting c_{13} to zero permits using the same coding to assemble the coefficients of the difference equation without testing for triangle type.

The mesh points and the corresponding components of the approximate potential $\underline{\varphi}$ are indexed from the slanting line in Figure 2 toward the axis; the points on the axis do not belong to the computing mesh because the value of φ is known there (50) and are not indexed; the indexing on line L + 1 continues that on L. A mesh point on the line L has in general two neighbors on the same line, two on the line below, L - 1, and two on the line above, L + 1. See the detail in Figure 2 at L = 11. With this indexing the matrix of the linear system approximating (47) becomes block-tridiagonal. The center block contains the coefficients of the approximate potentials on the line L;

the left and right blocks each have two non-zero diagonals, the coefficients of the potentials on the lines L-1 and L+1 . The number of points on a line is alternately the same and one greater than the number on the preceding line. Thus the order of the diagonal blocks and the left and right band widths, measured from the diagonal to the outer non-zero diagonal, grow in steps with L .

For each mesh region, the difference equation approximating (47) is a weighted sum of the potentials at the seven points of the star formed by the mesh point within the region and its six neighbors. The coefficients for the external points of the star are sums of c_{12}, c_{13}, etc.; the coefficient for the central point is a sum of c_{12}, c_{13}, etc. plus a sum of A_1, etc. The rule for forming the sums of the c's is to add the analogues of (99) and (103) as encountered in traversing the dodecagon in the positive direction with the signs reversed when a p_i or m_i is traversed against its direction (cf. (101)). The rule for the sum of A's is: for each triangle meeting the center of the star add to the center coefficient the A belonging to the vertex lying on the central mesh point.

The program to assemble the potential matrices is based upon the rectangular [K, L] indexing used by Winslow[9]. All coefficients (nine for each triangle) for the triangles in the mesh row between the lines L and L+1 are computed at one time. To facilitate applying

zero normal derivative boundary conditions (48), the coefficients which lie outside the liquid but occur in stars of boundary points are set to zero. Two matrix stores are used in turn and the rules described above are split into two parts. First the right half of the matrix for the line L is completed into one store; and then the left half of the matrix for the line L+1 is computed into the other store.

The zero value of the potential on the axis (54) is dealt with by setting to zero the coefficients which correspond to points that lie at intersections of stars with the axis. The boundary condition (48), zero normal derivative on the wall, is automatically accommodated for the line L=1 by setting the matrix store to zero and computing only the right half of the matrix; for other points on the wall, the setting of triangle coefficients zero outside the liquid enforces the boundary condition. Because the normal derivative on the free-surface is always accounted for by an explicit element, the matrix $-\lambda S^{-1}$ in (58) and $AG^{-1}\,\underline{h}^*$ in (81), a zero normal derivative boundary condition is implicit in the definition D_{11}. Consequently, only the left half of the matrix for the line LMAX-1, the free-surface, need be computed.

It is easy to verify that the matrices just described have the properties ascribed to $D(\lambda)$ in the discussion subsequent to (58).

The identification of the elements of (75) with the matrices just described is

(1) D_{12} and D_{11} are the left and diagonal blocks for $L = LMAX - 1$,

(2) D_{23}, D_{22}, and D_{21} are the three blocks for $L = LMAX - 2$,

(3) D_{32} is the right block for $L = LMAX - 3$, and

(4) D_{33} is the remainder of the matrix.

To see that the approximations (99) and (101) do yield, in general, asymmetric matrices, consider an isolated obtuse triangle among acute triangles (Figure 3 contains an example at the mesh point on the hemisphere where only two triangles meet.). Because all neighboring triangles are acute, any asymmetry in the matrix must come from the contribution from the triangle $P_1P_2P_3$. Suppose the mesh points are ordered so that P_1 preceeds P_2 on one mesh line. The matrix of contributions from m_1 to the diagonal block of the matrix belonging to the line P_1 and P_2 is

$$\begin{bmatrix} (c_{12} + c_{13}) & -c_{12} \\ (-c_{12} - c_{13}) & c_{12} \end{bmatrix}, \tag{104}$$

which is asymmetric unless $c_{13} = 0$. The exceptional case occurs if and only if the triangle is equilateral.

Matrix Manipulation. The program is designed to admit up to 80 points on the free-surface and up to 3000 components in the approximate potential. The number of mesh lines is restricted by the allocation of drum storage areas. In the runs reported here, the number of points on the free-surface varies from 25 to 65 and the number of mesh lines from 62 to 6 with fewer lines for the larger number of points.

The potential matrix is stored by block-rows corresponding to mesh lines. Each block-row can be compressed into a seven column array. Eight columns are needed to store the derived block-rows $[\, D_{32},\ D_{22},\ D_{21}\ L\,]$ and $[\, RD_{21},\ RD_{11}\ L\,]$ that occur in (75).

To carry out the modified Wielandt inverse-iteration restricted to the top two mesh lines, the matrix W of the linear system (78) is needed; and to carry out the full upsweep (77) the matrix $[DR_{33},\ DR_{32}]$ (76) is needed. To allow for the possibility of improving the eigenvector iteratively, it is desireable to retain the matrices DL_{33} and DI_{23}. Moreover, in solving the system (81), the matrices $[DL_{23},\ DL_{22}]$, $[DL_{21},\ DL_{11}]$, DR_{11}, and $[DR_{22},\ DR_{21}]$ are used. Here the notation of (76) is extended naturally.

The submatrices of the left and right factors of the potential matrix are stored by rows. The number of nonzero entries in each row is the left and right band width of the block-row to which the row belongs.

To compress these matrices the rows are stored end to end in groups separated by indices indicating the band width and the number of rows with this width. The factorization is carried out block-row by block-row. The results continue to be stored in left and right stores until the storage of the upcoming group of rows would result in more than 6562 entries in the store. At this point the store is emptied as a record into drum and/or tape.

The rows of the left factor are stored in natural order and, within each row, the entries are stored from left to right, from outer to central diagonal. With this order the left rows occur as used in the downsweeps and the smaller entries lead so that they can be used first in forming inner products. Because the right factors are used in upsweeps, in which the first row of the matrix is used last, the right rows are stored in reverse order. The entries are stored from right to left. The storage area assigned to right rows is filled from the bottom upward. Any initial zeros are eliminated in writing the record on drum. After all the factorization is complete, the order of the records that form $[\, DR_{33},\ D_{32}]$ is reversed as the records are written onto tape.

The matrix W, which may have up to 25,760 entries, is also constructed, partitioned into blocks 40 columns wide, and written on tape.

Clearly, the problem involves a large number of matrices, some of large order, that must be introduced into core storage in various sequences. Thus the programming problem for the UNIVAC 1108 is to devise a method to move a large number of matrices efficiently from drum storage to core in such a way that no time is lost in waiting for information. A subsidiary problem is to be able to reload the drum when it is desired to determine additional eigenvalue-vector pairs. The latter problem is solved by creating a restart tape which , as a matter of precaution, contains at the end of each major segment of the program, and also after determination of each eigenvalue-vector pair, all the output (future input) so far obtained. A drum loading routine, which is buffered to run at tape speed, can reload the drums at restart or, to facilitate independent running of major segments, at the beginning of each program segment.

To guarantee that the record read from tape or from drum is the one required, each record is provided with an eight word header descriptive of the contents of the record. The header is checked by the drum loading program and by the main programs before each use of the information.

The primary programming problem is solved by using a large core area as free storage. The Wielandt inverse-iteration program falls into four sections:

(1) computing the guess,

(2) carrying out the modified Wielandt inverse-iteration restricted to the two top lines,

(3) expanding the restricted potential throughout the tank (and iteratively improving the eigenvector, if possible), and

(4) presenting the output in tabular form.

To each section of the program corresponds a list of matrices in the order used. (Here output vectors, eigenmode, full tank potential, and eigenvector, are considered as matrices.)

A family of drum reading and matrix checking programs keep the free storage as full of information as possible. At the beginning of each list, the drum reading program fills the available space in the free store by using a UNIVAC 1108 program (NTRAN) to stack drum read orders. These orders are executed as soon as possible via the interrupt features of the UNIVAC 1108. As the main program needs information, it checks that the next unused area of the free store contains the desired information and, if necessary, holds up until it is available. As the main program finishes with the information in an area, it releases that area to the drum read program. The latter uses NTRAN to fill the released area with new information or waits until the released area grows large enough to accommodate the next record. The reading of new lists is initiated by the main program as early as possible to keep

the free store full. Running times of from 1 1/2 to 4 1/2 minutes for eight eigenvalue-vector pairs show that the procedure just described is reasonably effective. For a problem in which the W matrix had 17,030 entries considerable waiting occurred.

The Eigenvalue-vector Iteration. The efficacy of the modified Wielandt inverse-iteration in determining the eigenvalues can be judged from the size of the norm $\mathcal{N}$ (69) finally attained in the iteration. The relevant inequality,

$$1/\mathcal{N} \leq \lambda_k - \lambda^{(0)} ,$$

is in the wrong direction, that is, it bounds the computed eigenvalue $\lambda^{(0)}$ away from λ_k, the exact eigenvalue of the approximate matrix used in the computation. Moreover, what is wanted is a comparison of $\lambda^{(0)}$ with the exact eigenvalue of the continuous problem. Nevertheless $1/\mathcal{N}$ does indicate the general level of accuracy attained. Better error estimates would be appropriate, were the $\mathcal{N}$'s larger. For the runs reported here, $\mathcal{N}$ is generally of the order 10^4 or greater except for problems with center depth $h_o = 0.1$. The value of $\mathcal{N}$ within a run varies from eigenvalue to eigenvalue but tends to remain at the same level or to decrease slowly with increasing index. For Bond numbers $B_\alpha \geq 10$ and $h_o \geq 0.5$, an $\mathcal{N}$ of the order 10^5 is common.

As B_α decreases toward 0 , $\mathcal{N}$ tends to decrease slowly:

for $h_o = 3$, from 10^5 to 10^4 ;

for $h_o = 0.1$, from 10^3 to 10^2 .

As h_o decreases, $\mathcal{N}$ tends to decrease very slowly at first, and then has a rapid decrease between $h_o = 0.25$ and $h_o = 0.1$:

for $B_\alpha = 50$, from 10^5 to 10^3 ;

for $B_\alpha = 0$, from 10^4 to 10^2 .

For $h_o = 0.1$, $\mathcal{N}$ is of the order 10^3 for $B > 5$.

The domains for $h_o = 0.1$ are long and narrow compared with the others (cf. Figures 3 and 4). In order to get what seems to be an adequate number of mesh lines between the free surface and the tank wall so that the potential is represented, a fine mesh must be used on the free-surface. But the number of eigenvalues of the approximation matrix (65) is equal to the number of mesh points on the free-surface. Because (65) is an approximation to a continuous problem with an infinity of eigenvalues, the range of the eigenvalues of the approximate problem increases as the number of mesh points increases. Consequently, the matrix becomes more ill-conditioned as the number of mesh points increases. It is a fact of life that ill-conditioned linear systems are difficult to solve.

Two cases for $B_\alpha = 0$ and $\Theta = 5$ degrees, $h_o = 0.25$ and $h_o = 0.5$, with 50 mesh points on the free-surface, rather than the 25 used for the runs included in the tables, give values of $\mathcal{N}$ of the order 10^2. This suggests that the difficulty lies in the large number of mesh points rather than with the inadequacy of the mesh.

Eigenvectors computed by the Wielandt inverse iteration should have roughly half the number of correct digits that the corresponding eigenvalues have (cf. 69). Thus, in general, the eigenvectors should have about two digits of accuracy, sometimes more, and probably only one for the smaller values of B_α when $h_o = 0.1$.

When the free-surface is flat and the tank very deep, the eigenfunctions are proportional to $J_1(\lambda_k r)$ where λ_k is the k-th zero of $J_1'(r)$. The computed eigenvectors for the cases $B_\alpha = 0$ and $B_\alpha = 50$ with a flat surface, $\Theta = 0$ degrees, and $h_o = 3$, even with 40 mesh points on the free-surface, reproduce the shape of $J_1(\lambda_k r)$ with unexpected accuracy--at least one more digit than the observed accuracy of the corresponding eigenvalue indicates. For these two cases, the first eigenvector had at least three digits correct, if not four; the second eigenvector had two to three digits correct; and the fifth had one or two correct.

For the flat surface case with $B_\alpha = 0$, the calculated Fourier coefficients D_k (23) compare well with the theoretical values: four digits of accuracy for $k = 1$, three digits for $k = 2$ and 3 , and two digits for $4 \leq k \leq 9$. Thus although the first eigenvector is likely to be more accurate than the succeeding ones, the latter yield adequate Fourier coefficients. However, it is doubtful if the higher eigenvectors are sufficiently accurate to yield adequate results when extended to a potential throughout the tank.

Integration Techniques. An easily calculable approximation for the Fourier coefficient

$$D_k = \frac{\int_0^{r_w} h_k \, r^2 \, dr}{\int_0^{r_w} \Phi_k \, h_k \, r dr} \tag{23}$$

can be derived by observing that

$$h_k = \frac{g}{\omega_k} \Phi_{k_n} \tag{18}$$

holds. One consequence of (18) is that the product $D_k \, \Phi_k$, is independent of the normalization of Φ_k . Therefore, let Φ_k be normalized so that it is consistent with the approximate potential φ .

Because the integrals in (23) are to be evaluated on the equilibrium free-surface, it is appropriate to introduce arc length on the free-

surface as the variable of integration (ds = gdr) and to approximate the integrals on the same mesh that was used in the approximation of the free-surface operator. Thus, the denominator can be written as

$$\int_o^{r_w} \Phi h \, r \, dr = \frac{1}{\omega} \int_o^{s_w} \Phi \, \Phi_n \, r \, ds \tag{105}$$

$$= \frac{1}{\omega} \sum_j \int_{t_1}^{t_2} \Phi \, \Phi_n \, r \, ds \, ,$$

where $s_w = s_N$, the length of the meridian of the equilibrium free-surface. Making two approximations of the form (90), using (94), (73), and (60) give an approximation to the denominator in the form

$$\frac{1}{\omega} \sum_j \varphi_j \, \varphi_{n,j} \int_{t_1}^{t_2} r \, ds$$

$$= \frac{1}{\omega} \sum_j \varphi_j (a_j \, \varphi_{n,j}) = \frac{1}{\omega} \underline{\varphi}^T (A \, \underline{\varphi}_n) \tag{106}$$

$$= \frac{\lambda}{2\omega} \underline{\varphi}^T S^{-1} \underline{\varphi} = \frac{\lambda}{2\omega}$$

The last step follows because $\underline{\varphi}$ is a B-orthonormal vector. (Thus, the continuous potential should be normalized so that

$$\int_o^{r_w} \Phi \, hr \, dr = \frac{\omega}{2} \tag{107}$$

to have the normalization of the computing potential.)

The analogue to (106) for the numerator is

$$\int_0^{r_w} hr^2\, dr \doteq \frac{1}{\omega}\, \underline{r}\, (A\, \underline{\varphi}_n)$$

$$= \frac{\lambda}{2\omega}\, \underline{r}\, S^{-1}\, \underline{\varphi} \qquad (108)$$

where $\underline{r}$ is the vector of r-values at the mesh points on the free-surface. Hence, (106) and (108) imply that

$$D_k \doteq \underline{r}\, S^{-1}\, \underline{\varphi}_k \qquad (109)$$

is the computing approximation for the Fourier coefficients.

Suppressing the index k, introducing arc length as the variable of integration, transforming as in (105), and approximating as in (106) leads to the following approximate value for the integral V occurring in (42) and (43):

$$\int_0^{s_w} \Phi\, \Phi_n\, r\, ds \doteq \underline{\varphi}\, (A\, \underline{\varphi}_n) = \lambda/2\ . \qquad (110)$$

In setting up a set of weights to approximate the integrals (39) and (40) which occur in the definitions of the lateral force and the moment, the problem is that the potential and the coordinates of the wall are known only at the mesh points. Moreover, the linear distance between adjacent mesh points is computed in generating the potential matrix. These facts suggest approximating the entire integral by linear

interpolation at the mid-point of the chord between two adjacent mesh points. Let φ_i, φ_j, and φ_k be the potential values at three consecutive mesh points on the wall. Because the mean value of the potential is used in each of the two intervals, the approximations have the forms, in terms of the coefficients V and W,

$$V\varphi_i + V\varphi_j \quad \text{and} \quad W\varphi_j + W\varphi_k .$$

Hence, the weight assigned to φ_j is $V + W$. For computing purposes, it is desirable to make the replacement $\sin\beta = r_w$.

Forced Motion Analysis. For convenience these calculations are carried out by a separate program. The main program provides punched card output to serve as input to this program, namely a set of cards containing k, the index of the eigenvalue, h_o, $\cos\Theta$, B_α, ω^2_k, D_k, and $g_N(\partial\varphi_k/\partial n)_w$, the evaluation carried out at the intersection of the wall and the equilibrium free-surface. The last quantity is derived from the computed value of φ_n at the wall rather than by finite-difference techniques, which badly underestimate φ_n because the potential drops off very rapidly from the surface.

The programming to determine the vertical rise height in response to sinusoidal, square wave, and periodic pulse lateral perturbing acceleration is a straight forward exercise in evaluating the series (29), (30), and (31).

Recommendations. The principal difficulty with the problem is the unresolved conflict between the desire to reduce the truncation error by increasing the number of mesh points on the surface and the fact that more points make the linear system harder to solve. Two courses are open, direct attack or palliatives.

The most promising direct approaches are:

(1) to solve the linear system (78) by orthogonal triangularization and

(2) to double the precision of the arithmetic used.

Factoring the matrix of a linear system into the product of an orthogonal and a right triangular matrix tends to yield more accurate solutions and sometimes produces solutions that cannot be obtained by other methods. Direct triangular decomposition with partial pivoting was originally chosen because it is a standard, good method with familar coding. Doubling the precision is not prohibitive because all inner products are now accumulated using machine language double precision. The penalty is considerable reprogramming and a decrease in the size of problem that can be run.

The palliatives are:

(3) to introduce a variable mesh on the free-surface and

(4) to attempt to condition the matrix.

Clearly a variable mesh would allow the truncation error to be reduced in important regions while the number of mesh points remained unchanged. However, the existence of small mesh spacings in a problem tends to make the linear system more difficult to solve, so there is a penalty. An added advantage is that it will facilitate the development of suitable meshes. The problem of conditioning a matrix, that is, finding a transformation that makes a linear system easier to solve, is an active subject of research for many numerical analysts today. The probability of finding a good transformation is small for this problem.

Two directions in which the program, as a program, might be improved are:

(5) to make the mesh generation routine easier to use and

(6) to improve the guesses, in particular the strategy for dealing with skipped eigenvalues.

Because of the amount of human time consumed in developing suitable meshes, any improvement of the mesh generation would increase the program's usefulness.

Improvement of the guesses clearly saves computer time. The original design of using the actual solution of a nearby problem in constructing the guess might save significant running time.

RESULTS AND CONCLUSIONS

The Method. The problem of low gravity sloshing, where surface tension forces may dominate gravitational forces, has previously been investigated by approximate methods for right circular cylinders with flat bottoms (or infinite depth) and by experimental techniques.[2,3] This study is a first attempt to survey the problem by purely numerical (finite-difference) methods using a digital computer.

The highly curved equilibrium free-surface characterized by large departures from the horizontal plane is accurately represented by numerical methods--in contrast to the approximate representations used by others.[3] Restriction of the tank to right circular cylinders is not necessary. Here, in fact, the tank has a hemispherical bottom topped by a right circular cylinder--in principle, any reasonable tank shape can be studied. The assumption of a large depth is unnecessary. The physical difficulties, met in experiments, in obtaining proper combinations of liquids, dimensions, and tank materials to give desired Bond numbers and contact angles can be eliminated through numerical computation. Consequently, both surveys over wide parameter ranges and detailed examination of particular cases become feasible. The basic restriction inherent in the finite-difference approximation is that the contact angle be nonzero (although it can be quite small).

The demonstration of the utility of numerical calculation as a tool in surveying small amplitude motion of liquids under reduced gravity conditions is a major result of this work. The magnitude of the program to do this is indicated by the space needed to give a nonsuperficial, yet not too detailed, description in the preceding section of this report. In spite of its magnitude, the program runs fast enough to be a survey tool. The principal outputs from the numerical computation are

1. The normal mode eigenvalues ω_k^2 ;
2. The normal mode eigenfunctions Φ_k (both throughout the liquid and restricted to the equilibrium surface);
3. The eigenmodes, h_k, the shape of the perturbed surface in the kth mode; and
4. The Fourier coefficients D_k in the expansion $r = \sum D_k \Phi_k$.

Reducing the mass of results to engineering data, even for a single case, is a task requiring iteration among numerical analysts, programmers, and users. Consequently, even for the restricted set of calculations presented here, only a representative selection of the results accumulated can be presented.

In principle, the computations of the response to lateral perturbations is an exercise in evaluating Fourier series (see, for example, (29) - (31)). For sinusoidal perturbations no difficulty in interpreting the analysis is encountered. However, the calculations for square wave and periodic pulsing perturbation suggest that an attempt at a general analysis may be more misleading than helpful. Consequently, the program to aid an engineer in

carrying out a detailed analysis of laterally perturbed motion is as yet in a rudimentary stage. At present, cases needing detail in engineering practice should be investigated individually with output tailored to the judgements to be made.

For routine engineering work, a mechanical analog, an equivalent spring-mass oscillator, may suffice; and therefore, mechanical analog parameters for the fundamental mode are also discussed.

The Present Survey. The data reported here is basically a survey of small amplitude linearized sloshing over a range of Bond numbers and fill depths with a fixed contact angle of 5 degrees. This value is significantly smaller than that used in previous calculations.[2] The choice of 5 degrees is a compromise between (1) the desire to obtain results representative of the behavior of fluids with small contact angles and (2) the necessity to avoid numerical difficulties encountered in calculations within very thin wedges. The consistency of the results reported suggests that computations for contact angles less than 5 degrees may be successful. As pointed out earlier (page 70), the results for large depth with a flat interface agree with calculations by classical methods.

The axial Bond numbers $B_\alpha = \rho g_\alpha r_o^2/\sigma$ used in the survey range from 0 to 50. Depths, h_o, range from 0.1 to 3, measured along the center line between the free-surface and the hemispherical tank bottom. Figures 3 and 4 give

sample cross-sections of the liquid in equilibrium. For large h_o and small B_α, the cross-section resembles a domain bounded by two parallel straight lines and two nearly parallel circles (see Figure 1); for small h_o and large B_α, the equilibrium domain resembles a puddle in the bottom of the hemisphere. The range of parameters covers both the cases in which large depth analysis is applicable[2] and those in which the shape of the tank bottom may have a significant, if not dominant, effect.

The Eigenvalues ω_k^2. The variation of the first mode (fundamental) eigenvalue ω_1^2 as a function of Bond number B_α and liquid depth h_o is shown in Figure 5. For all values of B_α, ω_1^2 is an increasing function of h_o; and, for depths exceeding about 1 1/2 tank radii the hemispherical tank bottom ceases to have a significant effect. For depths greater than about 3/4 of the tank radius, ω_1^2 is a decreasing function of B_α. In contrast to other reports,[3] ω_1^2 for large depth and finite B_α decreases monotonically to 1.8411, the value for $B_\alpha = \infty$. For small depths, ω_1^2 first decreases and then increases with B_α. This behavior is consistent with the fact that $\omega_1^2 = 1$ for small depth with $B_\alpha = \infty$.[18]

Table I lists the first five eigenvalues ω_k^2 for all cases in the survey. Those in which the liquid wets the cylinder are above the dashed lines; those in which the liquid lies within the hemisphere are below. For $B_\alpha = 0$, all cases wet the cylinder and all ω_k^2 are increasing functions of depth. For $B_\alpha = 1$, ω_4^2 and ω_5^2 decrease and then increase with depth. For $B_\alpha \geq 2$, all higher eigenvalues ω_k^2, $k > 1$, show a minimum as a function of depth.

Because the minimum occurs near the dashed line which separates the two geometric domains, the higher eigenvalues appear to be decreasing functions of depth when the liquid lies within the hemisphere and increasing functions when the liquid wets the cylinder. Table I also shows that the higher eigenvalues tend to assume their "asymptotic", large-depth values at smaller depths than does the fundamental.

Dimensional sloshing frequencies $\bar{\omega}_k$ can be obtained from the values of Table I via the relation

$$\bar{\omega}_k = \omega_k \left((1+B_\alpha)\, \sigma/\rho r_o^3 \right)^{1/2} .$$

For convenience in calculation, the equilibrium depth along the axis, h_o, has been used in place of the liquid volume as the parameter in this study. Because volume is more frequently known than depth, Figure 6, which gives liquid depth as a function of volume for selected B_α, facilitates using the results in engineering calculations.

The Fundamental Eigenmode h_1. Because the emphasis in this survey is on results representative of the behavior of liquids with small contact angles, a detailed study of the dependence of eigenvalues and eigenmodes on contact angle Θ is not presented. However, the results of some test cases, contact angles of 90 and 60 degrees with $B_\alpha = 0$ and $h_o = 3$, show the dramatic effect of varying the contact angle: The eigenmode h_1 changes its shape--from concave to generally convex--as the contact angle is decreased

from 90 to 5 degrees. This is shown in Figure 7 (where the three eigenmodes have been normalized to a common value at $r = 1$). The first eigenmode becomes sharply peaked near the wall as the contact angle is reduced. However, its derivative must be zero at $r = 1$ to satisfy the fixed contact angle condition, which is built into the calculations. The fundamental eigenvalues ω_1^2 for these three cases are 6.24 for $\Theta = 90$ degrees, 5.04 for $\Theta = 60$ degrees, and 2.81 for $\Theta = 5$ degrees; the first two values agree well with earlier calculations by a different method.(2)

The dependence of the eigenmode shape on Bond number is significant at small contact angles. For $\Theta = 5$ degrees and $h_o = 3$, large depth, this is shown in Figure 8 for the fundamental eigenmode h_1. (Again the three curves are normalized to a common value at $r = 1$.) Although an examination of Table I would suggest that $B_\alpha = 50$ is close to the asymptotic range in so far as the first eigenvalue is concerned, Figure 8 indicates that this is not the case for eigenmodes. Albeit the fundamental for $B_\alpha = 50$ has acquired thoughout most of the tank the concave shape characteristic of very large Bond numbers, it still retains a convex region with a peak near the wall. By contrast, the eigenmodes for $\Theta = 90$ degrees do not vary with B_α provided the liquid depth is large.

Variation of the liquid depth for a given Bond number has surprisingly little effect upon the shape of the fundamental eigenmode under low gravity conditions. This is shown for the zero gravity case in Figure 9. Again by contrast, variation of depth when $B_\alpha = \infty$ produces significant change in the eigenmode shapes.(18)

Response to Lateral Perturbations. Most engineering interest centers on the vertical rise of the liquid at the wall when lateral accelerations perturb the equilibrium. For a sinusoidal perturbation of amplitude $\hat{B}_\tau$ and frequency ω_o, say $B_\tau = \hat{B}_\tau \sin \omega_o t$, the maximum excursion at the wall occurs at $t = \pi/2\omega_o$. For this t, (29) specializes to

$$h\Big]_{\substack{\theta=0 \\ r=r_w}} = \frac{\hat{B}_\tau}{1+B_\alpha} \sum_{k=1}^{\infty} \frac{1}{1-(\omega_o/\omega_k)^2} \frac{D_k \Psi_k(r_w)}{\omega_k^2} \tag{111}$$

where D_k, defined by (23), is the Fourier coefficient in the expansion $r = \sum D_k \Phi_k$ and

$$\Psi_k(r) = \omega_k h_k(r) = \left[(1+f_r^2)^{1/2} \frac{\partial \Phi_k}{\partial n} \right]_{z=f(r)} . \tag{112}$$

Because

$$D_k \Psi_k(r_w)/\omega_k^2 = (D_k/\omega_k) h_k(r_w) , \tag{113}$$

(111) is a linear combination of kth mode responses at the wall. For all cases in the survey, the quantities needed to evaluate (111) are tabulated for the first five normal modes: ω_k^2 in Table I, D_k in Table IIa, and $\Psi_k(r_w) = \omega_k h_k(r_w)$ in Table IIb.

The first five eigenmodes, $h_k(r)$, for $B_\alpha = 0$ and $h_o = 1/4$ are plotted in Figure 10. The vertical scale is compressed compared to the horizontal scale to accommodate the common normalization of the computations and Table IIb. The characteristics of the higher eigenmodes ($k \geq 2$) are

(1) their oscillatory nature; (2) the existence of a small region near the wall in which the magnitude is much larger than elsewhere in the tank; and (3) the decrease in size of this small region with k.

Examination of Table IIa and extrapolation of the trend in Figure 10 suggests that the D_k do eventually alternate in sign as k increases. The negative signs of D_2 for large B_α seem to continue a decreasing trend established for smaller values of B_α. The anomalies in sign of D_4 and D_5 for $B_\alpha = 0$ seem to be part of a family that travels to higher values of k with increasing B_α--it appears in D_5 for $B_\alpha = 1$ and 2 and can be traced in higher modes at larger B_α. (Scattered evidence has been produced to suggest that the alternation is reestablished beyond the anomaly.) Because the eigenmodes are normalized so that $h_k(r_w)$ alternate in sign, so do the columns in Table IIb. Thus, it turns out that the products $D_k \Psi_k$, $k \geq 2$, are generally negative for factors taken from a common line in Tables IIa and IIb. The exceptions are the anomalies just noted.

The products $D_k \Psi_k$ are independent of the normalization of Φ_k and h_k (page 71) and tend to be of comparable, moderate orders of magnitude for a common line in Tables IIa and IIb. Hence, the convergence of the series (111) depends mainly upon the imposed frequency ω_o being markedly different from the natural frequencies ω_k. For $\omega_o < \omega_1$, the growth of ω_k^2 with k enforces the convergence, and the five terms from Tables IIa and IIb have sufficed to give three significant figures, in general.

Figure 11 (all quantities are dimensionless) gives the maximum rise height h_w for the sinsusoidal perturbation $B_\tau = \hat{B}_\tau \sin \omega_o t$ calculated from (111) as a function of ω_o/ω_1, the ratio of the perturbing to the fundamental frequency. The plotted ordinate is $h_w/\hat{B}_\tau$ where $\hat{B}_\tau = \rho \hat{g}_\tau r_o^2/\sigma$ is the maximum value of the transverse Bond number; the parameters are the depth $h = \bar{h}/r_o$ and the axial Bond number $B_\alpha = \rho g_\alpha r_o^2/\sigma$. The expected resonance at $(\omega_o/\omega_1)^2$ is indicated. The effect of increasing B_α is to reduce the response to lateral perturbing accelerations. Note also that the effect of decreasing h_o is unnoticeable at $B_\alpha = 0$, but as B_α increases, the response is further reduced.

Although the responses to the square wave and the periodic pulsing lateral perturbing accelerations (see Figure 12) do not necessarily reach their maximum rise height at the wall for time $t = \pi/2\omega_o$, specializing (30) and (31) to this value of t leads to a useful comparison. The specializations are in view of (113) linear combinations of $h_k(r_w)$, namely:

Square wave:

$$h\Big]_{\substack{\theta=0 \\ r=r_w}} = \frac{\hat{B}_\tau}{1+B_\alpha} \frac{4}{\pi} \sum_{k=1}^{\infty} \left[\sum_{\substack{m=1 \\ m \text{ odd}}}^{\infty} \frac{(-1)^{\frac{m-1}{2}}}{m\left[1-(\frac{m\omega_o}{\omega_k})^2\right]} \right] \frac{D_k \Psi_k(r_w)}{\omega_k^2} \quad \text{and} \qquad (114)$$

Periodic pulse:

$$h\Big]_{\substack{\theta=0 \\ r=r_w}} = \frac{\hat{B}_\tau}{1+B_\alpha} \frac{4}{\pi} \sum_{k=1}^{\infty} \left[\sum_{\substack{m=1 \\ m \text{ odd}}}^{\infty} \frac{\sin \frac{m\delta\pi}{2}}{m\left[1-(\frac{m\omega_o}{\omega_k})^2\right]} \right] \frac{D_k \Psi_k(r_w)}{\omega_k^2} \qquad (115)$$

where D_k is given by (23), $\Psi_k(r)$ by (112), and $\delta = \Delta t\, \omega_o/\pi$ is the ratio of the pulse width to the half-period. The inner series in (114) and (115) are clearly convergent and depend only on the ratio ω_o/ω_k. However, the dominant term may occur very far out in the series if ω_k/ω_o is a close approximation to an odd integer. Worse yet, resonance occurs if ω_o is an odd submultiple of a natural frequency ω_k. An effect of the submultiple resonances is to admit negative rise heights at the wall. Consequently, evaluation of (114) and (115) in a survey for the cases reported here, even with ω_o restricted to $o < \omega_o < \omega_1$, is bound to yield "noisy" results. Nevertheless, because the evaluations are instructive, Tables IIIa and IIIb give the values of $h_w/\hat{B}_\tau$ obtained from (114) and (115) for selected ratios of ω_o/ω_1 (with the same parameters as used in plotting the sinusoidal perturbations). In Table IIIb, the value of δ is 0.01.

In Table IIIa, even though the entries are not maximum rise heights, the effect of the resonance at $\omega_o = \omega_1$ seems to be more pronounced than in the sinusoidal case--in fact, the positive values in the last columns lie well above the corresponding curves in Figure 11. In common with the sinusoidal case, the effect of decreasing B_α seems to be to reduce the response. Again, the effect of decreasing h_o is almost unnoticeable for $B_\alpha = 0$, but results in a marked reduction of the response as B_α increases. The five terms presented in Tables I, IIa, and IIb generally are sufficient to give three digits in evaluating (114) for Table IIIa.

However, to obtain consistent results in evaluating (115) for Table IIIb, it is necessary to use all the terms available: that is, $D_k \Psi_k(r_w)/\omega_k^2$ for $k = 6$, 7, and 8 are included in most of the sums--although these values may not be reliable. The results in Table IIIb tend to confirm the conclusions drawn from the sinusoidal and square wave cases. Both Table IIIa and IIIb support the observation made earlier, namely that the method is best applied to the analysis of specific cases with a limited set of parameters so that the submultiple resonances can be clearly identified.

In principle, by appropriate modification, say replacing $\Psi_k(r_w)$ by $\Psi_k(r)$, analogues for (111), (114), and (115) can be developed to trace as a function of time the behavior of the free-surface throughout the tank in response to a lateral perturbation. However, contemplation of Figure 10 and the implications of (114) and (115) suggests that perhaps more eigenmodes of higher accuracy are needed to yield reliable results when the present method is applied throughout the tank.

Mechanical analog parameters for first mode lateral sloshing are shown in Figures 13 and 14, namely: the nondimensional equivalent spring constant, lateral force, equivalent mass, and lateral force action point. Here the function of the spring constant plotted in Figure 13, namely $\kappa_1/(1+B_\alpha)$, and the sloshing mass $\mathcal{M}$ in Figure 14 both decrease strongly with B_α toward the asymptotic values for $B_\alpha = \infty$. For large depths, others[3] report (in the normalization used here) $\kappa_1/(1+B_\alpha)$ as slowly increasing and $\mathcal{M}$ as increasing toward the asymptotic value with B_α. However, the

results of test calculations using the present program for $\Theta = 90$ degrees and large depth check well, for all four parameters, with the closed form solutions for $\Theta = 90$ degrees in a deep flat-bottomed tank. Consequently, even though the results for $\Theta = 5$ degrees must be viewed with some caution, they are considered valid because they are computed by a program that checks well for $\Theta = 90$ degrees and large depth.

Parameters are presented only for fundamental mode. The reason is that the parameters depend upon the potential along the tank wall as well as upon the potential on the free-surface; the former is less reliable than the latter. Only the fundamental gives parameters accurate enough to use. The parameters for higher modes are available in principal and await more accurate potentials.

The present data for the mechanical analog may be used when it can be definitely established that the first term in the series (see (111), (114), or (115)) is dominant. In such cases, the nondimensional right-hand side of (41), (42), (43), and (44) needed to implement the mechanical analog can be read from Figures 13 and 14 (the actual ordinates in the former are $\kappa_1/(1+B_\alpha)$ and $F_{x_1}/(1+B_\alpha)h_w$.

In capsule, the results of this study are that it is possible to compute at least the first five normal sloshing frequencies in a cylindrical tank with a hemispherical bottom under low gravitational conditions when the

free-surface is highly curved because of surface-tension effects. The simultaneous determination of normal sloshing eigenmodes permits representing the small-amplitude free-surface response to periodic lateral perturbations by expanding the surface shape in a truncated Fourier series. A survey of these expansions (restricted to the tank wall) shows that increasing the axial Bond number or decreasing the depth tends to reduce the response to lateral perturbations. Still further results are equivalent mechanical analog parameters which simplify routine engineering calculations of first mode sloshing under low gravitational conditions.

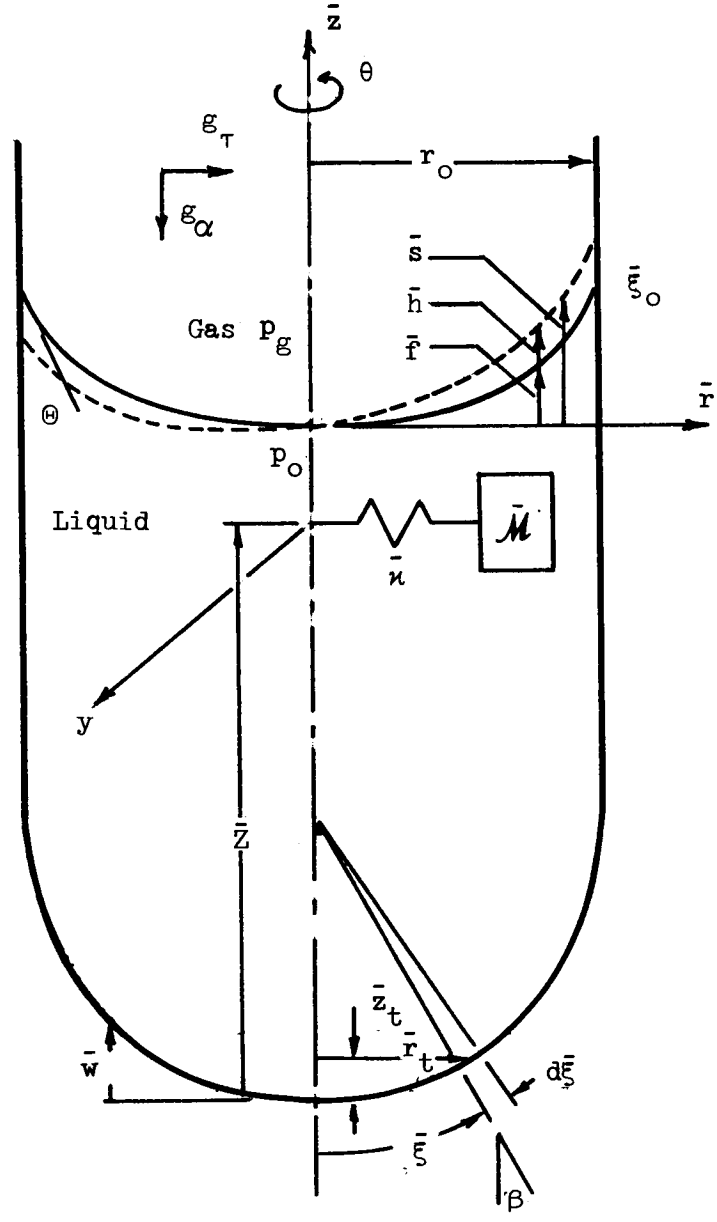

Container Geometry and Coordinate System

Figure 1

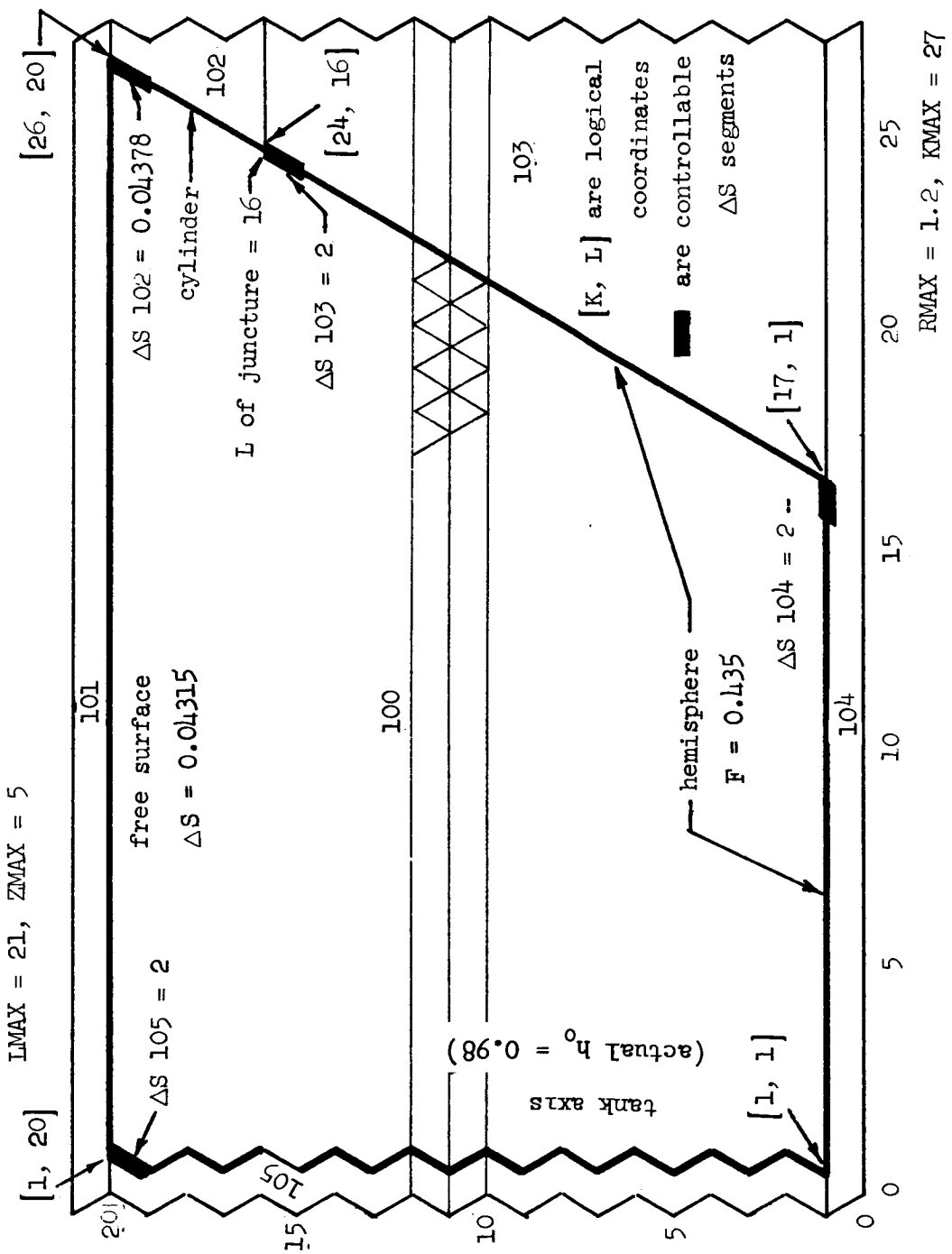

Logical Diagram for $B_\alpha = 50$, $h_o = 1$, @ = 5 degrees
25 free-surface computing points

Figure 2

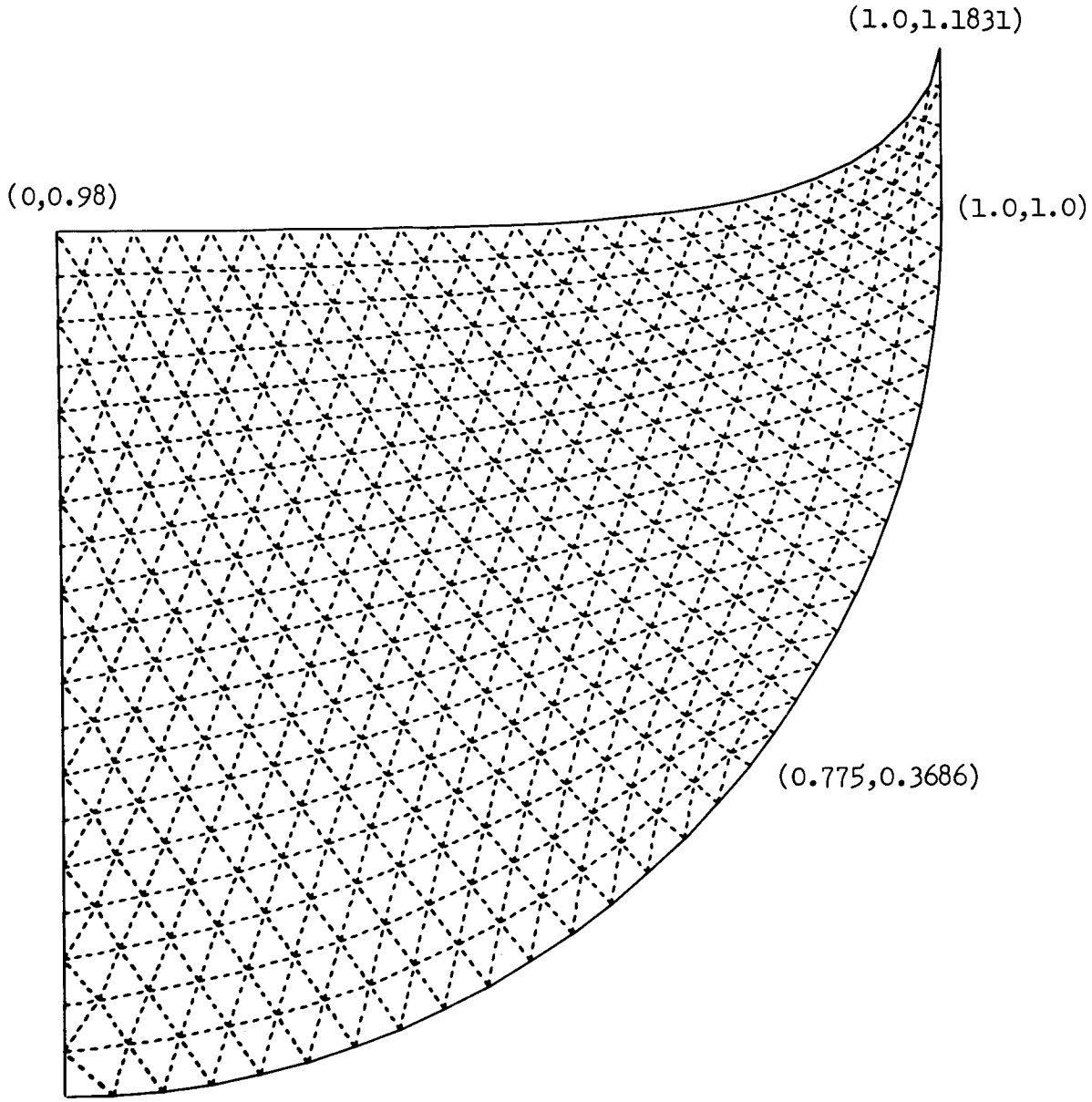

Physical Cross-section of D
Computing Mesh for $B_\alpha = 50$, $h_o = 1, \Theta = 5$ degrees
25 free-surface computing points

Figure 3

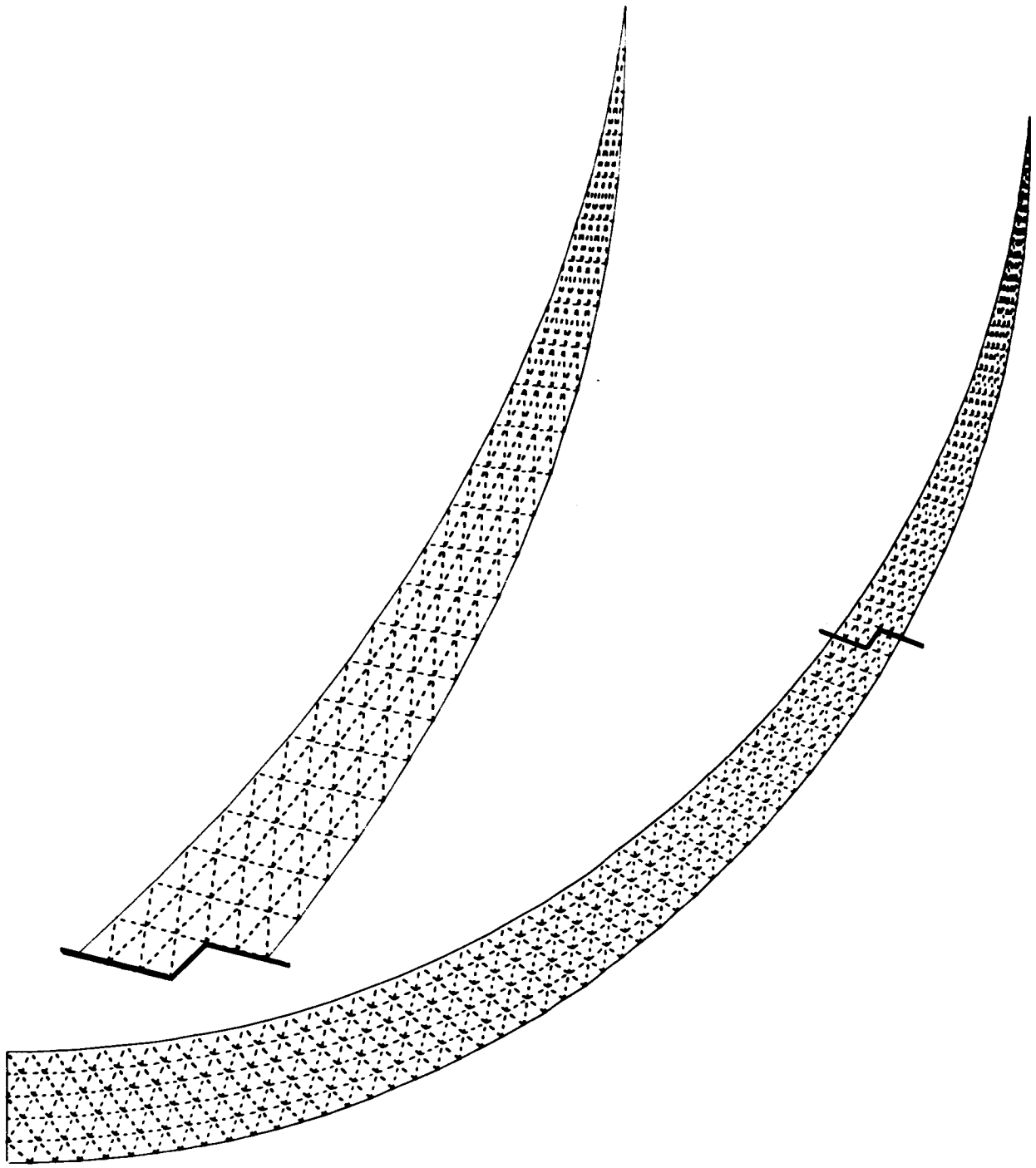

Computing Mesh for $B_\alpha = 0$, $h_o = 0.1$, $\Theta = 5$ degrees
65 free-surface computing points

Figure 4

TABLE I

Lateral Sloshing Eigenvalues
For Cylindrical Tank With Hemispherical Bottom
Θ = 5 degrees

Bond No. $B_\alpha = \rho g_\alpha r_o^2/\sigma$	Depth $h_o = \bar{h}_o/r_o$	Eigenvalues $\omega_k^2 = \bar{\omega}_k^2[(1+B_\alpha)\sigma/\rho r_o^3]^{-1}$				
		k = 1	2	3	4	5
0	3	2.81	34.6	137	353	723
	2	2.80	34.6	137	353	723
	1	2.69	34.0	136	353	723
	1/2	2.11	31.5	131	349	721
	1/4	1.33	24.8	113	314	675
	1/10	0.596	12.5	63.6	197	465
1	3	2.38	26.2	95.8	239	480
	2	2.38	26.2	95.8	239	480
	1	2.25	25.8	95.7	239	480
	1/2	1.65	23.6	92.0	235	477
	1/4	0.981	16.7	74.1	203	432
	1/10	0.403	12.5	73.0	239	578
2	3	2.21	22.4	78.3	191	380
	2	2.20	22.4	78.3	191	380
	1	2.07	22.1	78.3	191	381
	1/2	1.49	20.2	75.6	188	378
	1/4	0.717	11.8	54.2	154	338
	1/10	0.397	12.7	74.2	240	not produced
5	3	2.00	17.0	55.4	131	255
	1	1.85	16.8	55.3	131	255
	1/2	1.17	14.1	50.8	124	245
	1/4	0.615	9.93	45.7	129	279
	1/10	0.408	11.8	67.3	214	502
10	3	1.90	13.3	40.4	92.1	176
	2	1.90	13.3	40.4	92.2	177
	1	1.72	13.2	40.3	92.1	177
	1/2	1.02	10.4	35.1	83.5	164
	1/4	0.604	8.74	38.3	104.1	219
	1/10	0.434	10.6	58.2	180.5	417
20	3	1.85	10.2	28.6	62.5	117
	1	1.62	10.1	28.5	62.3	117
	1/2	0.941	8.11	25.5	58.9	114
	1/4	0.629	7.62	30.8	80.1	165
	1/10	0.475	9.34	48.1	144	325
50	3	1.84	7.54	18.2	36.7	65.2
	2	1.83	7.55	18.3	36.8	65.5
	1	1.58	7.48	18.2	36.6	65.1
	1/2	0.939	6.40	17.5	37.3	68.7
	1/4	0.701	6.41	22.1	52.7	103
	1/10	0.549	7.77	35.7	101	218

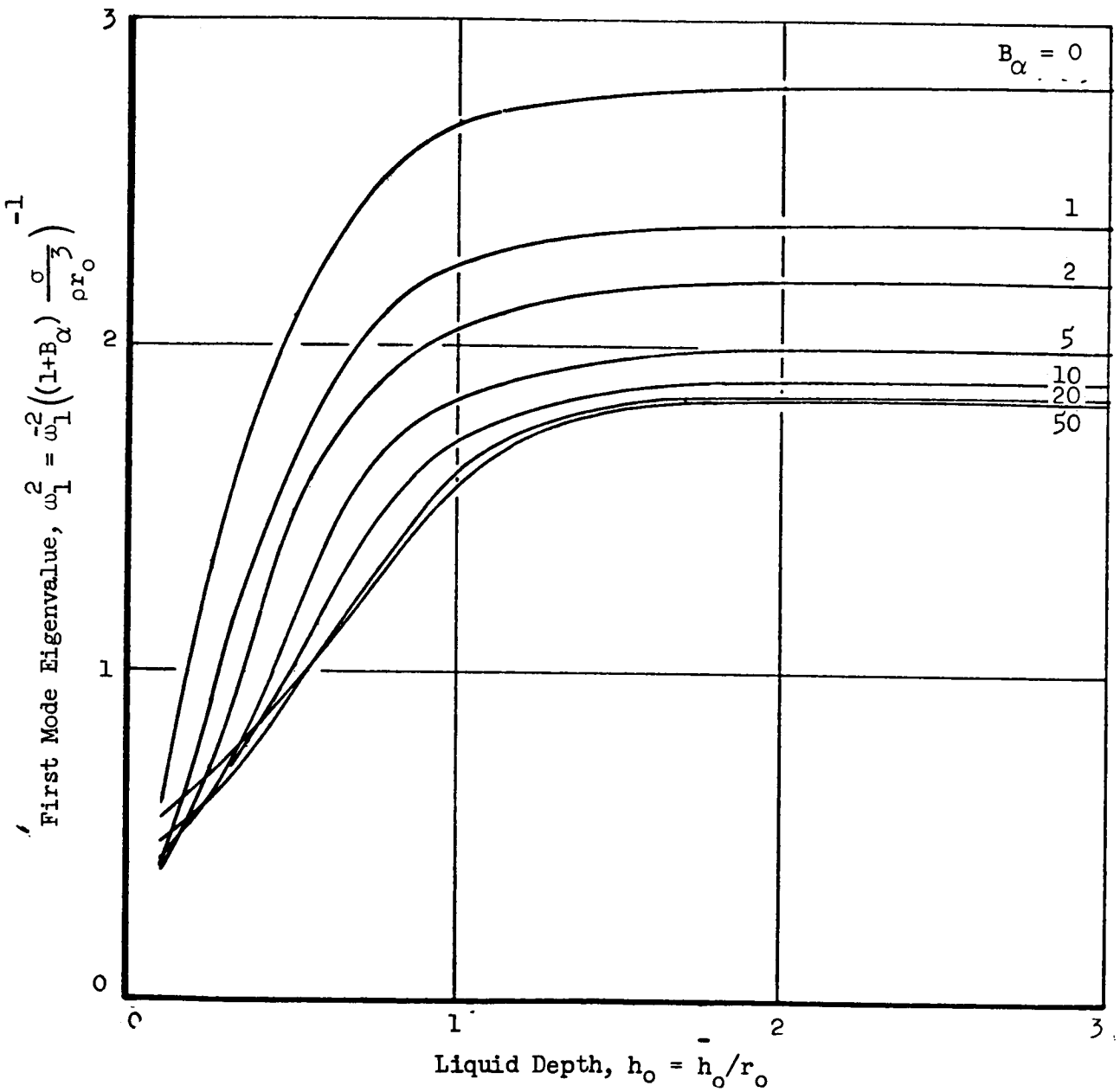

First Mode Eigenvalue for Lateral Sloshing in a Cylindrical Tank with Hemispherical Bottom

Θ = 5 degrees

Figure 5

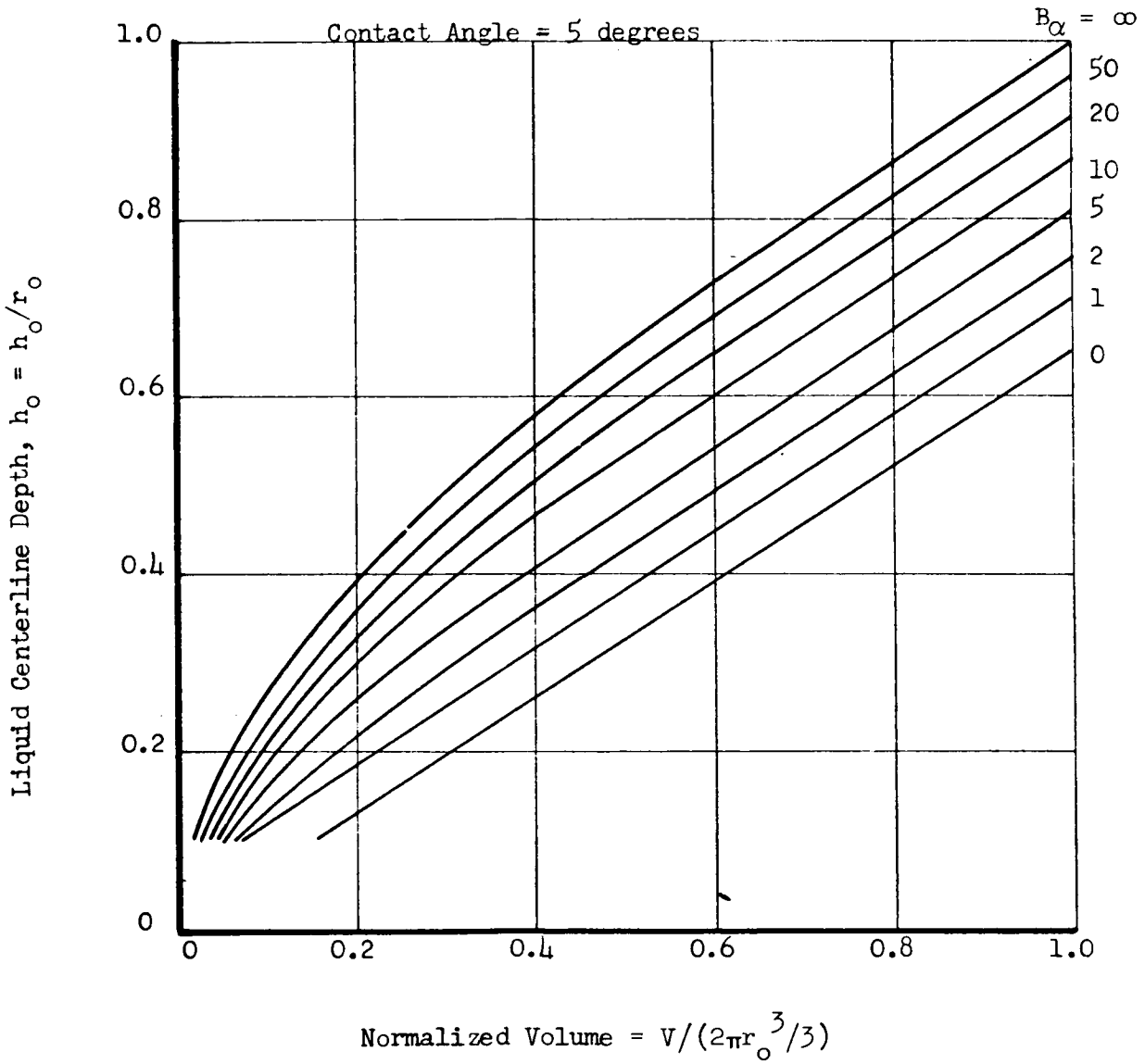

Liquid Centerline Depth - Tank Volume Relationship

Figure 6

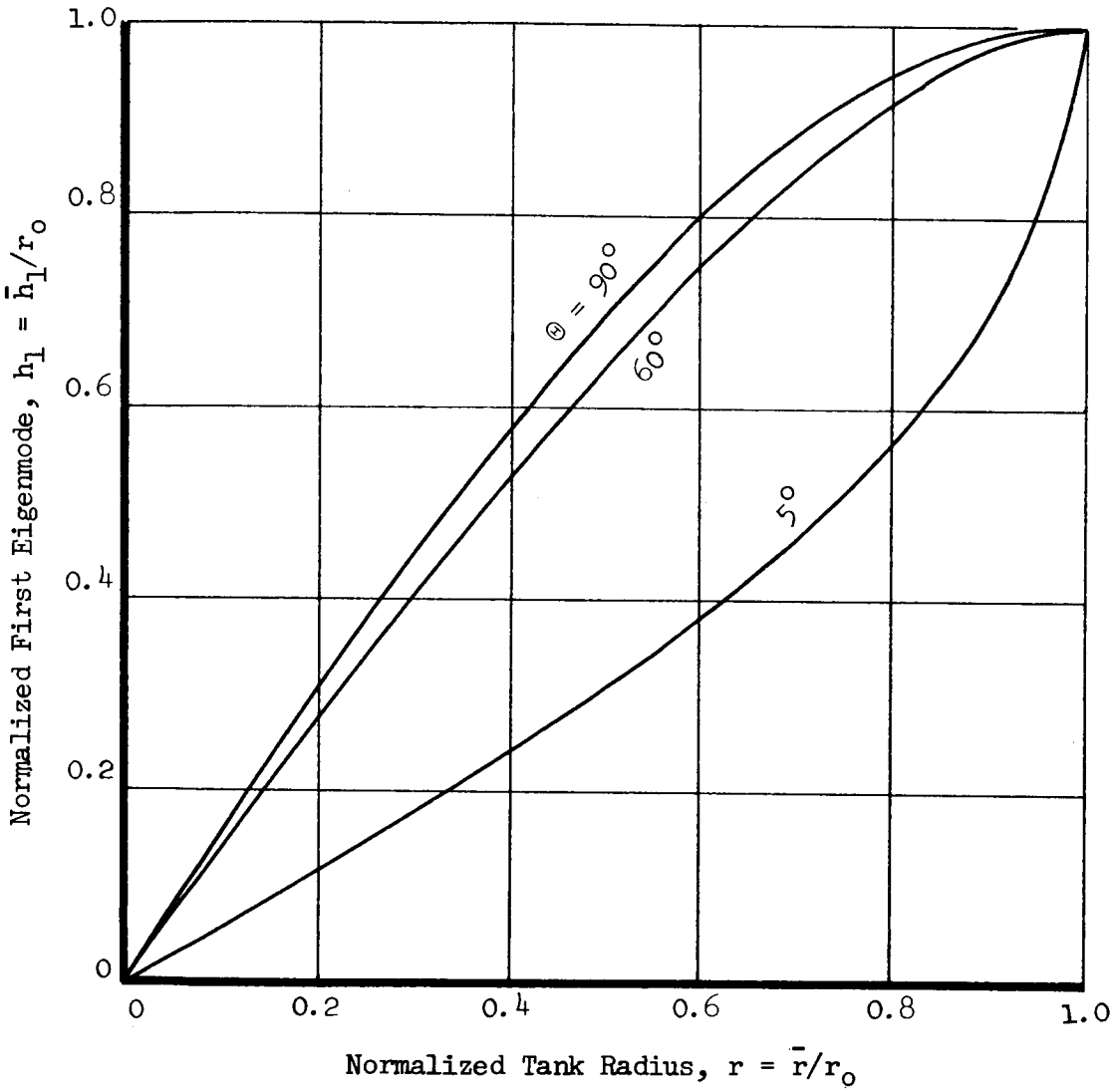

The Effect of Contact Angle on the First Eigenmode

$h_o = 3$, $B_\alpha = 0$

Figure 7

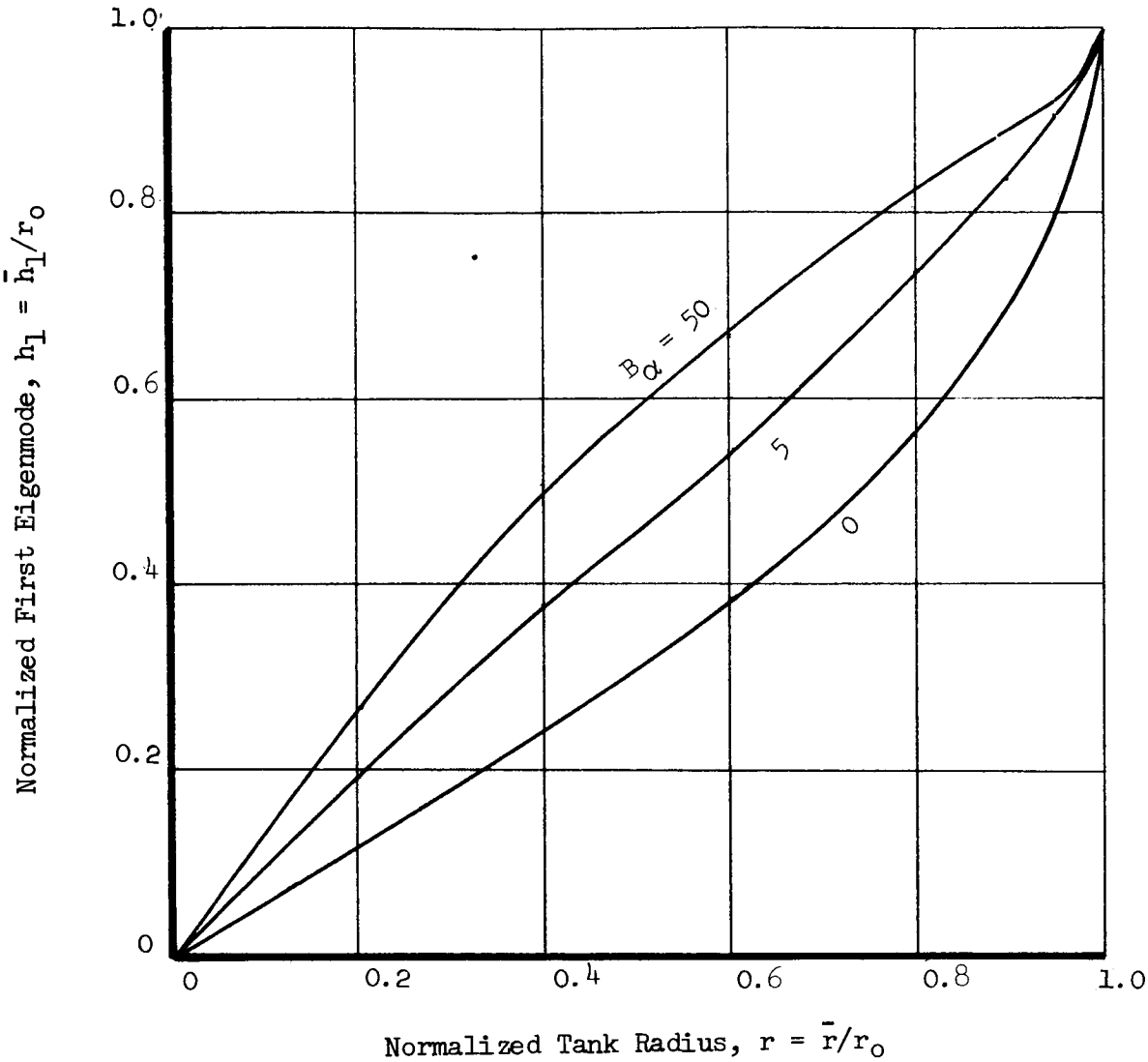

The Effect of Bond Number on the First Eigenmode
$h_o = 3$, $\Theta = 5$ degrees

Figure 8

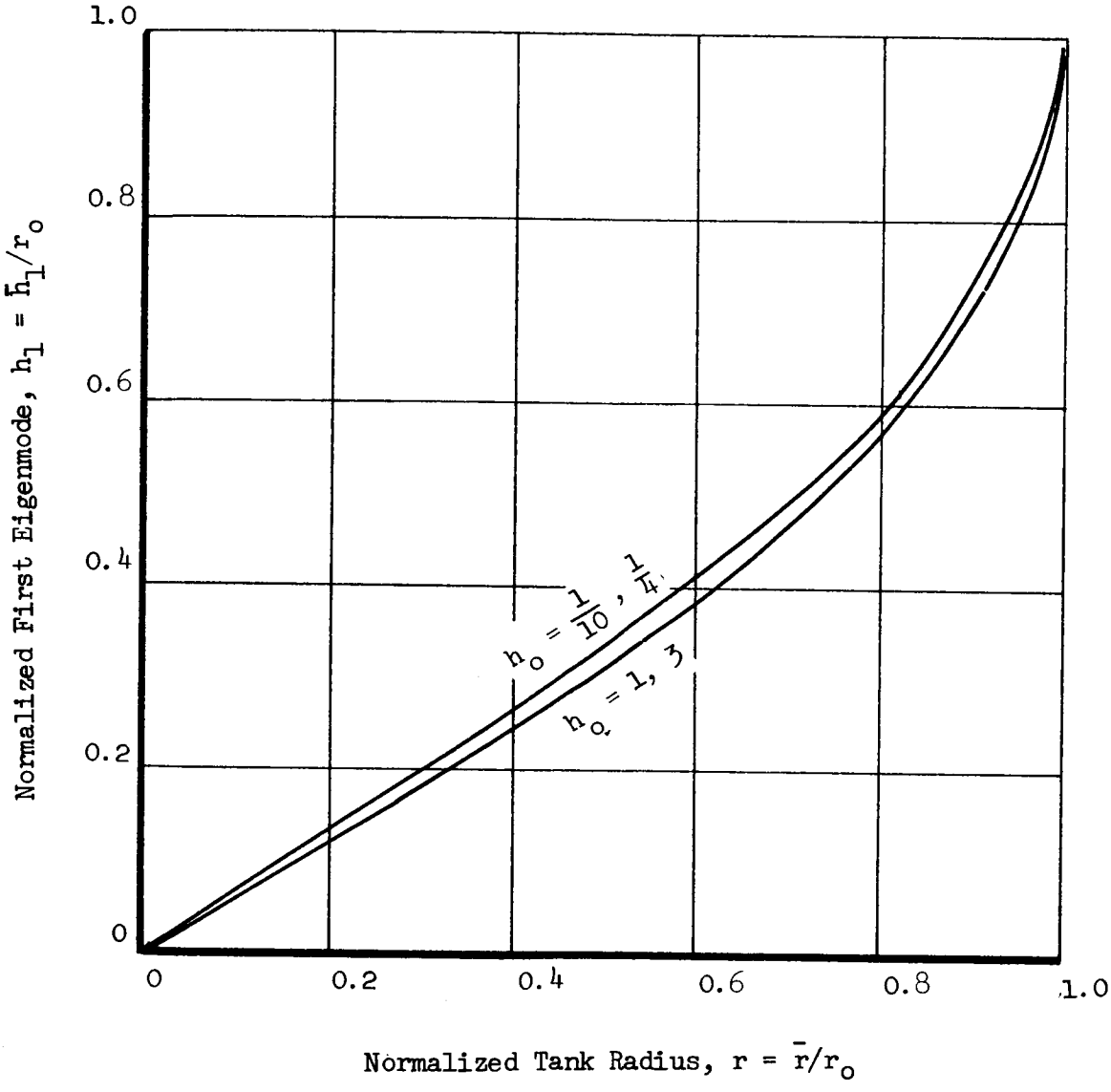

The Effect of Depth on the First Eigenmode
$B_\alpha = 0$, $\Theta = 5$ degrees

Figure 9

TABLE IIa

Fourier Coefficients

$$D_k = \left(\int_0^{r_w} r^2 h_k dr \right) \Big/ \left(\int_0^{r_w} \phi_k h_k r dr \right)$$

For Cylindrical Tank With Hemispherical Bottom
Θ = 5 degrees

Bond No. $B_\alpha = (\rho g_\alpha r_o^2/\sigma)$	Depth $h_o = \bar{h}_o/r_o$	k = 1	2	3	4	5
0	3	.492	.449-1	-.273-2	-.752-3	.325-3
	2	.492	.447-1	-.276-2	-.750-3	.325-3
	1	.493	.405-1	-.341-2	-.657-3	.344-3
	1/2	.494	.251-1	-.333-2	.199-3	.157-3
	1/4	.494	.143-1	-.163-2	.344-3	-.878-4
	1/10	.495	.980-2	-.638-3	.155-3	-.541-4
1	3	.548	.382-1	-.635-2	.195-3	.338-3
	2	.548	.381-1	-.636-2	.197-3	.337-3
	1	.549	.326-1	-.663-2	.397-3	.318-3
	1/2	.549	.177-1	-.425-2	.824-3	-.841-4
	1/4	.549	.155-1	-.163-2	.211-3	-.438-4
	1/10	.447	.124-1	-.764-3	.133-3	-.395-4
2	3	.579	.326-1	-.828-2	.111-2	.149-3
	2	.579	.325-1	-.828-2	.111-2	.149-3
	1	.578	.264-1	-.817-2	.131-2	.939-4
	1/2	.579	.140-1	-.455-2	.113-2	-.236-3
	1/4	.572	.232-1	-.227-2	.217-3	-.374-4
	1/10	.407	.110-1	-.792-3	.134-3	not produced
5	3	.621	.206-1	-.104-1	.303-2	-.625-3
	1	.621	.140-1	-.940-2	.309-2	-.717-3
	1/2	.621	.116-1	-.461-2	.126-2	-.299-3
	1/4	.555	.244-1	-.319-2	.472-3	-.931-4
	1/10	.348	.986-2	-.871-2	.151-3	-.440-4
10	3	.649	.821-2	-.103-1	.456-2	-.166-2
	2	.649	.801-2	-.102-1	.455-2	-.166-2
	1	.649	.171-2	-.835-2	.422-2	-.168-2
	1/2	.646	.158-1	-.674-2	.208-2	-.548-3
	1/4	.515	.233-1	-.372-2	.701-3	-.157-3
	1/10	.320	.937-2	-.957-3	.175-3	-.504-4
20	3	.671	-.609-2	-.782-2	.526-2	-.271-2
	1	.671	-.112-1	-.498-2	.420-2	-.241-2
	1/2	.638	-.183-1	-.820-2	.300-2	-.102-3
	1/4	.468	.221-1	-.421-2	.986-3	-.263-3
	1/10	.261	.913-2	-.106-2	.208-3	-.601-4
50	3	.687	-.269-1	-.115-2	.382-2	-.304-2
	2	.687	-.271-1	-.108-2	.379-2	-.303-2
	1	.687	-.271-1	.130-2	.221-2	-.217-2
	1/2	.599	.162-1	-.880-2	.400-2	-.176-2
	1/4	.412	.199-1	-.479-2	.143-2	-.463-3
	1/10	.215	.889-2	-.123-3	.272-3	-.817-4

Note: Tabulated numbers are in mantissa form; e.g. first number in k=3 column is -0.00273.

TABLE IIb

Unnormalized Eigenmode at Wall

$$\Psi_k(r_w) = \omega_k h_k(r_w) = \left[(1+f_r^2)^{1/2} \frac{\partial \Phi_k}{\partial n} \right]_{r=r_w}$$

For Cylindrical Tank With Hemispherical Bottom
Θ = 5 degrees

Bond No. $B_\alpha=(\rho g_\alpha r_o^2/\sigma)$	Depth $h_o=\bar{h}_o/r_o$	k = 1	2	3	4	5
0	3	.379+1	-.376+2	.119+3	-.258+3	.467+3
	2	.379+1	-.376+2	.119+3	-.258+3	.467+3
	1	.361+1	-.371+2	.119+3	-.258+3	.467+3
	1/2	.276+1	-.332+2	.116+3	-.257+3	.469+3
	1/4	.171+1	-.269+2	.103+3	-.241+3	.448+3
	1/10	.754	-.129+2	.550+2	-.142+3	.286+3
1	3	.320+1	-.300+2	.946+2	-.207+3	.379+3
	2	.320+1	-.300+2	.946+2	-.207+3	.379+3
	1	.300+1	-.298+2	.946+2	-.207+3	.379+3
	1/2	.215+1	-.277+2	.929+2	-.205+3	.377+3
	1/4	.126+1	-.191+2	.741+2	-.179+3	.346+3
	1/10	.487	-.679+1	.240+2	-.555+2	.103+3
2	3	.296+1	-.261+2	.818+2	.180+3	.331+3
	2	.295+1	-.261+2	.818+2	-.180+3	.331+3
	1	.274+1	-.260+2	.817+2	-.180+3	.331+3
	1/2	.194+1	-.239+2	.805+2	-.179+3	.331+3
	1/4	.917	-.117+2	.405+2	-.903+2	.163+3
	1/10	.516	-.697+1	.241+2	-.547+2	not produced
5	3	.268+1	-.200+2	.617+2	-.136+3	.252+3
	1	.244+1	-.200+2	.616+2	-.136+3	.252+3
	1/2	.152+1	-.170+2	.565+2	-.129+3	.242+3
	1/4	.820	-.853+1	.261+2	-.544+2	.942+2
	1/10	.613	-.756+1	.251+2	-.556+2	.100+3
10	3	.255+1	-.155+2	.464+2	-.102+3	.189+3
	2	.254+1	-.155+2	.464+2	-.102+3	.189+3
	1	.227+1	-.156+2	.464+2	-.102+3	.189+3
	1/2	.135+1	-.122+2	.362+2	-.773+2	.140+3
	1/4	.870	-.793+1	.226+2	-.455+2	.775+2
	1/10	.739	-.821+1	.262+2	-.568+2	.101+3
20	3	.249+1	-.118+2	.333+2	-.717+2	.132+2
	1	.216+1	-.119+2	.333+2	-.715+2	.131+3
	1/2	.130	-.928+1	.241+2	-.477+2	.820+2
	1/4	.991	-.786+1	.206+2	-.400+2	.669+2
	1/10	.920	-.900+1	.273+2	-.576+2	.101+3
50	3	.250+1	-.887+1	.213+2	-.430+2	.763+2
	2	.249+1	-.888+1	.214+2	-.431+2	.768+2
	1	.213+1	-.881+1	.213+2	-.429+2	.762+2
	1/2	.139+1	-.798+1	.176+2	-.323+2	.529+2
	1/4	.124+1	-.826+1	.192+2	-.353+2	.573+2
	1/10	.125+1	-.103+2	.285+2	-.756+2	.982+2

Note: Tabulated numbers in mantissa form. See Table IIa.

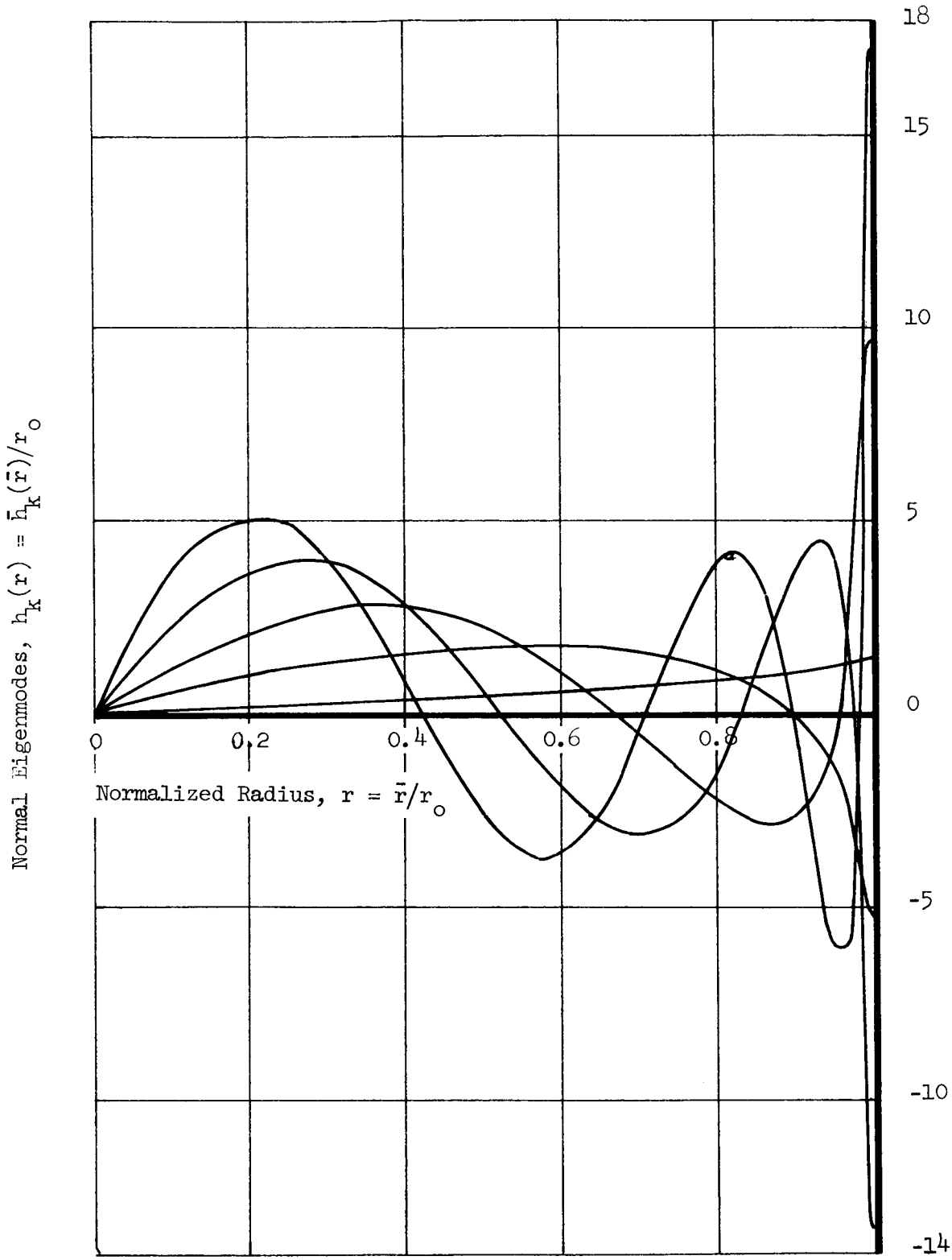

First Five Eigenmodes
$B_\alpha = 0$, $\Theta = 5$ degrees, $h_o = 0.25$

Figure 10

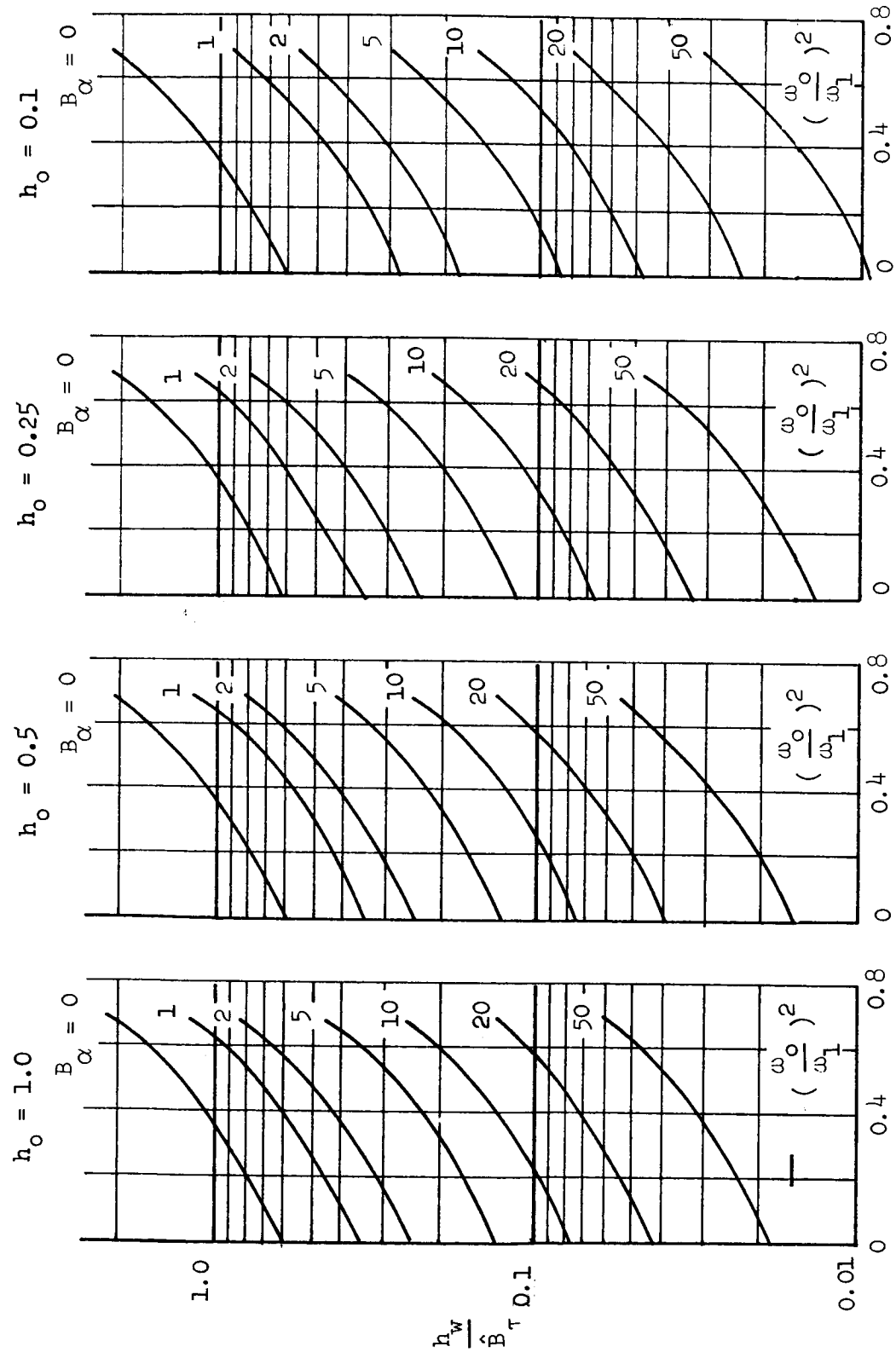

Lateral Sloshing Response to Sinusoidal Lateral Perturbing Acceleration
Cylindrical Tank with Hemispherical Bottom, Θ = 5 degrees

Figure 11

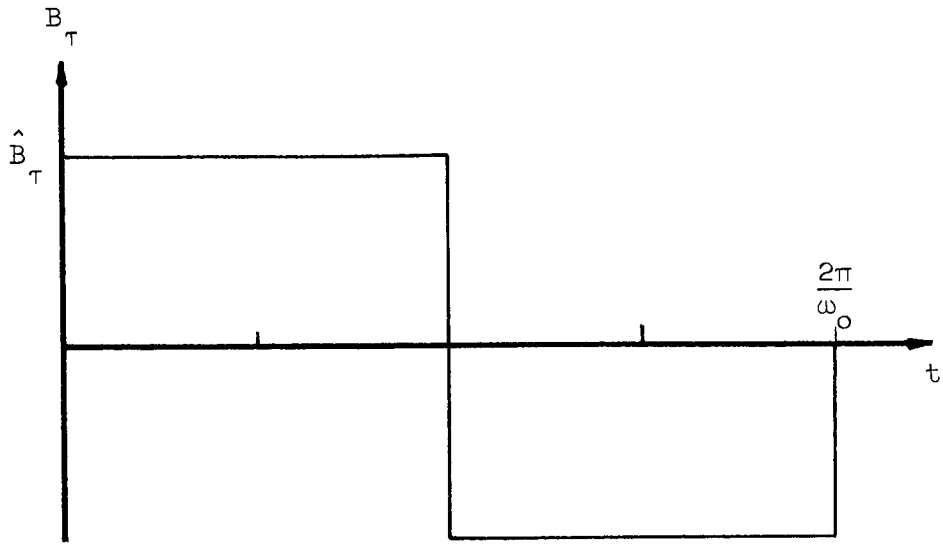

Square Wave Function

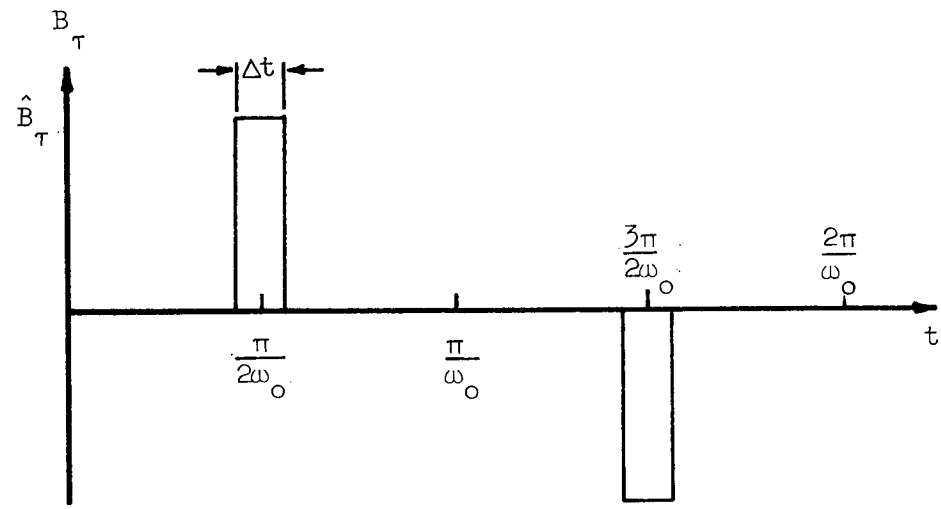

Periodic Pulse Function

Square Wave and Periodic Pulse Perturbing Accelerations

Figure 12

TABLE IIIa

Calculated Response
to
Square Wave Lateral Perturbing Acceleration
Θ = 5 degrees

$$\frac{h_w}{B_\tau} = \frac{\bar{h}_w}{r_o} \frac{\sigma}{\rho \hat{g}_\tau r_o^2}$$

Bond No. $B_\alpha = \rho g_\alpha r_o^2/\sigma$	Depth $h_o = \bar{h}_o/r_o$	$(\omega_o/\omega_1)^2$ = 0.01	0.03	0.1	0.2	0.5	0.7
0	3	.141+1	.128+1	-.159+1	.128+1	.262+1	.266+1
	2	.139+1	.127+1	-.160+1	.128+1	.267+1	.266+1
	1	.125+1	.128+1	-.175+1	.128+1	.557	.266+1
	1/2	.120+1	.120+1	-.160+1	.130+1	.156+1	.267+1
	1/4	.130+1	.178+1	-.191+1	.124+1	.166+1	.252+1
	1/10	.121+1	.125+1	-.185+1	.126+1	.160+1	.262+1
1	3	.580	.787	-.108+1	.722	.100+1	.148+1
	2	.585	.782	-.108+1	.722	.102+1	.148+1
	1	.631	.710	-.109+1	.710	.944	.148+1
	1/2	.656	.712	-.102+1	.718	.868	.150+1
	1/4	.646	.709	-.117+1	.675	.892	.156+1
	1/10	.532	.549	-.797	.552	.709	.114+1
2	3	.484	.458	-.768	.559	.649	.106+1
	2	.484	.458	-.770	.557	.649	.106+1
	1	.492	.423	-.748	.511	.657	.105+1
	1/2	.504	.457	-.723	.501	.607	.105+1
	1/4	.470	.490	-.674	.414	.608	.104+1
	1/10	.349	.360	-.520	.362	.461	.742
5	3	.234	.284	-.416	.256	.351	.564
	1	.244	.260	-.413	.252	.350	.562
	1/2	.248	.270	.212	.272	.370	.568
	1/4	.238	.254	-.349	.471	.309	.523
	1/10	.170	.186	-.296	.178	.228	.368
10	3	.142	.157	-.232	.150	.197	.334
	2	.142	.157	-.232	.150	.197	.333
	1	.150	.156	-.221	.147	.193	.329
	1/2	.147	.148	-.231	.160	.202	.349
	1/4	.126	.130	-.195	.136	.167	.282
	1/10	.906-1	.954-1	-.137	.100	.178	.197
20	3	.853-1	.823-1	-.127	.103	.111	.176
	1	.831-1	.882-1	-.129	.839-1	.112	.128
	1/2	.770-1	.999-1	-.130	.796-1	.108	.173
	1/4	.623-1	.697-1	.553	.701-1	.980-1	.146
	1/10	.473-1	.477-1	-.709-1	.476-1	.615-1	.100
50	3	.377-1	.379-1	-.557-1	.410-1	.520-1	.818-1
	2	.378-1	.379-1	-.558-1	.401-1	.521-1	.817-1
	1	.385-1	.380-1	-.519-1	.362-1	.452-1	.821-1
	1/2	.284-1	.423-1	-.499-1	.328-1	.446-1	.739-1
	1/4	.259-1	.267-1	-.421-1	.261-1	.362-1	.586-1
	1/10	.181-1	.187-1	-.277-1	.193-1	.240-1	.403-1

Note: Tabulated numbers in mantissa form. See Table IIa.

TABLE IIIb

Calculated Response
to
Periodic Pulse Lateral Perturbing Acceleration
of Width $0.01\ \pi/\omega_o$ for $\Theta = 5$ degrees

$$\frac{h_w}{\hat{B}_\tau} = \frac{\bar{h}_w}{r_o} \frac{\sigma}{\rho \hat{g}_\tau r_o^2}$$

Bond No. $B_\alpha = \rho g_\alpha r_o^2/\sigma$	Depth $h_o = \bar{h}_o/r_o$	$(\omega_o/\omega_1)^2 =$ 0.01	0.03	0.1	0.2	0.5	0.7
0	3	-.122	.273-1	.684-1	-.760-2	.986-1	.384-1
	2	-.113	.270-1	.699-1	-.790-2	.102	.384-1
	1	-.263-1	.301-1	.987-1	-.880-2	-.628-1	.385-1
	1/2	-.306-1	.248-1	.203	-.170-2	.131-1	.395-1
	1/4	-.544-1	.375	.970-1	-.920-2	.310-1	.381-1
	1/10	-.400-3	.259-1	.121	-.900-2	.194-1	.357-1
1	3	-.438-1	-.144-1	.694-1	-.820-2	.228-1	.188-1
	2	-.405-1	-.128-1	.689-1	-.810-2	.252-1	.173-1
	1	-.890-2	.490-2	.754-1	-.560-2	.136-1	.208-1
	1/2	-.120-2	-.730-2	.653-1	-.180-2	.920-2	.240-1
	1/4	-.820-2	.103-1	.375-1	-.930-2	.100-1	.273-1
	1/10	-.100-3	.990-2	.509-1	-.290-2	.660-2	.164-1
2	3	-.430-2	.127-1	.503-1	-.131-1	.830-2	.122-1
	2	-.340-2	.129-1	.507-1	-.128-1	.840-2	.123-1
	1	.940-2	.250-1	.467-1	-.670-2	.960-2	.137-1
	1/2	.390-2	.560-2	.462-1	-.380-2	.520-2	.146-1
	1/4	.134-1	.480-2	.516-1	-.128-1	.670-2	.168-1
	1/10	.330-2	.890-2	.333-1	-.160-2	.510-2	.110-1
5	3	-.740-2	.142-1	.233-1	-.120-2	.340-2	.750-2
	1	.430-2	.200-2	.242-1	.300-3	.380-2	.810-2
	1/2	.390-2	.460-2	-.797-1	-.230-2	.580-2	.790-2
	1/4	.130-2	.000	.242-1	.299-1	.340-2	.800-2
	1/10	.400-3	-.170-2	.600-2	-.110-2	.250-2	.520-2
10	3	.100-3	.200-2	.154-1	-.120-2	.230-2	.350-2
	2	.500-3	.260-2	.155-1	-.120-2	.240-2	.390-2
	1	-.320-2	.260-2	.135-1	.700-3	.300-2	.450-2
	1/2	.240-2	.320-2	.151-1	-.300-2	.260-2	.170-2
	1/4	.100-3	.220-2	.122-1	-.600-3	.170-2	.400-2
	1/10	-.100-3	.240-2	.880-2	-.160-2	-.490-2	.270-2
20	3	-.120-2	.150-2	.780-2	.180-2	.100-2	.330-2
	1	.900-3	.220-2	.790-2	-.100-3	.130-2	-.230-2
	1/2	-.180-2	.630-2	.550-2	-.400-3	.100-2	.230-2
	1/4	.200-2	.120-2	-.106	-.600-3	.180-2	.200-2
	1/10	.400-3	.700-3	.450-2	-.100-3	.700-3	.130-2
50	3	-.100-3	.900-3	.370-2	.200-3	.500-3	.800-3
	2	.200-3	.800-3	.370-2	-.500-3	.500-3	.100-2
	1	.300-3	.400-3	.330-2	-.400-3	.800-3	.110-2
	1/2	.360-2	.200-3	.290-2	-.300-3	.600-3	.700-3
	1/4	.200-3	.300-3	.250-2	.000	.400-3	.140-2
	1/10	.000	.300-3	.180-2	-.100-3	.200-3	.600-3

Note: Tabulate numbers in mantissa form. See Table IIa.

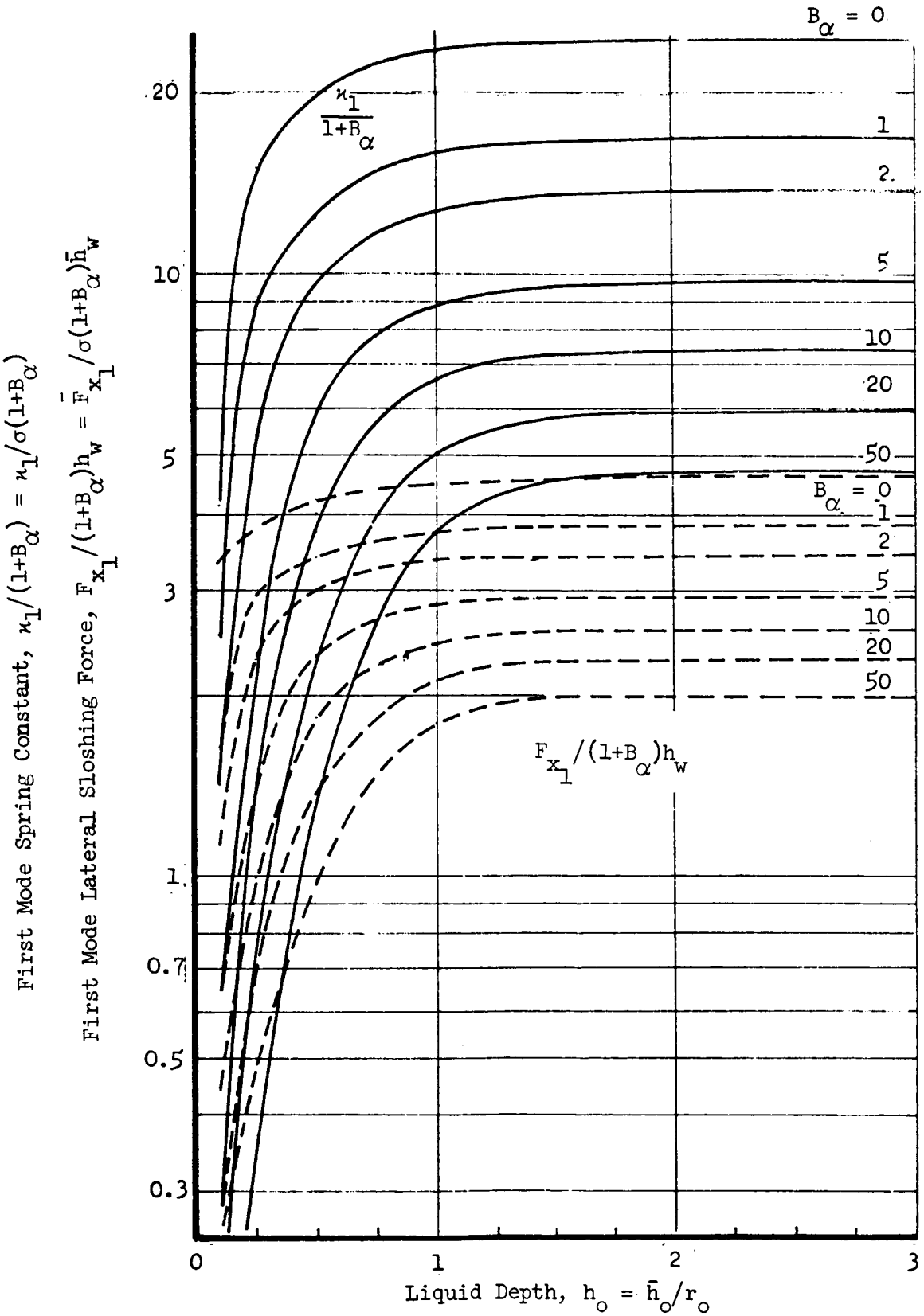

First Mode Mechanical Analog Spring Constant and Lateral Force
Cylindrical Tank With a Hemispherical Bottom

Θ = 5 degrees

Figure 13

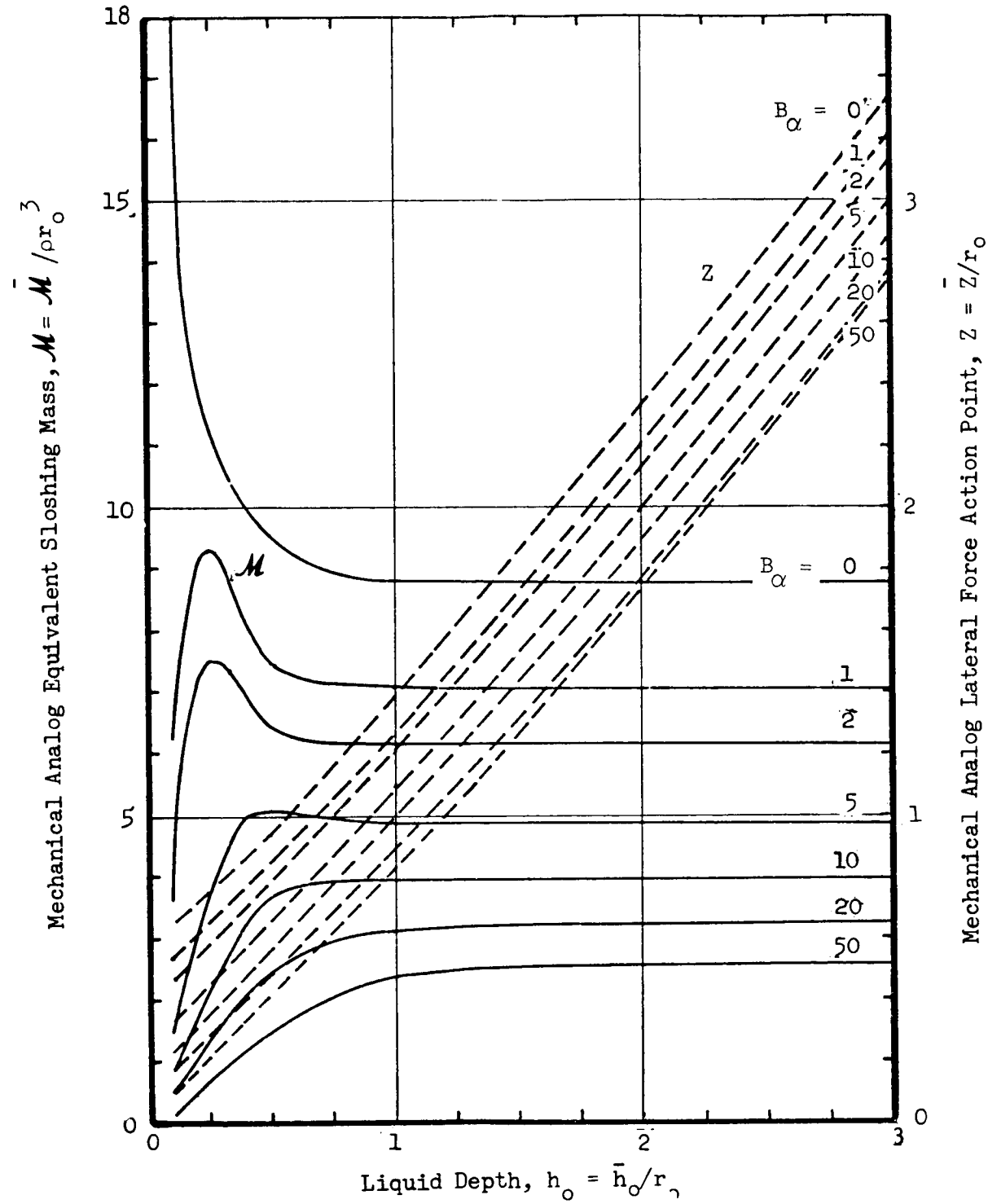

First Mode Mechanical Analog Sloshing Mass and Lateral Force Action Point for Lateral Sloshing in a Cylindrical Tank With a Hemispherical Bottom
Θ = 5 degrees

Figure 14

REFERENCES

1. Lamb, H., Hydrodynamics, Dover, 1955, Ch. IX.

2. Satterlee, H. M. and Reynolds, W. C., The Dynamics of the Free Liquid Surface in Cylindrical Containers Under Strong Capillary and Weak Gravity Conditions, Stanford University Dept. Mech. Engr. rpt. no. LG-2, Stanford, Calif., May 1, 1964.

3. Dodge, F. T. and Garza, L. R., Experimental and Theoretical Studies of Liquid Sloshing at Simulated Low Gravities, TR rpt. no. 2, Contract NAS 8-20290 by Southwest Research Inst. for Geo. C. Marshall Spaceflight Center, 20 Oct. 66.

4. Moiseev, N. N., and Petrov, A. A., The Calculation of Free Oscillations of a Liquid in a Motionless Container, Advances in Applied Mechanics, vol. 9, Academic Press, New York, 1966, pp 91-154.

5. Abramson, N. H. (ed) The Dynamic Behavior of Liquids in Moving Containers, NASA SP-106, 1966.

6. Davis, P. J., and Rabinowitz, P.; Advances in Orthonormalizing Computation, Advances in Computers, vol. 2, Academic Press, New York, 1961, p 79.

7. Satterlee and Reynolds, op. cit. pg 50.

8. Satterlee and Reynolds, op. cit. pp 37-8.

9. Winslow, Alan M., An Irregular Triangle Generator, UCRL-7880, Univ. of Calif., Lawrence Radiation Laboratory, Livermore, Calif., Aug. 25, 1964.

10. Winslow, A. M., Numerical Solution of the Quasi-Linear Poisson Equation in a Nonuniform Triangle Mesh, J. Comp. Physics, vol. 1,no. 2, (1966/67), to appear.

11. Kellogg, R. B., Difference Equations on a Mesh Arising from a General Triangulation, Math. Comp. 18 (1964) 203-210.

12. Varga, R. S., Matrix Iterative Analysis, Prentice-Hall, Inc., Englewood Cliffs, N. J., 1962, pp. 161-173.

REFERENCES, Cont.

13. Ostrowski, A. M., On the Convergence of the Rayleigh Quotient Iteration for the Computation of Characteristic Roots and Vectors, I, II, III, IV, V, VI, Arch. Rat. Mech. Anal. 1 (1957/58) 233-241, 2 (1958/59) 423-428, 3 (1959), 325-40, 3 (1959) 341-347, 3 (1959), 472-481, 4 (1959/60) 153-165.

14. Gantmacher, F. R., The Theory of Matrices, vol. I, Chelsea Publishing Co., New York, 1959, Chapter X, Paragraphs 6 and 7, pp. 310-326.

15. Wilkinson, J. H., The Algebraic Eigenvalue Problem, Oxford Univ. Press, Oxford, 1965, pp. 221-232 and 619-629.

16. Wilkinson, J. H., Rounding Errors in Algebraic Processes, Prentice-Hall, Inc., Englewood Cliffs, N. J., 1963, pp 142-147.

17. Reynolds, W. C., Saad, M. A., and Satterlee, H. M., Capillary Hydrostatics and Hydrodynamics at Low g. Stanford Univ. Dept. Mech. Engr. rpt no. LG-3, Stanford, Calif., Sept. 1, 1964, p 52.

18. Budiansky, B., Sloshing of Liquids in Circular Canals and Spherical Tanks, J. of the Aerospace Sciences, 27(1960) 161.

DISTRIBUTION LIST FOR SUMMARY REPORT

Contract NAS3-7119

Address	Number of Copies
1. National Aeronautics and Space Administration Washington, D. C. Attn: RV-1/Warren Keller	2
2. NASA-Lewis Research Center 21000 Brookpark Road Cleveland, Ohio 44135	
Attn: Spacecraft Technology Procurement Section (M.S. 54-2)	1
Attn: Technology Utilization Office (M.S. 3-19)	1
Attn: Technical Information Division (M.S. 5-5)	1
Attn: Library (M.S. 60-3)	2
Attn: Spacecraft Technology Division	
a. C. C. Conger (M.S. 54-1)	1
b. W. J. Masica (M.S. 54-3)	1
c. D. A. Petrash (M.S. 54-1)	25
d. E. W. Otto (M.S. 54-1)	1
Attn: Report Control Office (M.S. 5-5)	1
3. NASA Scientific and Technical Information Facility P. O. Box 33 College Park, Maryland 20740 Attn: NASA Representative RQT-2448	6
4. Southwest Research Institute 8500 Culebra Road San Antonio, Texas 78206 Attn: Dr. H. Norman Abramson	1
5. Dr. Marvin Adelberg 4043 Cody Road Sherman Oaks, California 91403	1
6. TRW Space Technology Laboratory One Space Park Redondo Beach, California 90278	
Attn: R. Pravin Bhuta	1
Attn: Dr. R. E. Hutton	1

Address	Number of Copies
7. University of Washington Seattle, Washington 98105 Attn: Dr. C. P. Costello	1
8. Bell Aerosystems Buffalo, New York 14240 Attn: Minas Ensanian	1
9. University of California Los Angeles, California 90024 Attn: Dr. K. E. Forster	1
10. Advanced Technology Laboratoris General Electric Company Schenectady, New York 12301 Attn: Dr. Novak Zuber Attn: Mr. R. F. Gaertner	1 1
11. Massachusetts Institute of Technology Cambridge, Massachusetts 02139 Attn: Dr. Peter Griffith	1
12. Space and Information Systems Div. North American Aviation, Inc. 12214 Lakewood Blvd. Downey, California 90241 Attn: Donald J. Simkin Attn: Dr. Francis C. Hung	1 1
13. Midwest Research Institute 425 Volker Boulevard Kansas City, Mo. 64110 Attn: Dr. Sheldon Levy	1
14. Washington State University Pullman, Washington 99163 Attn: Dr. John H. Lienhard	1
15. University of Michigan Ann Arbor, Michigan 48106 Attn: Dr. John A. Clark Attn: Dr. H. Merte, Jr.	1 1

Address:	Number of Copies
16. Astronautics/Propulsion Martin Denver Division Denver, Colorado 80201 Attn: Howard L. Paynter Mail Stop T-14	1
17. Marshall Space Flight Center Huntsville, Alabama 35812 Attn: Frank Swalley Attn: Gordon Platt	1 1
18. Spacecraft Thermodynamics Dept. Lockheed Missile & Space Company Sunnyvale, California 94008 Attn: Dr. Hugh M. Satterlee	1
19. Manned Spacecraft Center 2101 Webster-Seabrook Road Houston, Texas 77058 Attn: Jerry C. Smithson (Mail Stop EP-21)	1
20. Mechanical Engineering Dept. Tufts University Medford, Massachusetts 02155 Attn: Dr. Lloyd Trefethen	1
21. NASA-John F. Kennedy Space Center Kennedy Space Center, Florida 32899 Mr. J. P. Claybourne /MC	1
22. Office National D'Etudes Et De Recherches Aerospatiales 29, Avenue de la Division LecLerc 92 Chatillon France Attn: par Michel Delattre Attn: par Jean Maulard	1 1
23. AFWL Kirtland Air Force Base, New Mexico Attn: Capt. C. F. Ellis/WLPC	1

Address	Number of Copies
24. Aerospace Corporation P. O. Box 95085 Los Angeles, California 90045 Attn: Library Technical Documents Group	1
25. Westinghouse Astronuclear Laboratories Electric Propulsion Laboratory Pittsburgh, Pennsylvania 15234 Attn: H. W. Szymanowski	1